Repetitive Control of Wind Turbines

Group 1032

Master's thesis, 2012/2013

AALBORG UNIVERSITET

Aalborg University
Institute of Electronic Systems
Frederik Bajers Vej 7
9220 Aalborg
Denmark
Tel +45 9940 8600
http://es.aau.dk

Title:
Repetitive Control by
Individual Pitch
of Wind Turbines

Theme:
Automation and Control

Project period:
September 3rd 2012 to
June 6th 2013

Project group:
1032

Participants:
Ayub Zap Tashkilot
Attila Todor Veress
Kim Udengaard Pedersen

Supervisors:
Rafael Wisniewski, AAU
Christoffer Sloth, AAU

Pages: 177

Copies: 9

Attachments: 1 DVD

Finished: 06-06-2013

Synopsis:

Wind turbines with a large rotor span, often encounter inhomogeneous wind field, resulting into stress induced on the vital parts of the turbine. Some of these phenomena in the wind field are repetitive, to a certain extend. By means of individual pitch control these disturbances can be minimized. This is investigated by first deriving a linearised state space model at a wind velocity of 18 m/s. To drive the model, a wind profile is designed. The developed turbine model is verified with respect to the nonlinear NREL FAST 5 MW simulation model for wind velocities from 12 m/s to 24 m/s, the third operating region, for which it is desired to design the control scheme.
Three controllers are designed. A collective pitch controller by means of PI controllers. An individual pitch controller using Multi-bladed Coordinate Transformation. The second individual pitch controller is done by using repetitive control scheme. In order to estimate the unmeasured states Kalman filter is used. To validate, the designed controllers are implemented on NREL FAST 5 MW wind turbine for comparison with its baseline controller. According to the results, the Coleman transformation is outperforms the baseline controller in reducing the blade displacement. The repetitive controller on the other hand has better results, by minimising the fatigue on all the components of the turbine with one drawback, increased pitch actuation.

PREFACE

This report is a master's thesis, written at the section for Automation and Control at the department of Electronic Systems at Aalborg University.
The group would like to thank main supervisors Professor Rafael Wisniewski and Post doc. Christoffer Sloth for their supervision and guidance throughout the project. A further thank goes to research assistant Fabiano Daher Adegas and associate Professor Peter Fogh Odgaard for their guidance.

Reading Guidelines
The report includes a number of citations, which are made according to, [Manwell et al., 2009, p.12] with the surname of the first author written, if consecutive authors the surname is followed by 'et al.'. Next the year of publication, and on which page the reference is found. Page reference is only used if the reference is made to books, projects or papers with large number of pages. A list of all the used sources is given in the Bibliography on page 141, and on the enclosed DVD.
References to Sections, Equations, Figures and Tables looks like: Figure 1.4 on page 6, for reference to a figure, where the first integer corresponds to the corresponding chapter and the second integer represents its consecutive position in the chapter. The last integer is the page at which the reference is found.
For simplicity 10^5 is written as $10e5$ throughout the report.
A nomenclature describing acronyms, abbreviations and symbols is found on page **??**, and is included as loose arks for ease the reading.
A DVD is attached on the inside of the back cover of the report. The DVD contains various articles used for references, relevant scripts, data, and a digital version of the report.

Ayub Tashkilot

Attila Todor Veress

Kim Udengaard Pedersen

CONTENTS

Part I

Introduction

1 INTRODUCTION

A short introduction in some of the renewable energies available nowadays, is given in this chapter. Their independent pros and cons are elaborated, with a conclusion minded on countries with a high average wind velocity, thus wind conversion is seen as the optimal solution for converting renewable energy to electricity. To understand the evolution of the windmills to wind turbines a summary of the wind turbine history is presented, ending with an explanation of the different mechanical parts of a modern wind turbine. These parts are exposed to a lot of stress and if not treated with caution, leading to early degradation or even to system failure. Some of these stress factors are caused by the repetitive wind changes throughout the rotor span at every revolution. A solution is proposed by means of individual pitch actuation and torque control in order to prevent fatigue caused by these forces. The project scope is then made on behalf of the ideas proposed in this chapter, followed by the requirement specifications. The chapter ends by stating the acceptance test.

1.1 Motivation

The continuous evolution of technologies involve an increase in energy demand. This energy production should be cheap and pollution free, to ensure a low price for the consumer and the stability of Earth. Due to the fact that the fossil-fuel power stations and nuclear plants are expensive to operate, costly to maintain and pollute the environment, a new solution had to be found. This solution should uphold a more convenient electricity production, from both economical and environmental friendly point of view. Known solutions such as using biomass, photovoltaic power, wind harnessing and hydro power plant, just to name a few, are depicted in Figure 1.1. These are beneficial regarding lowering the CO2 pollution.

Figure 1.1: Different types of renewable energy sources. Respectively photovoltaic, hydroelectric, wind energy and biomass [alternativeenergysource.org, 2011].

Biomass

Biomass is organic waste. This is e.g. used as fuel for various energy consumers like vehicles or power plants. During the production the waste is first separated from the non-organic materials and then refined for e.g. use in a power plant. This procedure may use more energy, than produced, thus it is not as beneficial as other approaches.

Photovoltaic

The photovoltaic panels, capture solar radiation and transform it into electrical energy. Photovoltaic power plants are size wise large [alternativeenergysource.org, 2011], thus for smaller countries it is not as suitable as other consents. Furthermore, it does not produce any power during the night. Though this form of renewable energy is CO2 emission free when it generates power, it is not as suitable for countries with an average low number of sunny days over a year. The annual solar radiation for the world is shown in Figure 1.2.

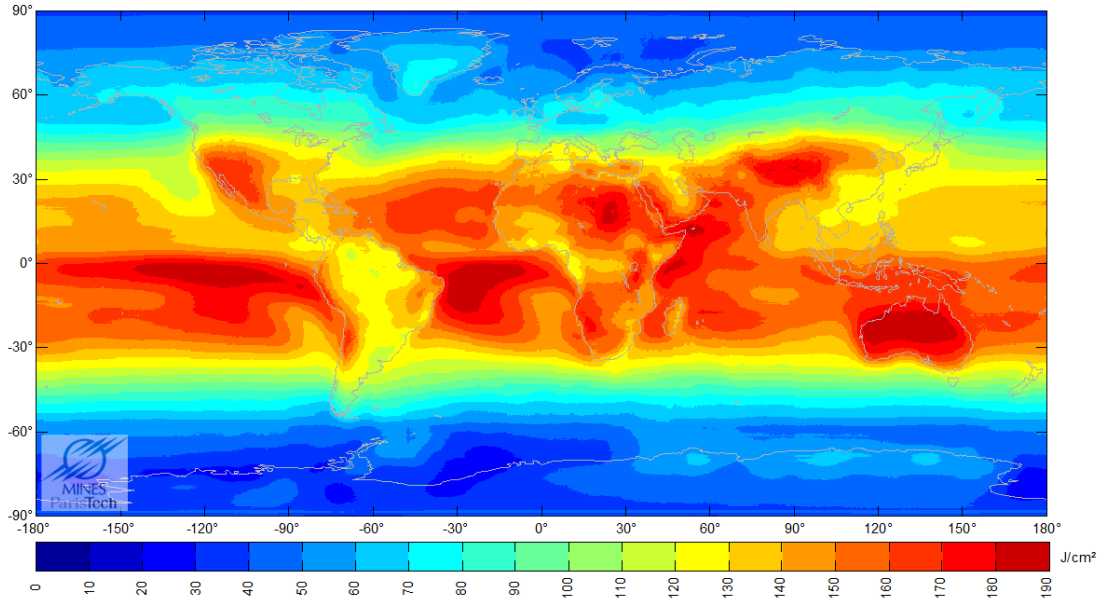

Figure 1.2: Annual average solar radiation from 1990 to 2004 [Armines, 2008].

Hydroelectric

By using the natural forces of the water flow, the hydroelectric power plant is very efficient. Though the process needs a dam and a large water reservoir for the generators to work efficiently. This method also makes it possible to contribute with extra electrical power, when an extra boost in the electric grid is needed. Though this method is very CO2 friendly, some countries do not have these large water reserves and therefore have to look other places to obtain renewable energy.

Wind Energy

An alternative to the mentioned renewable energy sources is harnessing the wind e.g. by using wind turbines. This is especially beneficial for countries with an average high wind velocity, which typical are countries with open spaces, like coastal lines and open fields, where the wind is free to roam. The average global wind velocity distribution for 2008 is shown in Figure 1.3.
The electric power distributor of Denmark, DONG, has foreseen the effectiveness of using wind turbines in Denmark for years, and have invested in this technology. According to [EWEA, 2012] around 30% of the power in Denmark is produced by wind turbines and the number is still increasing.

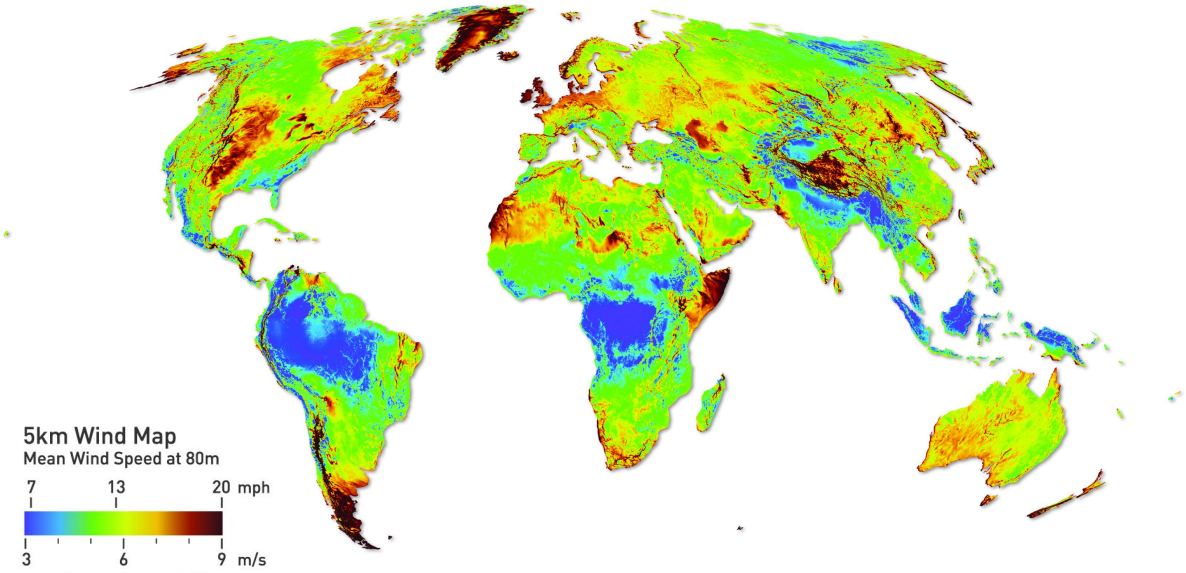

Figure 1.3: Average global wind velocity [3Tier, 2008].

The previously presented energy production techniques are weighted with respect to the geographical position and natural resources of Denmark. These are following elaborated upon:

- Using biomass as renewable energy is a good way to reuse waste, but as previously mentioned it is often costly refining it.
- Denmark does not have any larger mountains with natural water reservoirs, and therefore the hydroelectric power plants are not suitable.
- As seen in Figure 1.2 on the preceding page the annual solar radiation is of course highest along the equator, and thus the position of a country with respect to latitude, is important. Since Denmark lies high on this curve, it is not as suited for solar energy harvesting as e.g wind energy harvesting.
- In Figure 1.3 Denmark lies in the high end of the scale with respect to annual mean wind velocity. This subject is thus worth investigating, as an alternative to fossil fuels and CO2 reduction.

Thus the wind turbine is chosen for a renewable plant. To get an understanding of how the wind turbine has evolved to its present shape, its history is shortly presented in the following section.

1.2 The History of Harnessing the Wind

Man has tried to harness the immense power of the wind throughout decades. According to [Manwell et al., 2009, p.10-13], the first recorded usage of a windmill dates back to the Persians in 644 A.D. The mill is shown in Figure1.4.

Figure 1.4: Windmill made by the Persians from 644 A.D. [Mawer, 2012].

Through many years, windmills have been used for pumping water up from wells or for grinding grain. But by the invention of electricity and the generator, a new use of the kinetic energy in the wind was invented. The first known fully automatically operating horizontal axis wind turbine, was built by Charles Brush from Ohio in 1888 [Manwell et al., 2009, p.15]. Though it was first during the late 1960's the wind turbine got its breakthrough again. This was mainly because of the rising demand in electrical power which resulted in a rapid decrease in fossil fuels. To slow down the increasing depletion of the oil reserves, an alternative had to be found, and the wind turbine became more attractive as an investment.
Engineers made use of the windmill's ability to turn the kinetic power of the wind into a rotational force. Instead of using the rotational force for grinding grains, they used it to run a generator, and thus turning the power of the wind into electrical power. Though the vertical axis wind turbines are still used today, the main wind turbine seen in the country sides are the up-wind, horizontal axis wind turbine, variable speed, variable pitch, with three blades as depicted in Figure 1.5. This is mainly because the horizontal axis wind turbine is more efficient than the vertical axis wind turbine.

Figure 1.5: Horizontal axis wind turbine [Technologies, 2012].

1.3 Preliminary Analysis

A horizontal axis wind turbine consist of three main fuselages: tower, nacelle, and rotor. These parts are illustrated in Figure 1.6 with their appertaining mechanics.

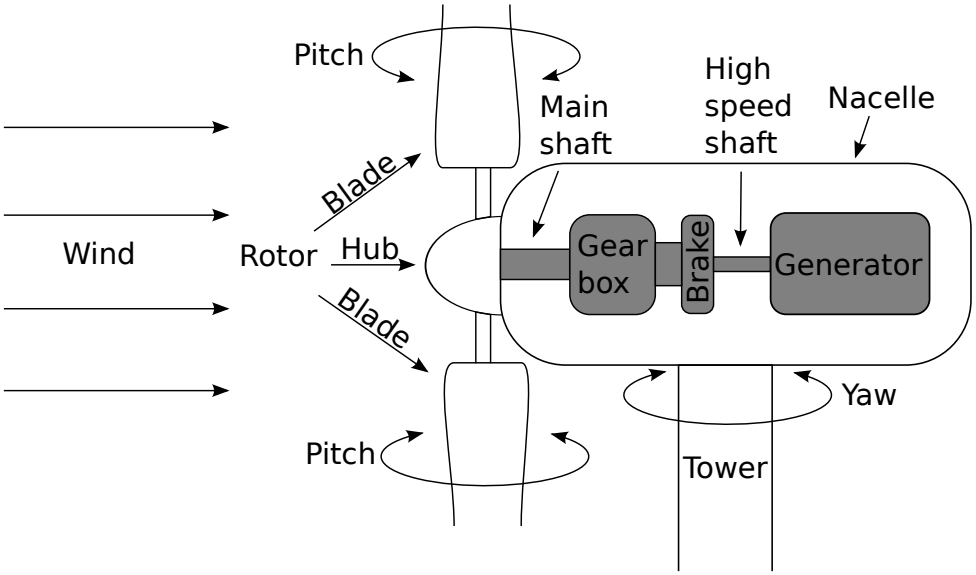

Figure 1.6: Components of a typical up-wind horizontal axis wind turbine.

When the rotor is in an upwind position, meaning that the wind is parallel with the nacelle as depicted in Figure 1.6, the kinetic energy of the wind affects the blades and induces an angular velocity to the rotor. To determine the mean wind velocity and ensure that the turbine is upwind, an anemometer and a wind wane is installed on the top of the nacelle. To keep the nacelle in an upwind position, motors are installed in the joint between the tower and the nacelle, and is controlled with respect to the wind vane. This rotating motion is called yawing. To be able to get the most kinetic energy out of the wind, the blades are able to revolve around their own axis, called pitching. The blades are attached to the hub by individual motors thus resulting in the possibility of individual pitching. To get the angular velocity from the main shaft up to speed, for the generator to be able to convert it to the power used in the power grid, a gearbox is installed. The gearbox is connected to the generator through a high speed shaft. The power accumulated through the generator, by means of power electronic converters is lead to the consumers through the power grid.

Basic Control Strategy

The basic insight of a horizontal axis wind turbine is given, which leads to an elaboration on the general control scheme noted by [Burton et al., 2001, p.471] and [Manwell et al., 2009, p.359]. This scheme is shortly presented.

For the turbine to be operational, a certain amount of kinetic energy has to be present in the wind. Usually the turbine begins producing electricity at a wind velocity of 3-5 m/s, also called the cut-in wind speed, and shuts down at approximately 25 m/s, also called the cut-out wind speed. It reaches its nominal, or rated wind speed at around 11-14 m/s. These numbers of course vary from one wind turbine to the other depending on what environment it is designed for. The states mentioned are shown in Figure 1.7, where

the cut-in wind speed is noted by **A**, the nominal wind speed as **C** and the cut-out wind speed as **D**.

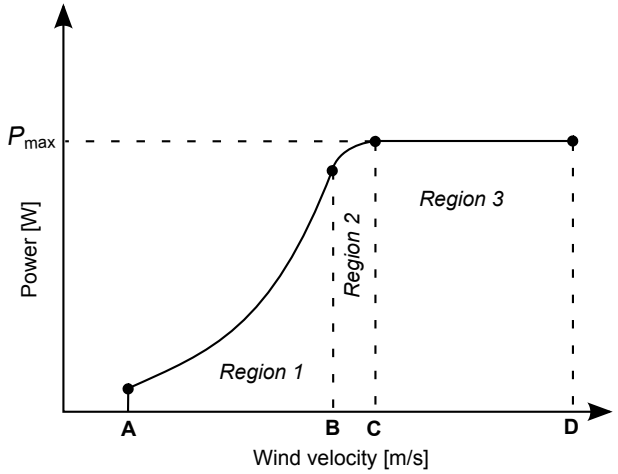

Figure 1.7: Power output characteristic according to a rising wind velocity.

During the region between the cut-in wind speed and nominal wind speed, the blades are set at an optimal pitch angle, meaning that the blades are pitched so they harness as much wind as possible. Further the torque is increased as the wind velocity increases, until **C** is reached. From **B** to **C** a transition from controlling the torque to controlling the pitch is made. This is a very critical point, where the turbine could endure a lot of stress if not controlled properly. This is often done by using a bumpless transfer or gain scheduling. From nominal wind velocity, **C** until the cut out wind speed **D**, the blades starts pitching out, which is called feathering. In this area, the torque is at its maximum value and is not change.
The limitation in power output, noted from point **C** to **D**, is for prolonging the lifespan of the turbine, otherwise the mechanics of the turbine would degrade rapidly. Further by not shutting down at point **C** the turbine is able to work under a larger wind span. The representation of the torque dynamics is depicted in Figure 1.8, where the bold letters corresponds to the ones of Figure 1.7. It is noted that, when enough wind is present to run the turbine at point **A**, the turbine generates little power, which rises until **B** is reached. This region if often denoted *Region 1*. From **B** to **C** the power output rises rapidly and stays there until the cut-out wind velocity is reached. The region from **B** to **C** is often denoted *Region 2*. It is thus desired to keep the turbine in the area from **C** to **D** to get the maximum power output. This region is noted *Region 3*.

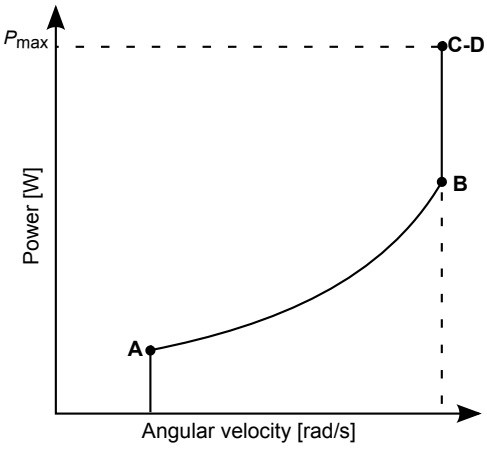

Figure 1.8: Representation of the torque characteristic of the generator with rising wind velocity.

In the case where these limitations would be neglected, the maximum power $P_{\max}$, would rise linearly, from **B** and forth, with respect to the wind velocity and the angular velocity of the rotor. This scheme is not possible with todays materials, because they are not able to withstand the immense powers of the nature, when run freely.

1.4 The Evolutionary Aerodynamic Impact on Wind Turbines

Because of the increasing power demand and interest in renewable energy, turbine manufacturers try to meet it, by building larger turbines, so they are able to cover a larger area of the wind field, and thus produce more power per wind turbine. As the turbines gets larger, the rotor area also increases, resulting in new problems. These are e.g. an increase in the mean wind velocity as height is increased, the wake from e.g. wind turbine farms becomes larger as the rotor span increases and the tower shadow is present for a longer time, because of the larger tower which carries the heavier nacelle and rotor. These disturbances are further elaborated in the following part.

Wind Shear

The change in wind velocity with respect to hight is called wind shear. Wind shear is the change in the vertical and, or horizontal wind velocity [Bianchi et al., 2007, p.24-25]. Though in this report it is mainly vertical wind shear (also called speed shear) that is considered. It occurs because of e.g. obstructions due to terrain, building, weather phenomenas or because of the friction with the surface of the ground. An example is seen in Figure 1.9.

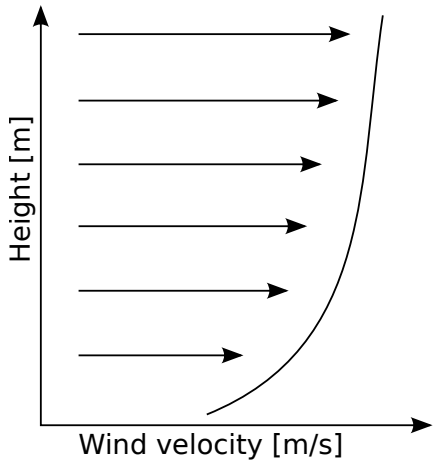

Figure 1.9: Representation of a general vertical wind shear, where the wind velocity is displayed with vector arrows.

Though the wind field looks uniform at given heights in Figure 1.9, it is highly dynamic. A given wind field consists of everything from small eddies, to large dips or increase in wind velocity. The period of these phenomena are stochastic.

Wind Wake

Another wind phenomena that influences the turbine is the wind wake. It can occur in wind farms, as turbulences and wind deficit, V_{H^-}, caused by the rotational movement of the rotor, from a turbine in front

of another turbine, as noted in Figure 1.10. The spacing between turbines is often noted by D_0, which is the rotor diameter. There are two main types of wakes, near and far. Far wake occurs from approximately 2 to 5 D_0 downstream, [Vermeer et al., 2003, p.489], where a typical spacing for turbines in wind farms are 5 to 10 D_0 and 1.5-3 D_0 in the crosswind, depending on the size of the turbine [NREL, 2013], though the wake deficit is noticeable after 15 D_0. Thus only far wake is investigated. When turbines are aligned, it is possible that the next turbine in line encounters what is called a full wake. This is the most severe case of wake for a turbine, and can decrease power production and increase the loads. Researchers from [Energy Research Centre of the Netherlands, 2009] have investigated these effects on the consecutive turbines and found that from a distance of 5 D_0 the increase in loads rose to 45% and at 9.5 D_0 by 10%. Though it is mainly the second turbine in a row that encounters the highest increase in loads where as the effect (difference in wind velocity from turbine to turbine) on the consecutive turbines are less severe.

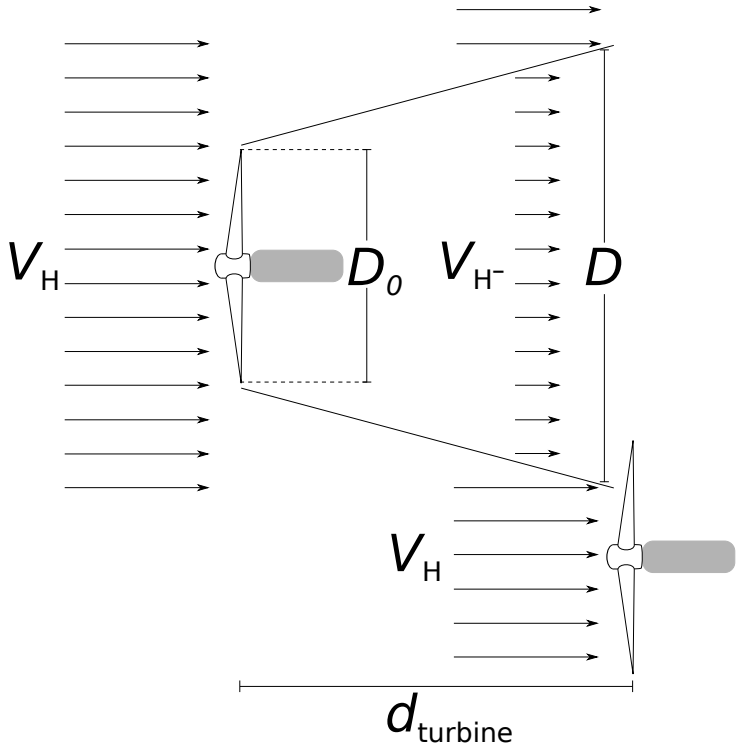

Figure 1.10: Wind wake caused by a turbine. V_{H} is the oncoming wind velocity at hub height for the first turbine in line. V_{H^-} is the wind velocity after the the first wind turbine. D_0 is the diameter of the wind turbine, D is the diameter of the wake at a given distance and d_{turbine} is the distance from one turbine to the next.

Tower Shadow

One of the self afflicting disturbances of the turbine is tower shadow. This occurs when a blade passes the tower at its vertical downward position, π rad, depicted in Figure 1.11(b).

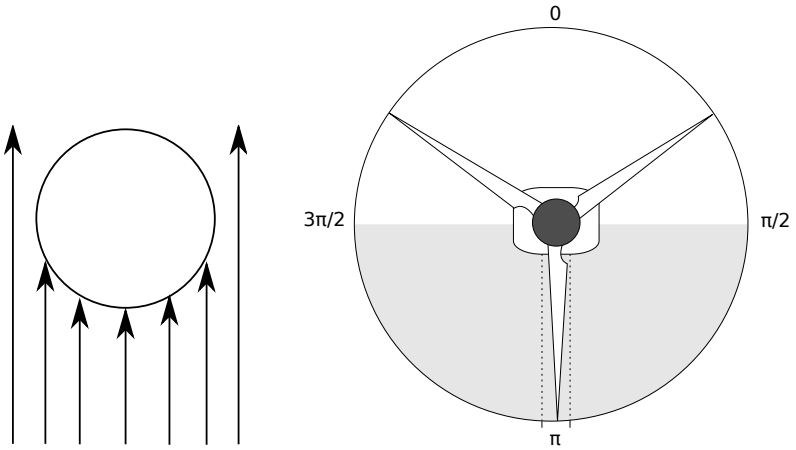

(a) Wind velocity decreasing when hitting a structure, depicted by the length of the vector arrows. The circle denotes the tower seen from above.

(b) The area at which the turbine encounters tower shadow is marked light gray. The tower is depicted with stippled lines at the azimuth angle π rad.

Figure 1.11: Tower shadow noted from looking down on the tower, and straight onto the turbine.

At this angle the wind velocity is decreased as noted in Figure 1.11(a), by the length of the vector arrows. The turbine encounters the tower shadow at a frequency of $3P$, meaning three times per rotor revolution, one for each blade.

The Effect on the Turbine

According to [Manwell et al., 2009, p.143] the negative effects these aerodynamic changes may cause are:

- Blade vibrations.
- Significant material fatigue.
- Increased peak forces.
- Blade stall.

These transient changes affects the structure and the mechanical parts of the turbine in a negative way. Some of the strain these changes inflict on the turbine can be diminished. This is concerning the wind shear, wake and tower shadow which are repetitive changes to a certain extend. These changes can be approximated in time, though wake is able to change its position, velocity and intensity, or not bee present at all, though it does not change instantaneously. The same can be said about the wind shear.

Following the project scope is presented on behalf of the investigations made.

1.5 Project Scope

Throughout the Introduction, the repetitive changes which the rotor of a turbine encounters due to the wind, have been investigated. Following the project scope is elaborated with respect to these repetitive changes:

Is it possible to reduce the periodic loads on the components of a modern wind turbine operating in above-rated region, by means of individual pitch control?

The considered case is outlined in Figure 1.12, which is considered a small section of a wind turbine park.

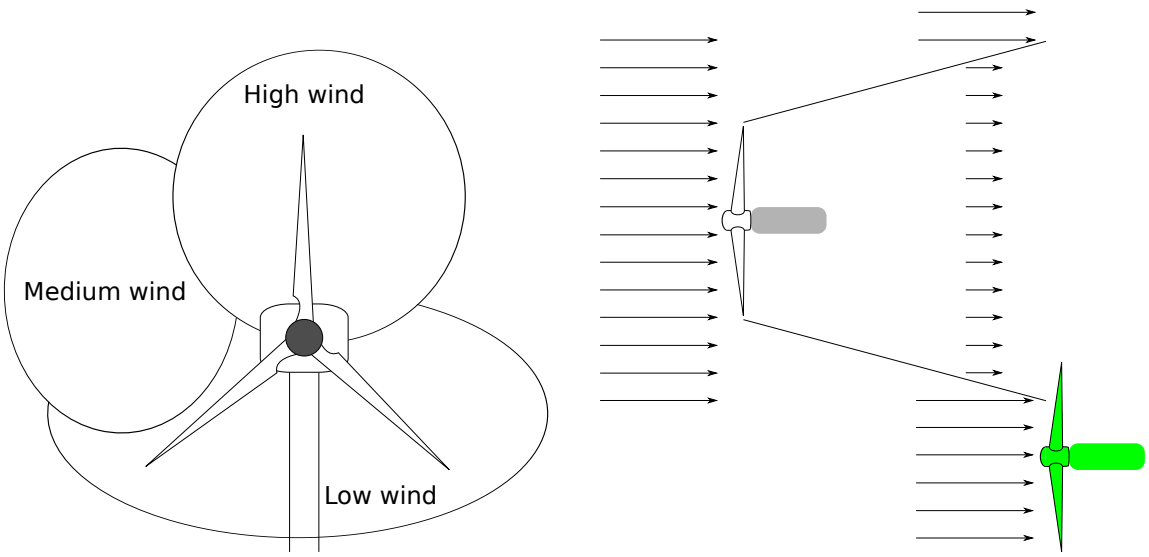

(a) Change in wind velocity noted from horizontal view

(b) Change in wind velocity, with respect to wake, noted from bird perspective.

Figure 1.12: Repetitive disturbances.

The turbine depicted green in Figure 1.12(b), is the one considered throughout the report, though both of the turbines have the same characteristics. The repetitive changes in wind velocity are noted in Figure 1.12(a), as areas. These are noted fixed for a certain time frame.

In the following section the requirements for the given wind turbine are clarified. Further an acceptance test is set with respect to proving the stated project scope.

2 REQUIREMENT SPECIFICATIONS

Considering the project scope noted in Section 1.5, and the results of the investigations through Section 1.4 on page 9, controlling the pitch angles and the torque applied on the generator (variable speed - variable pitch), seems beneficial cost wise and implementation wise. The approach is similar to the control scheme used by the nonlinear benchmark NREL (National Renewable Energy Laboratory) FAST (Fatigue, Aerodynamics, Structures and Turbulence) 5 MW wind turbine model [Jonkman and Jr., 2005]. Throughout the project, the model is noted FAST model. The wind turbine model and control design, are made with respect to the nonlinear NREL FAST 5 MW wind turbine. Throughout the report, when the NREL FAST 5 MW wind turbine is mentioned, it is only the nonlinear model that is considered. This wind turbine is chosen because of its extended usage as benchmark model, and the fact that it is open source. The operating area of interest is the above rated, *Region 3*, where the turbine has its maximum output. In this region, the NREL 5 MW wind turbine operates for wind velocities from 11.4 m/s and cuts off at 25 m/s. The inputs for the FAST model are the pitch angles and the torque of the generator, while the output are the corresponding control signals. A set of limitations are imposed according the specifications of the FAST model, also listed in Appendix D on page 161. The requirements are stated as following:

1. The power produced by the wind turbine should be kept constant at all time, at 5 MW with an error tolerance of $\pm 1\%$, for wind velocities from 12 to 24 m/s.

2. The angular velocity of the generator should be kept constant at all time at 122.9 rad/s, with an error tolerance of $\pm 1\%$, for wind velocities from 12 to 24 m/s.

3. The fatigue present on the blades of the wind turbine should be minimised compared to the already existing controller of the NREL FAST 5 MW turbine.

4. The pitch action should be individual and minimised compared to the existing pitch control of the NREL FAST 5 MW turbine.

5. The generator torque should be kept constant at the reference value of 43050 Nm, with an error tolerance of $\pm 1\%$, for wind velocities from 12 to 24 m/s.

Acceptance test

To verify the requirements above, an acceptance test is set up, composed with respect to the following:

- Setup.
- Purpose.
- Success criteria.

Setup

The Acceptance tests are run in `MATLAB`'s `Simulink` environment, in which the FAST 5 MW turbine already is implemented by NREL. Thus for implementation ease this environment is chosen. The performance of the derived controller is implemented on the FAST 5 MW turbine, and compared to the baseline NREL 5 MW controller. The turbine is tested under the circumstances which a wind turbine in the open could encounter, described in Section 1.4 on page 9. Though because the FAST 5 MW turbine environment does not have wind wake, this is not tested for the FAST model, but a wake model is made for the control model on which it is tested. The input disturbances are kept the same in all the tests, for later comparison.

Purpose

The purpose of the acceptance test is to verify whether the controller is able to obey the requirements stated on page 15, on the FAST 5 MW turbine.

Success criteria

The test is considered passed if all the requirements listed on page 15 are fulfilled. The results of the acceptance test are elaborated in Chapter 14.1 on page 123.

Following an outline of the report is given, for the reader to have an overview of the report.

2.1 Outline

The project scope and requirements specifications are stated, leading to a short overview of each chapter throughout the report. The main thought behind it, is to provide an overview of the project for the reader.

Chapter 3: Wind Model
This chapter gives an overview on the wind model, used as a disturbance for the linearised model. It consists of a Kaimal filter, wind shear, tower shadow and a wake model. The wind model is made with respect to a wind field which a wind turbine could encounter in reality.

Chapter 4: Aerodynamic Model
This chapter presents how the aerodynamic forces, caused by the kinetic energy of the wind, affects the structure and mechanical parts of the turbine. The equation for the force of torque and the force of thrust are derived using the final element method. The forces are then obtained with respect to pitch angle, angular velocity of the rotor and tip speed ratio. However, the resulting equations are nonlinear, thus a linearisation is performed and elaborated thoroughly in appendix, as it is considered trivial for the information flow.

Chapter 5: Mechanical and Structural Models
This chapter presents each of the mechanical models, which the turbine is composed of. First, deriving the tower and blades, continued by the drive-train and generator. As the generator model is nonlinear, a linearisation is performed and elaborated on in appendix. Finally the pitch model is developed for the individual pitch purposes.

Chapter 6: Combined Model
This chapter merges the models, developed in the previous two chapters Aerodynamic and Mechanical Model, and the final model for the wind turbine is derived, which is used for control design and as system model throughout the simulations. An overview is also given on the systems inputs, states, outputs and disturbances respectively.

Chapter 7: Model Validation
This chapter presents the performance of the developed model in comparison with the nonlinear NREL FAST 5 MW wind turbine, having a wind disturbance input corresponding to the third control region. The chapter concludes on the comparison of the linearised model with respect to the FAST 5 MW model at the end.

Chapter 8: System Analysis
This chapter provides an analysis of the linearised model used for designing the controllers. The open loop stability is elaborated using Hurwitz stability criterion. The reachability and observability of the system are verified using gramians. Following, the model discretization is performed using a zero order hold. The obtained linearised and discretised model is further used for control purpose.

Chapter 9: Control Introduction
This chapter gives a short overview on the three control designs that follow. It further elaborates on the overall control scheme and the measurements used for control purpose of the different parts of the turbine.

Chapter 10: Collective Pitch Control
This chapter presents the basic control scheme used for stabilising the closed loop linear model. This is accomplished by designing two PI controllers, with purpose of keeping the output power and angular velocity of the rotor constant. This is later used in both the multi-bladed coordinate transformation and the repetitive control scheme.

Chapter 11: Individual Pitch Control by Multi-bladed Coordinate Transformation
This chapter gives an overview on the multi-bladed coordinate transformation, also known as the Coleman transformation. The multi-bladed coordinate transformation is an individual pitch control scheme. The control is accomplished by means of traditional PI controllers. It is used to minimise the 1P loads caused by the individual blade bending due to wind disturbances. Following, an implementation if the controller on the developed linear discrete wind turbine model is elaborated. The results of the implementation are then compared to the results of the developed collective pitch control scheme, ending with a conclusion on the performances of multi-bladed coordinate transformation.

Chapter 12: Repetitive Control
This chapter gives an overview on how a repetitive controller works. This is followed by an elaboration on the general steps required to design an repetitive controller. In order to persuade the reader that this approach is optimal, an implementation of the repetitive controller scheme is made on the linearised pitch system, with results of the simulation. A conclusion based on the obtained results is drawn. By having the necessary knowledge and understanding of the repetitive controller, the implementation on the linear discrete wind turbine model is presented in detail. The chapter ends by concluding on the performances of the repetitive controller with respect to the previously designed controllers: collective pitch control and individual pitch control using multi-bladed coordinate transformation.

Chapter 13: Acceptance Tests
This chapter provides a set of tests with respect to the acceptance tests presented in the Introduction chapter. The developed controllers are implemented on the NREL FAST 5 MW wind turbine software, where the performances are tested and elaborated upon. These tests lead to the conclusion of the project.

Chapter 14: Conclusion
This chapter gives the overall conclusion of the project with respect to the project scope, requirement specifications and acceptance test results.

Chapter 15: Further Work
This chapter gives an overview of the stage at which the project is, and provides further information on continuing the design, for both model and control.

Part II

Modelling

This chapter concerns the derivation of the linear control model, used in Chapter 9 on page 65, for design a controller upon. In each of the following sections, the sub-models of the parts which a wind turbine is composed of, are explained and derived. The nonlinear dynamics are linearised and elaborated in Appendix C on page 157. Linearising the nonlinear dynamics of the model, is chosen because of its extended use throughout control derivation. An overview of how the forces affects the different parts of the turbine, is given in the following section.

Models Overview

The kinetic energy of the wind applied on the blades of a turbine produces an aerodynamic force that induces an angular rotation on the rotor. This is the force of torque, $F_{\mathrm{Q}}(t)$, noted in Figure 2.2. It is then passed through a low speed shaft to the gearbox, for increasing the angular velocity. The gearbox is connected to the generator by a high speed shaft. By applying a torque to the generator, a mechanical energy is induced. A diagram of the procedure from harvesting the wind to mechanical power, is presented in Figure 2.1.

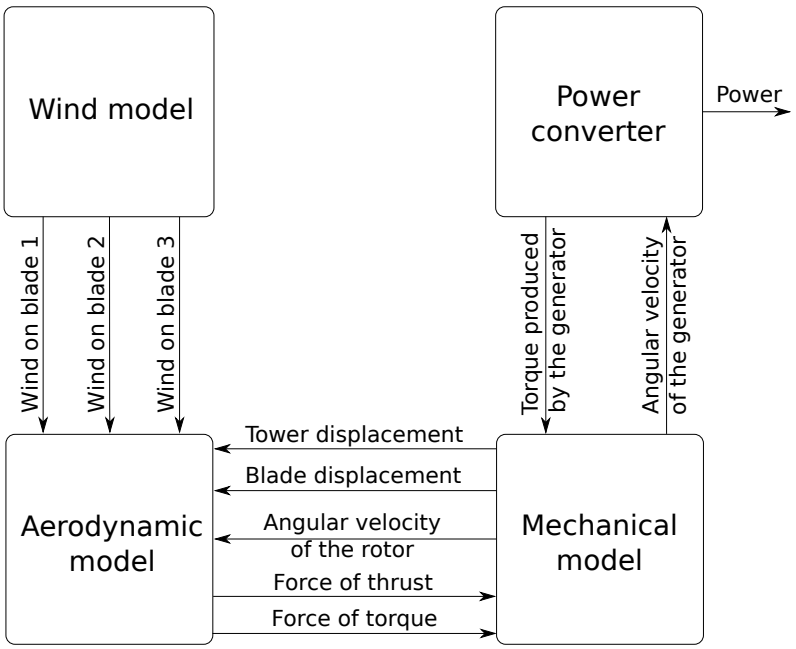

Figure 2.1: Wind turbine modeling parts, and its interconnection.

The aerodynamic forces affect the mechanical structure of the wind turbine, along with the angular velocity of the rotor and the structural displacement (tower and blades displacement). The most important dynamics of the wind turbine are shown in Figure 2.2 and Figure 2.3.

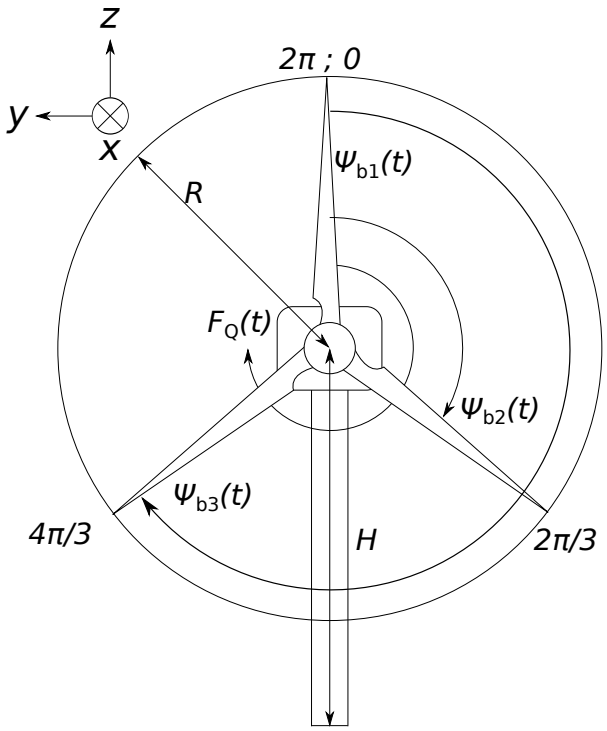

Figure 2.2: Aerodynamic torque applied to the rotor by the wind.

As noted in Figure 2.2, the force of torque, $F_Q(t)$, is applied to the rotor as a result of the oncoming wind velocity. This is in the direction of the x-axis. R is the rotor radius, H is the height from the ground to the middle of the rotor, also known as hub height. The spacing of the blades are of $2\pi/3$ respectively. The angle of each individual blade, with respect to the rotor, is shown by $\psi_{bi}(t)$, where the i indicates the blade number. As a result of the wind velocity in the direction of x, the turbine is also affected by a thrust force. This effect is displayed in the Figures 2.3.

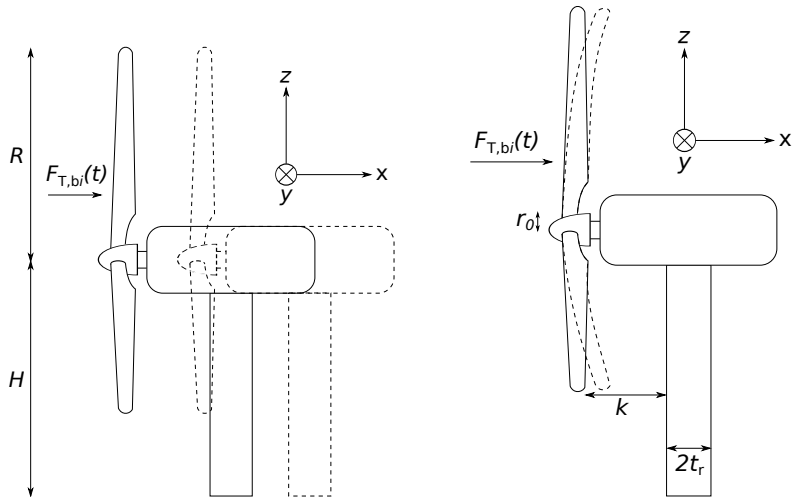

(a) Tower bending.

(b) Flap wise bending of the blades.

Figure 2.3: Tower and blade dynamics taken into consideration with respect to the model derivation.

In Figure 2.3(a), the tower bending is represented as a displacement of the tower. It is caused by the force

of thrust, $F_{\mathrm{T,b}i}(t)$, which is perpendicular to the lifting force that acts on each blade. In Figure 2.3(b) the force of thrust is noted only on the blades. This make the blades bend flap-wise, with respect to a fixed point in the center of the rotor. The distance from the edge of the hub to its apex is denoted by r_0, and the diameter of the tower is noted by $2t_{\mathrm{r}}$.

The mentioned forces and dynamics are used to derive a model for a wind turbine in the following chapters.

3 WIND MODEL

The wind model, noted in Figure 3.1, is the driving force of the wind turbine. Its profile is made with respect to each individual blade noted by the three arrows.

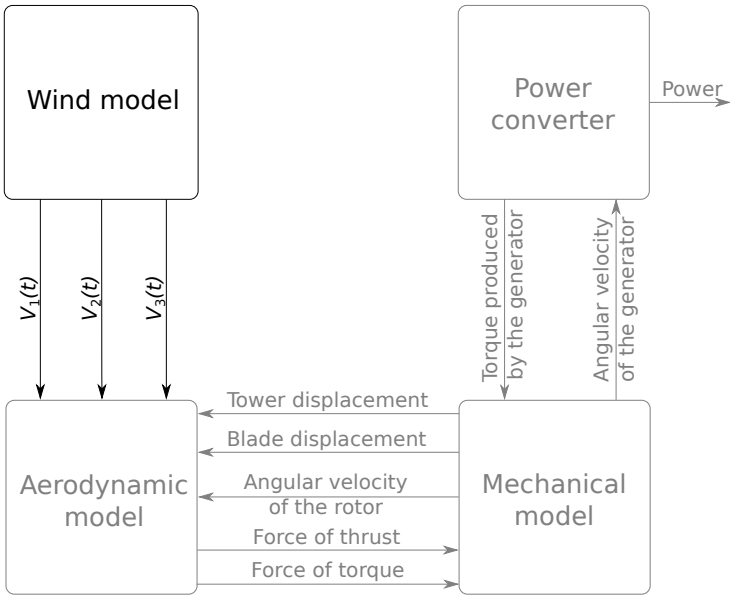

Figure 3.1: An overview of what effect the wind model has on the turbine.

Though the wind is normally perceived as uniform with the occasional gusts, it is very dynamic in reality. Further by encountering obstacles, the wind can become more dynamic. The derived wind profile is made with respect to:

- Wind shear.
- Tower shadow.
- Turbulence.
- Wake.

The effect of these forces are described in Chapter 1.4 on page 9. By summing them, a wind profile complex enough to encompass these aspects is derived as:

$$V_i(t) = V_{\mathrm{K},i}(t) + V_{\mathrm{s},i}(t) + V_{\mathrm{ts},i}(t) + V_{\mathrm{w},i}(t) \qquad \text{for } i = 1,\ 2,\ 3 \qquad [\mathrm{m/s}] \quad (3.1)$$

Where:

$V_i(t)$	is the total wind affecting blade $i = 1,\ 2,\ 3$	[m/s]
$V_{\mathrm{K},i}(t)$	is the turbulence affecting blade $i = 1,\ 2,\ 3$	[m/s]
$V_{\mathrm{s},i}(t)$	is the wind shear affecting blade $i = 1,\ 2,\ 3$	[m/s]
$V_{\mathrm{ts},i}(t)$	is the tower shadow affecting blade $i = 1,\ 2,\ 3$	[m/s]
$V_{\mathrm{w},i}(t)$	is the wake affecting blade $i = 1,\ 2,\ 3$	[m/s]

The equations used in modeling the wind shear and tower shadow are proven in Paper [Dolan and Lehn, 2006] and the derivation of each is briefly clarified following.

Wind Shear

According to [Dolan and Lehn, 2006], the wind shear can be approximated as:

$$V_{\mathrm{ws},i}(t) = \frac{2V_{\mathrm{H}}(t)}{3R^2} \cdot \sum_{b=1}^{3}\left[\frac{R^3 Z_0}{3H}\cos(\psi_{\mathrm{b}i}(t)) + \frac{R^4 Z_0(Z_0-1)}{8H^2}\cos^2(\psi_{\mathrm{b}i}(t)) + \frac{R^5 Z_0(Z_0-1)(Z_0-2)}{30H^3}\cos^3(\psi_{\mathrm{b}i}(t)) - \left(\frac{r_0^3 Z_0}{3H}\cos(\psi_{\mathrm{b}i}(t)) + \frac{r_0^4 Z_0(Z_0-1)}{8H^2}\cos^2(\psi_{\mathrm{b}i}(t)) + \frac{r_0^5 Z_0(Z_0-1)(Z_0-2)}{30H^3}\cos^3(\psi_{\mathrm{b}i}(t))\right)\right] \quad [\mathrm{m/s}] \tag{3.2}$$

Where:

$V_{\mathrm{H}}(t)$	is the mean wind at hub height	[m/s]
R	is the rotor radius	[m]
r_0	is the radius from rotor apex to where the blade profile starts	[m]
$\psi_{\mathrm{b}i}(t)$	is the azimuthal angle at time t for blade i	[°]
Z_0	is the empirical wind shear exponent	[mm]
H	is the hub hight	[m]

It is noted that the wind shear exponent changes with respect to the terrain. Examples are given in Table 3.1.

Terrain	**Wind shear exponent (Z_0) [mm]**
Open water	0.1
Crops	0.2
Heavy trees	0.25
Urban areas with tall buildings	0.4

Table 3.1: Wind shear exponent, Z_0, with respect to terrain, [Manwell et al., 2009, p.46].

Z_0 can vary from 0.1 to 1, where 1 notes most obstruction by the terrain. In Denmark most turbines are erected on open planes or fields, often used by farmers for crops, thus an exponent of $Z_0 = 0.2$ is used. By using this shear coefficient, the implemented result is noted in Figure 3.2. The profile is excited by a wind velocity of 18 m/s, and a shear $Z_0 = 0.2$, the blades encounter an additional wind velocity of approximately 0.45 m/s, at their vertical upright position. A decrease in wind velocity is noted when the

blades are moving towards their vertical downward position. Here the wind velocity is approximately 17.35 m/s.

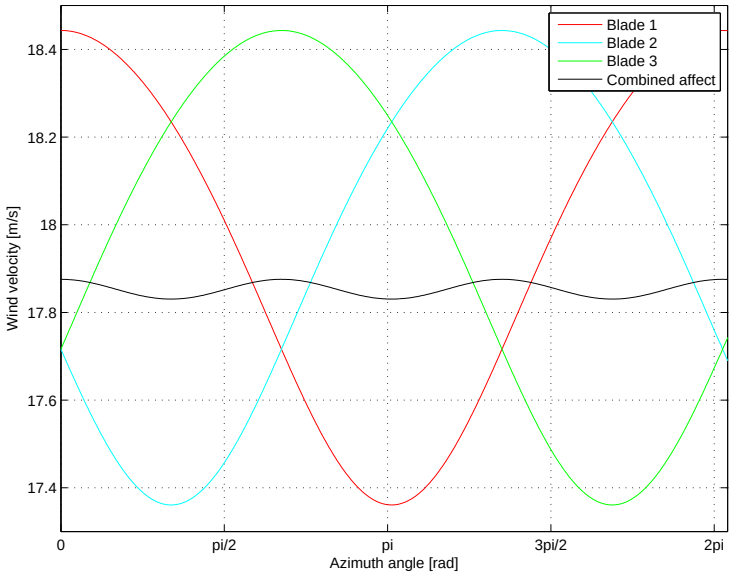

Figure 3.2: Changes in wind velocity on the blades and tower/turbine due to wind shear.

The forces, acting on the rotor are noted by the black line which oscillates around approximately 17.85 m/s. This bias compared to the mean wind velocity of 18 m/s, is due to the wind shear exponent Z_0. When making Z_0 larger, the amplitude increases, and vice versa.

In addition to the decrease of wind velocity for the blade in a downward position, is tower shadow. It is explained following.

Tower Shadow

It is proven that when wind encounters an object its velocity decreases at the epicenter, and accelerates when going around the object. This is elaborated in Chapter 1.4 on page 9. By using the tower shadow model from [Dolan and Lehn, 2006], these factors are taken into account. The tower shadow is derived as:

$$V_{\mathrm{ts},i}(t) = \frac{2mV_{\mathrm{H}}(t)}{3sR^2}\sum_{b=1}^{3}\left[\frac{t_{\mathrm{r}}^2\ln\left(R^2\sin^2(\psi_{\mathrm{b}i}(t))+k_{\mathrm{d}}^2\right)}{2\sin^2(\psi_{\mathrm{b}i}(t))} - \frac{t_{\mathrm{r}}^2\ln\left(r_0^2\sin^2(\psi_{\mathrm{r,\,bi}}(t))+k_{\mathrm{d}}^2\right)}{2\sin^2(\psi_{\mathrm{b}i}(t))} + \frac{t_{\mathrm{r}}^2k_{\mathrm{d}}^2}{\sin^2(\psi_{\mathrm{b}i}(t))\left(R^2\sin^2(\psi_{\mathrm{b}i}(t))+k_{\mathrm{d}}^2\right)} - \frac{t_{\mathrm{r}}^2k_{\mathrm{d}}^2}{\sin^2(\psi_{\mathrm{b}i}(t))\left(r_0^2\sin^2(\psi_{\mathrm{b}i}(t))+k_{\mathrm{d}}^2\right)}\right] \quad [\mathrm{m/s}] \quad (3.3)$$

where

$$m = 1 + \frac{Z_0(Z_0-1)(R^2)}{8H^2} \quad (3.4)$$

Where:

$V_{\mathrm{H}}(t)$	is the mean wind at hub height	[m/s]
t_{r}	is the tower radius	[m]
r_0	is the distance from starting point of the blade to the rotor center	[m]
R	is the radius of the rotor area	[m]
n	is defined as $\frac{r_0}{R}$	[·]
s	is defined as $1-n^2$	[·]
H	is the hight of the tower from the ground to the rotor apex	[m]
$\psi_{\mathrm{b}i}(t)$	is the azimuthal angle of blade i with respect to the rotor area, at time t	[°]
k_{d}	is the distance from blade origin to the middle of the tower	[m]

By implementing Equation 3.3 in MATLAB, the effect of the tower shadow is clearly noted in Figure 3.3.

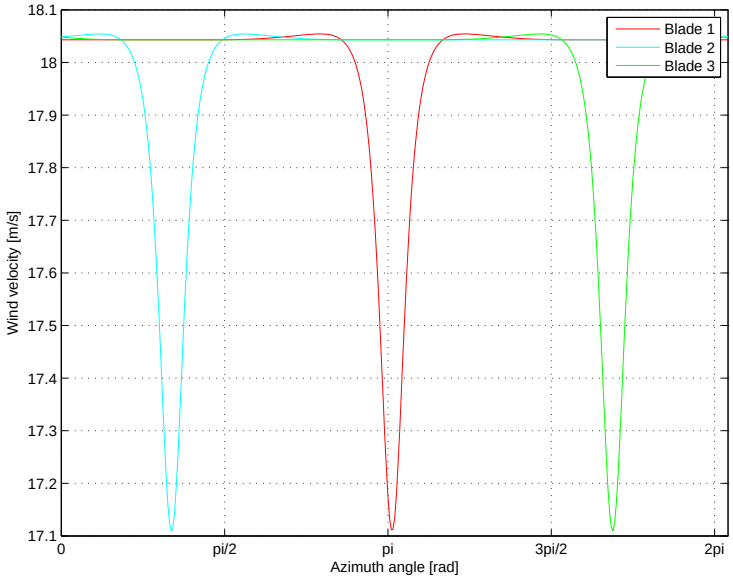

Figure 3.3: Wind disturbances caused by tower shadow.

Through calculations, [Dolan and Lehn, 2006] has found that the tower shadow only affects the blades for azimuth angles from $\pi/2$ rad$\leq \psi_{\mathrm{b},i}(t) \leq 3\pi/2$ rad, which is also noted in Figure 3.3. If this is not taken into considerations when implementing, the tower shadow would appear twice, because of the sine function in Equation 3.3. Another component of the wind profile, is the turbulence. This is elaborated in the following section.

Turbulence

For the mean wind velocity to resemble the real wind, turbulence $V_{\mathrm{K},i}(t)$, is needed in the wind profile. The two models, Von Karman and Kaimal, have been investigated because of their already proven resemblance to a real turbulence. They have further been used in the wind turbine industry by e.g. the implementation in the FAST model. One of the differences amongst them is, that the Kaimal spectrum is able to give a more realistic profile. This is e.g. noted by the fact that Von Karman is isotropic, invariant with respect to the wind direction, where the Kaimal spectrum has different standard deviations for the lateral and vertical turbulences (horizontal turbulence is 80 percent and vertical turbulence is 50 percent of the longitudinal turbulence). Because of the possibility to extend the model, and have a more realistic

turbulence profile, the Kaimal spectrum is used. It is given as the power spectrum density (the frequency domain) by:

$$S_k(f) = \sigma_k^2 \frac{4\frac{L_k}{V_{\mathrm{H}}(t)}}{\left(1+6f\frac{L_k}{V_{\mathrm{H}}(t)}\right)^{\frac{5}{3}}} \quad [\mathrm{dB/Hz}] \quad (3.5)$$

where:

L_k	is the velocity component integral scale parameter	$[\cdot]$
k	is the velocity components, u, v or w	$[\cdot]$
f	is the frequency of the turbulence	[Hz]
$V_{\mathrm{H}}(t)$	is the mean wind velocity at hub hight	[m/s]
σ_k^2	is the variance with respect to the turbulence intensity, TI	$[\cdot]$

The velocity component is composed of three parameters, u, v and w. These are the representation of the wind affecting the turbine in the directions x, y and z respectively. The variance, σ_k^2, is derived by using the turbulence intensity, TI, which is given by Table 3.2,

Class $[\cdot]$	**TI** $[\%]$
A	16
B	14
C	12

Table 3.2: Turbulence intensity classes from the standard IEC 61400-1 3^{rd} edition, [Analysis and Program, 2009]

and is calculated using the following equation:

$$\sigma_{\mathrm{u}} = \frac{TI}{100} V_{\mathrm{H}}(t) \quad [\mathrm{m/s}] \quad (3.6)$$

The turbulence intensity has by definition three classes, given by the IEC 61400-1 3^{rd} edition. These are defined as the turbulence intensity at a wind velocity of 15 m/s. The turbulence intensity is then substituted into Equation 3.6, and the standard deviation is calculated. The connection between three velocity components u, v and w for the standard deviation are

$$\sigma_{\mathrm{v}} = 0.8\sigma_{\mathrm{u}} \quad [\cdot] \quad (3.7)$$

$$\sigma_{\mathrm{w}} = 0.5\sigma_{\mathrm{u}} \quad [\cdot] \quad (3.8)$$

L_{k} is also calculated by the IEC 61400-1 3^{rd} edition standard. It is given by:

$$L_{\mathrm{u}} = 8.1 \cdot \Lambda \quad [\cdot] \quad (3.9)$$

$$L_{\mathrm{v}} = 2.7 \cdot \Lambda \quad [\cdot] \quad (3.10)$$

$$L_{\mathrm{w}} = 0.66 \cdot \Lambda \quad [\cdot] \quad (3.11)$$

Λ is the turbulence scale parameter, and is given by $\Lambda = 0.7 \cdot \min\{60\text{ m, Hub height}\}$. The Kaimal filter is implemented using the model developed by [Iov et al., 2004]. The resulting profile is given in Figure 3.4, which is excited with a wind velocity of 1 m/s and a turbulence intensity of 12 %.

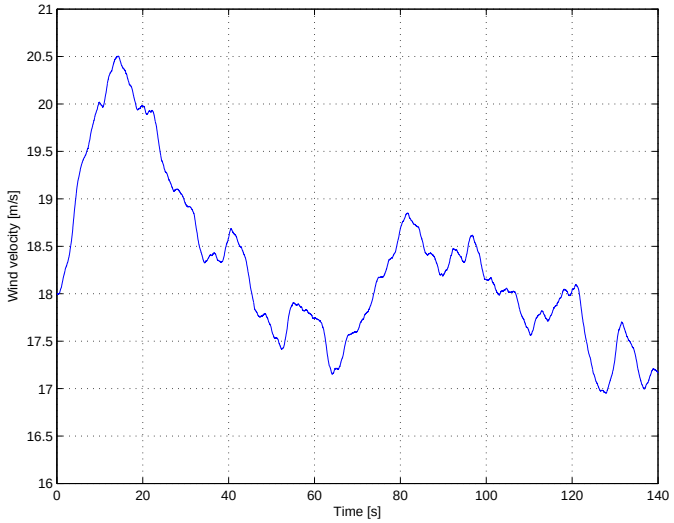

Figure 3.4: The turbulence caused by the Kaimal filter at a mean wind velocity of 18 m/s.

For the wind profile to be complete a wake field is needed. This is described in the following section.

Wake Model

The main focus in this report are repetitive changes. This subject is superimposed by adding a wake model for a specific part of the rotor area. In this area the wind velocity deficits due to the presence of another turbine in front. The wake model is made with respect to [Jensen, 1983, p.6], and stated following:

$$V_{\mathrm{w},i}(t) = V_{\mathrm{H}}(t)\left(1 - \frac{2}{3}\left(\frac{R}{R + c_{\mathrm{e}} \cdot d_{\mathrm{turbine}}}\right)^2\right) \quad [\mathrm{m/s}] \quad (3.12)$$

Where:

$V_{\mathrm{H}}(t)$	is the wind speed at hub height	[m/s]
R	is the rotor radius	[m]
c_{e}	is the entrainment constant	[·]
d_{turbine}	is the distance from the first turbine to the subsequent	[m]

Equation 3.12 makes a top-hat, thus for having a more real distribution, Equation 3.13 is applied to d_{turbine} and R.

$$f(\psi) = \frac{1 + \cos(9 \cdot \psi)}{2}; \qquad \text{for } \psi \leq 20^\circ \quad (3.13)$$

This gives the more realistic wake shaped as a sine. The wake model is corrected to the wake deficit made according to [Frandsen, 2007, p.29], where the velocity deficit is calculated by:

$$V_{\mathrm{wd}} = \frac{1}{2} V_{\mathrm{H}}(t) C_{\mathrm{t}} \left(\frac{D}{D_0}\right)^2 \quad [\mathrm{m/s}] \quad (3.14)$$

Where

$$D = D_0(1 + \beta_0)s \quad [\mathrm{m}] \quad (3.15)$$

$$d_{\mathrm{s}} = \frac{d_{\mathrm{turbine}}}{D_0} \quad [\cdot] \quad (3.16)$$

Where:

$V_{\mathrm{H}}(t)$	is the wind velocity at hub height	[m/s]
C_{t}	is the thrust force coefficient	[·]
D_0	is the rotor diameter	[m]
D	is the width of the wake at the consecutive wind turbine	[m]
β_0	is the turbulence parameter	[·]
d_{s}	is the non-dimensional downwind distance	[·]
d_{turbine}	is the distance from the first turbine to the consecutive	[m]

The C_{t} value is determined in Appendix B on page 151, thus through calculations an approximate deficit of 0.84 m/s is given. The value is subtracted from $V_{\mathrm{H}}(t)$, thus the wake depicted in Figure 3.5 is used.

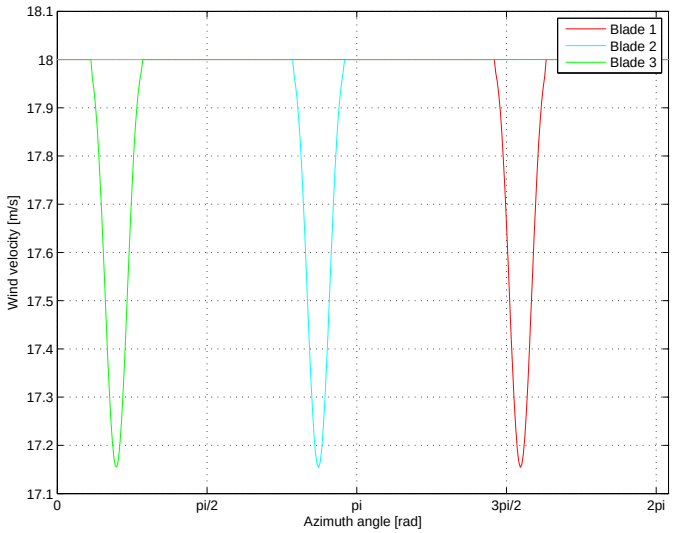

Figure 3.5: The wind profile on each blade when affected by a wake.

Total Wind Field

By adding the wind velocities, and including the turbulence, the final wind field is given in the following equation:

$$V_i(t) = V_{\mathrm{K},i}(t) + V_{\mathrm{s},i}(t) + V_{\mathrm{ts},i}(t) + V_{\mathrm{w},i}(t) \qquad \text{for } i = 1,\ 2,\ 3 \qquad [\mathrm{m/s}] \quad (3.17)$$

The final wind profile is presented in Figure 3.6, though it should be noted when comparing to Kaimal representation in Figure 3.4 on the facing page, one revolution, 2π rad, is made in approximately 5 seconds, with respect to the optimal angular velocity of the rotor given in Appendix D.2 on page 163.

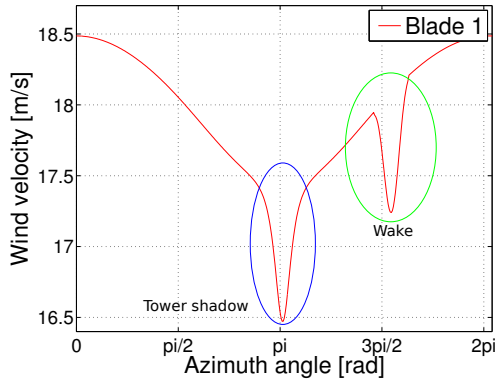

(a) The total wind field for blade 1 without Kaimal spectrum.

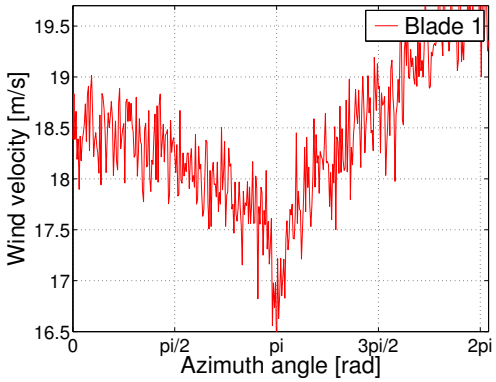

(b) The total wind field for blade 1 with Kaimal spectrum.

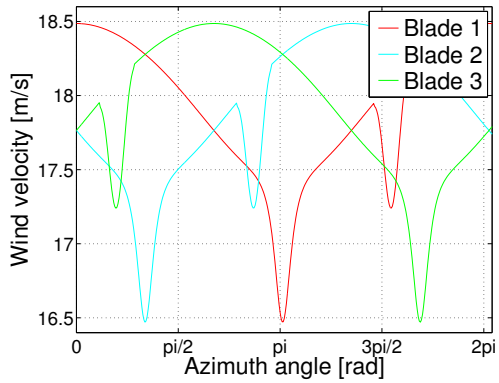

(c) The total wind field for all three blades without Kaimal spectrum.

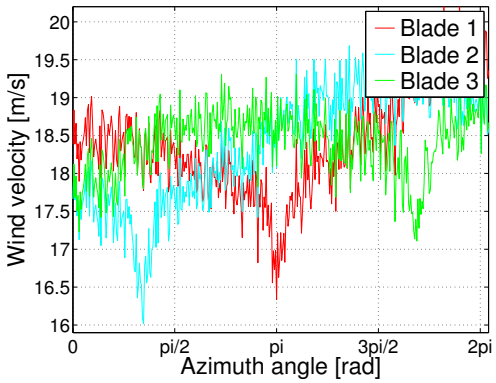

(d) The total wind field for all three blades with Kaimal spectrum.

Figure 3.6: Wind profile for the linearised mode, including tower shadow, wind shear, wake and white Gaussian noise for transient dynamic resemblance.

When comparing Figure 3.4 with the Figures 3.6 downward spikes are noted. An example is shown by the light green marking, and the blue marking in Figure 3.6(a). These are caused by the tower shadow and wake respectively. The shear is noted by the sine which stretches from 0 to 2π. This wind profile contains the main components needed to resemble the realistic wind. As noted in Figure 3.6(c) and Figure 3.6(d) the wind profile is applied on each individual blade. White Gaussian noise is used to resemble the transient dynamics of the wind. Following a control model for the turbine is derived, with thought of implementation as a state space for `MATLAB Simulink`.

4 Aerodynamic Model

As the wind profile is derived, the next step is to investigate the effect of these forces on the turbine. The aerodynamic model is developed with respect to the finite element model, which is elaborated following. When deriving the force of thrust and the force of torque, it is noted that these terms consist of nonlinearities, thus for the linearised model derivation, they need to be linearised. This is elaborated in Appendix C on page 157. The effect of these forces on the system are noted in Figure 4.1.

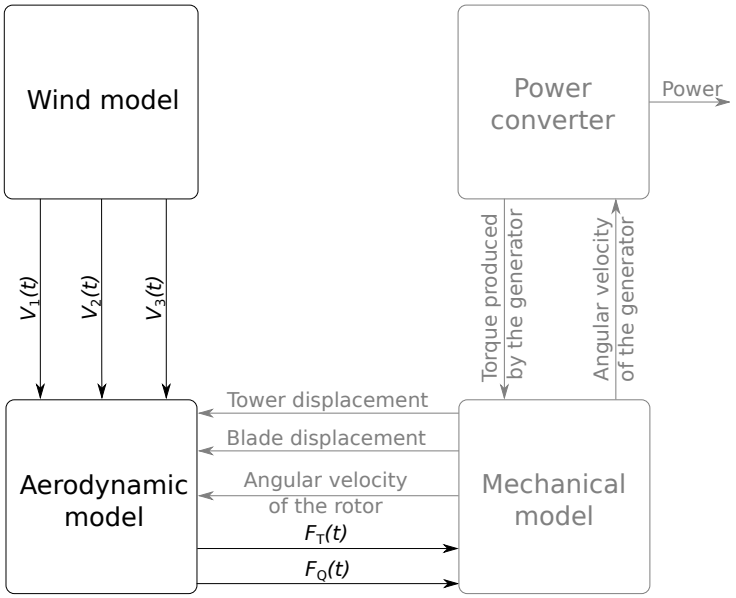

Figure 4.1: An overview of the effect the aerodynamic model has on the turbine and its interconnections.

4.1 Finite Element Model

The following derivations are made according to [Bianchi et al., 2007, p.10]. The rotor is noted ideal with an infinite number of thin blades, where the wind inflow is seen through a tube. In order to determine the maximum power, the power and thrust coefficients C_p and C_t respectively, the Bernoulli equation is used. This derivation is elaborated in Appendix B on page 151. The determined coefficients are used in the following for calculating the forces affecting the turbine.

The cross section of the blades are shaped like airfoils, and considered to be composed of an infinite number of infinitesimal airfoils. The forces acting on the airfoil, including the angle of attack which is the angle between the oncoming wind on the rotor and the chord line, are presented in Figure 4.2.

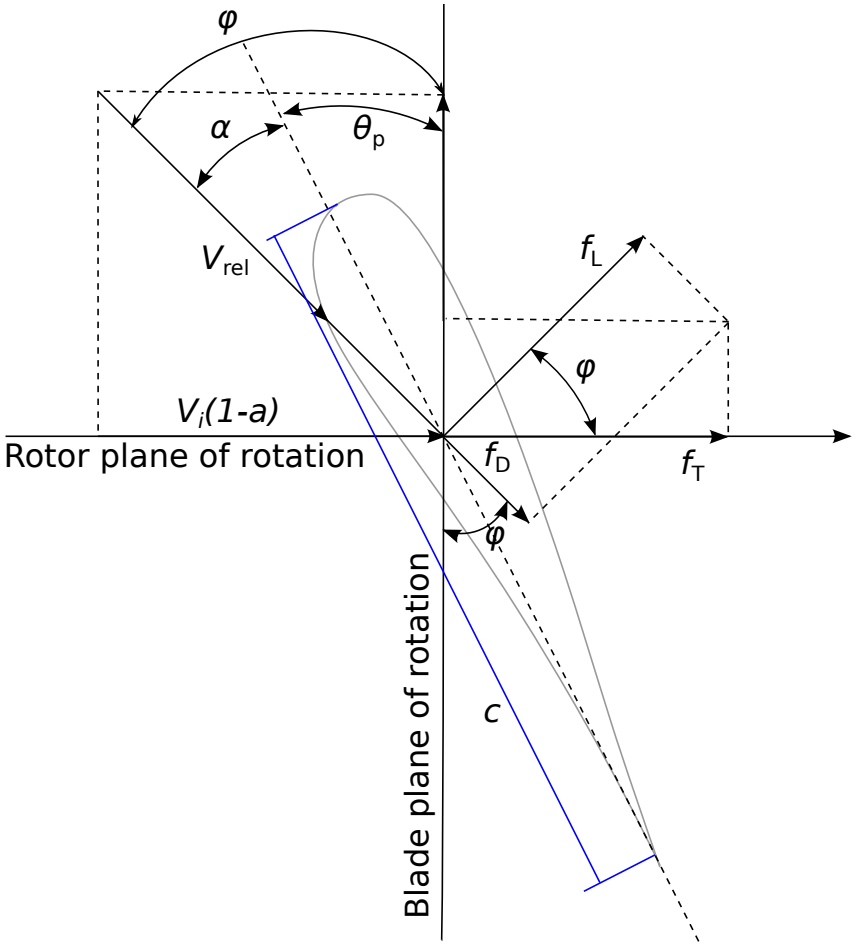

Figure 4.2: Forces acting on a blade element, [Bianchi et al., 2007].

Where:

a	is the interference factor	[H]
$V_{\mathrm{rel}}(t)$	is the relative velocity of the wind	[m/s]
$V_i(t)(1-a)$	is the horizontal wind velocity onto the blades	[m/s]
$\alpha(t)$	is the angle of attack	[°]
φ (t)	is the angle of the relative wind	[°]
$\theta_{\mathrm{p}}(t)$	is the pitch angle	[°]
$f_{\mathrm{L}}(t)$	is the lift force	[N]
$f_{\mathrm{D}}(t)$	is the drag force	[N]
$f_{\mathrm{T}}(t)$	is the normal force contributing to the force of thrust	[N]
c	is the chord length	[m]

The lift force coefficient is perpendicular to the relative wind, thus the lift coefficient is given as:

$$C_{\mathrm{L}}(t) = \frac{f_{\mathrm{L}}(t)}{\frac{1}{2}\rho A V_{\mathrm{rel}}^2(t)} \qquad [\cdot] \quad (4.1)$$

Where:

A	is the area of the disc ($A = \pi R^2$)	[m^2]
ρ	is the density of the air	[$\mathrm{kg/m}^3$]

The drag force is parallel to the relative wind and its coefficient is given as:

$$C_{\mathrm{D}}(t) = \frac{f_{\mathrm{D}}(t)}{\frac{1}{2}\rho A V_{\mathrm{rel}}^2(t)} \qquad [\cdot] \quad (4.2)$$

These force coefficients are functions of the angle of attack, lift and drag force. If the lift force decreases, the drag force increases, thus both forces are dependent on each other.
Due to the forces acting on the blades, a pressure difference from one side of the airfoil to the other produces a lift force. To further investigate how these aerodynamic forces affect the mechanical parts of the turbine, the blade element moment theory approach is used. These forces are noted in Figure 4.2, from which the following equations are derived:

$$\varphi(t) = \theta_{\mathrm{p}}(t) + \alpha(t) \qquad [^\circ] \quad (4.3)$$

$$f_{\mathrm{L}}(t) = \frac{1}{2}\rho C_{\mathrm{L}}(\alpha(t)) c V_{\mathrm{rel}}^2(t) \qquad [N] \quad (4.4)$$

$$f_{\mathrm{D}}(t) = \frac{1}{2}\rho C_{\mathrm{D}}(\alpha(t)) c V_{\mathrm{rel}}^2(t) \qquad [N] \quad (4.5)$$

$$f_{\mathrm{T}}(t) = f_{\mathrm{L}}(t)\cos(\varphi(t)) + f_{\mathrm{D}}(t)\sin(\varphi(t)) \qquad [N] \quad (4.6)$$

$$f_{\mathrm{Q}}(t) = f_{\mathrm{L}}(t)\sin(\varphi(t)) - f_{\mathrm{D}}(t)\cos(\varphi(t)) \qquad [N] \quad (4.7)$$

Note that by increasing the drag force, the torque decreases which results in a power reduction of the turbine. At the same time this causes an increase of the thrust force, leading to more wear on the rotor. The piecewise thrust force is given by:

$$f_{\mathrm{T}}(t) = \frac{1}{2}\rho c V_{\mathrm{rel}}^2(t)[C_{\mathrm{L}}(t)\cos(\varphi(t)) + C_{\mathrm{D}}(t)\sin(\varphi(t))] \qquad [N] \quad (4.8)$$

By integrating along the surface of the blade the total force is given:

$$F_{\mathrm{T}}(t) = \frac{1}{2}\rho\pi R^2 V_i^2(t) C_{\mathrm{t}}(\lambda(t), \theta_{\mathrm{p}}(t)) \qquad [N] \quad (4.9)$$

The piecewise force of torque on the blade, is given by multiplying the piecewise force of thrust by the radius of the rotor:

$$f_{\mathrm{Q}}(t) = f_{\mathrm{T}}(t) R \quad (4.10)$$

$$f_{\mathrm{Q}}(t) = \frac{1}{2}\rho c V_{\mathrm{rel}}^2(t)[C_{\mathrm{L}}(t)\sin(\varphi(t)) - C_{\mathrm{D}}(t)\cos(\varphi(t))] R \qquad [N] \quad (4.11)$$

By integrating along the surface of the blade, the total force of torque is given:

$$F_{\mathrm{Q}}(t) = \frac{1}{2}\rho\pi R^3 V_i^2(t) C_{\mathrm{q}}\left(\lambda(t), \theta_{\mathrm{p}}(t)\right) \qquad [\mathrm{N}] \quad (4.12)$$

with respect to the torque coefficient C_{q}. The power produced by the rotor is given as:

$$P(t) = \frac{1}{2}\rho\pi R^2 V_i^3(t) C_{\mathrm{p}}\left(\lambda(t), \theta_{\mathrm{p}}(t)\right) \qquad [\mathrm{W}] \quad (4.13)$$

where the torque and power coefficients satisfy

$$C_{\mathrm{q}}(t) = \frac{C_{\mathrm{p}}(t)}{\lambda(t)} \qquad [\cdot] \quad (4.14)$$

The torque and power coefficients are explained in Appendix B on page 151.
By expressing the torque as a function of the power developed by the rotor, the following relation is given:

$$F_{\mathrm{T}}(t) = \frac{P(t)}{\omega_r(t)} = \frac{1}{2\omega_{\mathrm{r}}(t)} \rho \pi R^2 V_i^3(t) C_{\mathrm{p}}\left(\lambda(t), \theta_{\mathrm{p}}(t)\right) \quad [\mathrm{N}] \quad (4.15)$$

where $\lambda(t)$ is the tip-speed-ratio defined as

$$\lambda(t) = \frac{\omega_{\mathrm{r}}(t) R}{V(t)} \quad [\cdot] \quad (4.16)$$

where:

R	is the rotor radius	[m]
$\omega_{\mathrm{r}}(t)$	is the angular velocity of the rotor	[rad/s]
$V_i(t)$	is the wind velocity onto the turbine	[m/s]

The nonlinearities of the force of torque $F_{\mathrm{q}}(t)$ and the force of thrust $F_{\mathrm{t}}(t)$, are linearised in Appendix C on page 157, for implementation in the state space model. Following the mechanical models are derived.

5 Mechanical and Structural Models

This chapter provides an overview of the mechanics, structural parts and the power conversion of a wind turbine. The connection between the power converter, mechanical and structural models within the turbine, is displayed in Figure 5.1. By investigating these parts, a linear state space model is derived, for later use in the controller design.

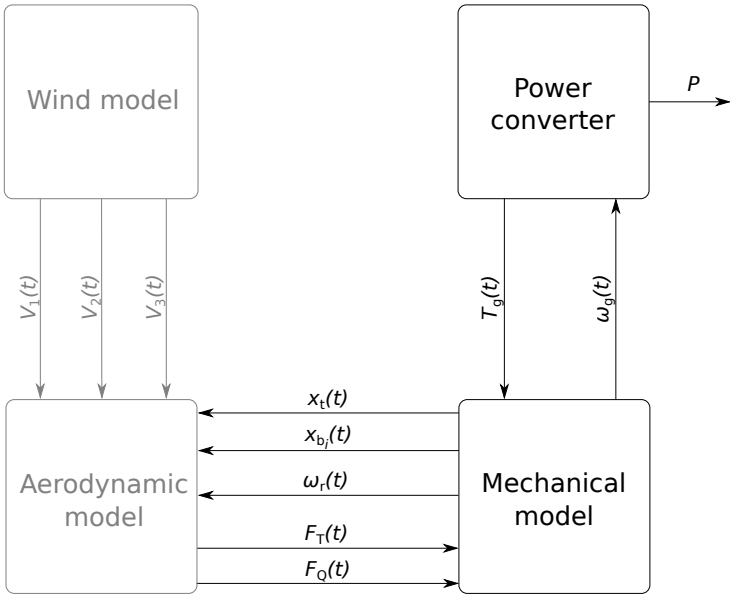

Figure 5.1: An overview of what effect the mechanics, structural parts and the power conversion has on the turbine.

The tower model is elaborated following.

5.1 Tower and Blade Modeling

As the wind exerts a thrust force on the wind turbine, the tower begins to oscillate backwards and forwards, from its initial position. The displacement and velocity, noted by x_t and $\dot{x}_t$ respectively, depend on the spring and damping constants of the tower, which is modeled as a second order mass-spring-damper. The force exerted by the wind on the tower is $F_{T,t}(t)$.

$$F_{T,t}(t) = M_t\ddot{x}_t(t) + B_t\dot{x}_t(t) + K_t x_t(t) \quad [\text{N}] \quad (5.1)$$

Where:

$F_{\mathrm{T,t}}(t)$	is the force of thrust acting on the tower	[N]
M_{t}	is the tower mass	[kg]
B_{t}	is the tower damping constant	[N/(m/s)]
K_{t}	is the spring constant	[N/m]

It is important to consider the backward motion of the tower, relative to the wind velocity. This motion induces a decrease in the wind velocity, and increases wind velocity when moving forward. Thus the wind velocity at the rotor is also influenced by the tower displacement as noted in the following equation:

$$V_{\mathrm{rel}}(t) = V_{\mathrm{H}}(t) - \dot{x}_{\mathrm{t}}(t) \quad [\mathrm{m/s}] \quad (5.2)$$

Where:

$V_{\mathrm{rel}}(t)$	is the relative wind velocity	[m/s]
$V_{\mathrm{H}}(t)$	is the horizontal wind velocity	[m/s]

The tower dynamics is modeled as a displacement in the direction parallel to the horizontal wind velocity, also known as fore-aft. In addition to the forces applied in the fore-aft direction, the blades are also contributing to the displacement of the tower. These are also modeled as mass-spring-damper systems. The forces acting on the blades and the tower are displayed in Figure 5.2.

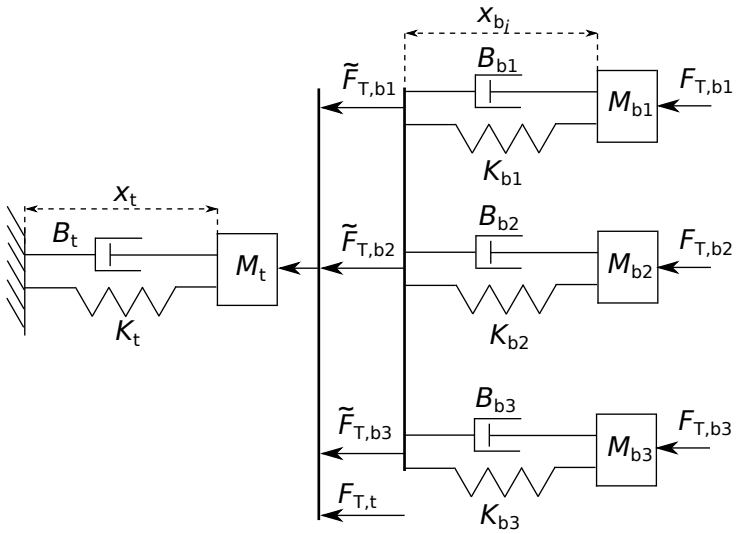

Figure 5.2: Tower bending affected by the thrust force, $F_{\mathrm{T,t}}$ and $F_{\mathrm{T,b}i}$, applied on the tower and each individual blade. $\tilde{F}_{\mathrm{T,b}i}$ are the resulting forces from the blade i onto the tower.

The initial position of the blades, according to the x-axis (fore-aft direction), is set with respect to the initial position of the tower. If a force is applied on one of the blades, a resulting blade deflection, $x_{\mathrm{b}i}(t) - x_{\mathrm{t}}(t)$, is given. According to these dynamics a model for the tower and blades is derived:

$$F_{\mathrm{b}i}(t) = M_{\mathrm{b}i}\ddot{x}_{\mathrm{b}i}(t) + B_{\mathrm{b}i}(\dot{x}_{\mathrm{b}i}(t) - \dot{x}_{\mathrm{t}}(t)) + K_{\mathrm{b}i}(x_{\mathrm{b}i}(t) - x_{\mathrm{t}}(t)) \quad [\mathrm{N}] \quad (5.3)$$

Isolating the acceleration of the blades, $\ddot{x}_{\mathrm{b}i}(t)$, from Equation 5.3, results in:

$$\ddot{x}_{\mathrm{b}i}(t) = \frac{F_{\mathrm{b}i}(t) - B_{\mathrm{b}i}(\dot{x}_{\mathrm{b}i}(t) - \dot{x}_{\mathrm{t}}(t)) - K_{\mathrm{b}i}(x_{\mathrm{b}i}(t) - x_{\mathrm{t}}(t))}{M_{\mathrm{b}i}} \quad \left[\mathrm{m/s^2}\right] \quad (5.4)$$

When deriving Equation 5.4 according to Figure 5.2, the following representation of the tower and blades equation is obtained:

$$F_{\mathrm{T,t}}(t) + \tilde{F}_{\mathrm{T,b1}}(t) + \tilde{F}_{\mathrm{T,b2}}(t) + \tilde{F}_{\mathrm{T,b3}}(t) = M_{\mathrm{t}}\ddot{x}_{\mathrm{t}}(t) + B_{\mathrm{t}}\dot{x}_{\mathrm{t}}(t) + K_{\mathrm{t}}x_{\mathrm{t}}(t) \quad [\mathrm{N}] \quad (5.5)$$

$F_{\mathrm{T,t}}(t)$ is the force applied onto the tower directly, where $\tilde{F}_{\mathrm{T,b}i}(t)$ is the force applied onto the tower as a result of the force affecting the blades. By rewriting the forces as, mass times acceleration, the following equation is derived:

$$\begin{aligned} F_{\mathrm{T,t}}(t) + F_{\mathrm{T,b1}}(t) - B_{\mathrm{b1}}(\dot{x}_{\mathrm{b1}}(t) - \dot{x}_{\mathrm{t}}(t)) - K_{\mathrm{b1}}(x_{\mathrm{b1}}(t) - x_{\mathrm{t}}(t)) \\ + F_{\mathrm{T,b2}}(t) - B_{\mathrm{b2}}(\dot{x}_{\mathrm{b2}}(t) - \dot{x}_{\mathrm{t}}(t)) - K_{\mathrm{b2}}(x_{\mathrm{b2}}(t) - x_{\mathrm{t}}(t)) \\ + F_{\mathrm{T,b3}}(t) - B_{\mathrm{b3}}(\dot{x}_{\mathrm{b3}}(t) - \dot{x}_{\mathrm{t}}(t)) - K_{\mathrm{b3}}(x_{\mathrm{b3}}(t) - x_{\mathrm{t}}(t)) \\ = M_{\mathrm{t}}\ddot{x}_{\mathrm{t}}(t) + B_{\mathrm{t}}\dot{x}_{\mathrm{t}}(t) + K_{\mathrm{t}}x_{\mathrm{t}}(t) \quad [\mathrm{N}] \quad (5.6) \end{aligned}$$

Since the thrust force acting on the tower, $F_{\mathrm{T,t}}$, is small compared to the forces acting on the tower as a result of the forces on the individual blades, $\tilde{F}_{\mathrm{T,b}i}$, it is neglected, which result in the following equation, where the tower acceleration, $\ddot{x}_{\mathrm{t}}$, is isolated:

$$\begin{aligned} \ddot{x}_{\mathrm{t}}(t) = [\, & F_{\mathrm{T,b1}}(t) + F_{\mathrm{T,b2}}(t) + F_{\mathrm{T,b3}}(t) \\ & + (B_{\mathrm{b1}} + B_{\mathrm{b2}} + B_{\mathrm{b3}} - B_{\mathrm{t}})\dot{x}_{\mathrm{t}}(t) + (K_{\mathrm{b1}} + K_{\mathrm{b2}} + K_{\mathrm{b3}} - K_{\mathrm{t}})x_{\mathrm{t}}(t) \\ & - (B_{\mathrm{b1}}\dot{x}_{\mathrm{b1}}(t) + K_{\mathrm{b1}}x_{\mathrm{b1}}(t) + B_{\mathrm{b2}}\dot{x}_{\mathrm{b2}}(t) + K_{\mathrm{b2}}x_{\mathrm{b2}}(t) + B_{\mathrm{b3}}\dot{x}_{\mathrm{b3}}(t) + K_{\mathrm{b3}}x_{\mathrm{b3}}(t))]\,/M_{\mathrm{t}} \quad \left[\mathrm{m/s^2}\right] \quad (5.7) \end{aligned}$$

5.2 Strain Gauge

The blade dynamics are noted in the previous section where a model for the tower and blades were derived. The flap wise displacement, noted $x_{\mathrm{b}i}$, is used as the blade displacement for the strain gauges.

5.3 Pitch Actuator

The pitch actuators are modeled as a first order system with constraints for the pitch rate and maximum and minimum pitch angles, noted in Table D.2 on page 163. The reference pitch angle is given by $\theta_{\mathrm{p}i,\,\mathrm{ref}}$, with the time constant τ_θ.

$$\theta_{\mathrm{p}i,\,\mathrm{ref}}(t) = \tau_\theta\dot{\theta}_{\mathrm{p}i}(t) + \theta_{\mathrm{p}i}(t) \quad [^\circ] \quad (5.8)$$

$$\dot{\theta}_{\mathrm{p}i}(t) = \frac{1}{\tau_\theta}\theta_{\mathrm{p}i,\,\mathrm{ref}}(t) - \frac{1}{\tau_\theta}\theta_{\mathrm{p}i}(t) \quad [^\circ] \quad (5.9)$$

5.4 Drivetrain

The drive train is grouped by the *Rotor* and the *Generator*, as depicted in Figure 5.3.

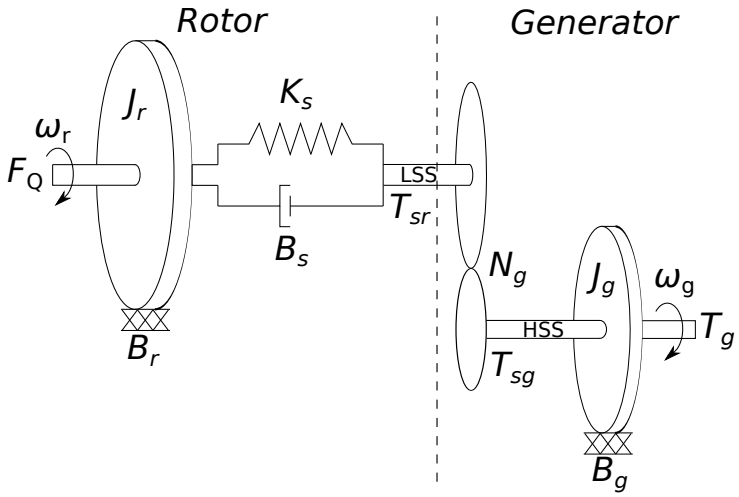

Figure 5.3: Drivetrain model with the low speed shaft shaft (LSS) on the *Rotor* side, the gearing depicted in the middle as the two circles, and the high speed shaft (HSS) on the *Generator* side. The high speed shaft is connected to the generator.

The input of the system is the torque force, $F_{\mathrm{Q}}(t)$, affecting the *Rotor*, by inducing an angular velocity ω_{r} on it. This force is induced onto the low speed shaft, which inertia and friction are given as J_{r} and B_{r} respectively. Because of the large torque from the rotor, a twist is applied on the low speed shaft, thus modeled as a damper B_{s} and spring K_{s} system.

A gearbox, with the gearing ratio N_{g}, is used to get the angular velocity up to speed for the generator to produce power. The generator and gearbox are connected by a high speed shaft. The high speed shaft is noted as rigid, thus its dynamics are not the same as the low speed shaft, and is modeled by an inertia J_{g} with friction B_{g}. A torque $T_{\mathrm{g}}(t)$ can be applied to the generator, which is connected to the high speed shaft, in order to convert the angular velocity to power.

The relation between the *Rotor* and *Generator* is denoted by the two torques, $T_{\mathrm{sr}}(t)$ and $T_{\mathrm{sg}}(t)$, through the gearbox. Using the gathered knowledge, the outputs for the torques are given as:

$$T_{\mathrm{sr}}(t) = B_{\mathrm{s}}\Delta\dot{\Omega}(t) + K_{\mathrm{s}}\Delta\Omega(t) \quad [\mathrm{Nm}] \quad (5.10)$$

$$T_{\mathrm{sg}}(t) = \frac{T_{\mathrm{sr}}(t)}{N_{\mathrm{g}}} \quad [\mathrm{Nm}] \quad (5.11)$$

where the torsional angle $\Delta\Omega(t)$ is given as:

$$\Delta\Omega(t) = \Omega_{\mathrm{r}}(t) - \frac{\Omega_{\mathrm{g}}(t)}{N_{\mathrm{g}}} \quad [\mathrm{rad}] \quad (5.12)$$

$$\Delta\dot{\Omega}(t) = \dot{\Omega}_{\mathrm{r}}(t) - \frac{\dot{\Omega}_{\mathrm{g}}(t)}{N_{\mathrm{g}}} \quad [\mathrm{rad/s}] \quad (5.13)$$

and its velocity is given by:

$$\dot{\Omega}_{\mathrm{r}}(t) = \omega_{\mathrm{r}}(t) \quad [\mathrm{rad/s}] \quad (5.14)$$

$$\dot{\Omega}_{\mathrm{g}}(t) = \omega_{\mathrm{g}}(t) \quad [\mathrm{rad/s}] \quad (5.15)$$

The following equations are derived with respect to Figure 5.3 on the preceding page, giving the angular acceleration for rotor, Equation 5.16, and the generator, Equation 5.17.

$$\dot{\omega}_{\mathrm{r}}(t) = \frac{F_{\mathrm{Q}}(t) - T_{\mathrm{sr}}(t) - B_{\mathrm{r}}\omega_{\mathrm{r}}(t)}{J_{\mathrm{r}}} \quad \left[\mathrm{rad/s^2}\right] \quad (5.16)$$

$$\dot{\omega}_{\mathrm{g}}(t) = \frac{T_{\mathrm{sg}}(t) - T_{\mathrm{g}}(t) - B_{\mathrm{g}}\omega_{\mathrm{g}}(t)}{J_{\mathrm{g}}} \quad \left[\mathrm{rad/s^2}\right] \quad (5.17)$$

By substituting all the equations form 5.10 to 5.15 into Equation 5.16, Equation 5.18, the angular acceleration of the rotor, is derived. By substituting all the equations from 5.10 to 5.15 into Equation 5.17, Equation 5.19, the angular acceleration of the generator, is derived.

$$\dot{\omega}_{\mathrm{r}}(t) = \frac{F_{\mathrm{Q}}(t) - B_{\mathrm{r}}\omega_{\mathrm{r}}(t) - B_{\mathrm{s}}\left(\omega_{\mathrm{r}}(t) - \frac{\omega_{\mathrm{g}}(t)}{N_{\mathrm{g}}}\right) - K_{\mathrm{s}}\Delta\Omega(t)}{J_{\mathrm{r}}} \quad \left[\mathrm{rad/s^2}\right] \quad (5.18)$$

$$\dot{\omega}_{\mathrm{g}}(t) = \frac{\frac{B_{\mathrm{s}}\left(\omega_{\mathrm{r}}(t) - \left(\omega_{\mathrm{g}}(t)/N_{\mathrm{g}}\right)\right) + K_{\mathrm{s}}\Delta\Omega(t)}{N_{\mathrm{g}}} - B_{\mathrm{g}}\omega_{\mathrm{g}}(t) - T_{\mathrm{g}}(t)}{J_{\mathrm{g}}} \quad \left[\mathrm{rad/s^2}\right] \quad (5.19)$$

5.5 Converter

A simple converter model is used to exert a torque T_{g} to the angular velocity of the generator, ω_{g}, resulting in an power output. This is done by the drivetrain transferring potential energy, absorbed by the rotor, to the generator. The converter is modeled as:

$$P(t) = \eta_{\mathrm{g}}\omega_{\mathrm{g}}(t)T_{\mathrm{g}}(t) \quad [\mathrm{W}] \quad (5.20)$$

where:

$P(t)$	is the power	[W]
η_{g}	is the efficiency	$[\cdot]$
$\omega_{\mathrm{g}}(t)$	is the angular velocity of the generator	[rad/s]

As noted in Equation 5.20, nonlinearities are present. For implementation in the state space, linear models are desired, thus a linearisation is performed in Appendix C.3 on page 159. The generator torque $T_g(t)$, from Equation 5.20, is not able to change instantaneously because of the inertia of the rotor. Thus, a model is derived, using a first order linear system, with the desired torque reference $T_{\mathrm{g,ref}}(t)$, and imposed with a time constant τ_T, which gives the following equation:

$$T_{\mathrm{g,\,ref}}(t) = \tau_{\mathrm{T}}\dot{T}_{\mathrm{g}}(t) + T_{\mathrm{g}}(t) \quad [\mathrm{Nm}] \quad (5.21)$$

$$\dot{T}_{\mathrm{g}}(t) = \frac{1}{\tau_T}T_{\mathrm{g,\,ref}}(t) - \frac{1}{\tau_{\mathrm{T}}}T_{\mathrm{g}}(t) \quad [\mathrm{Nm/s}] \quad (5.22)$$

The main models affecting the turbine are explained, and derived for further implementation in a combined linear state space system. The linearisation of the nonlinear models are presented in Appendix C on page 157. Following the neglected model dynamics are elaborated.

5.6 Neglected Model Dynamics

In order to keep the design model as simple as possible, some of the systems dynamics are neglected. Though by neglecting these dynamics, the model should still have the same behavior as the more complex FAST 5 MW model. Subsequently the neglected dynamics with a corresponding reason are mentioned.

- The dynamics of the yawing is neglected.

  - The yawing system of the nacelle is seen as ideal. Thus the rotor is always in an perfect upwind position.

- The blades are seen as stiff edgewise, but able to bend flap-wise, thus resulting in the first mode flap wise dynamics.

  - Though a blade has more degrees of freedom, it is possible to neglect some of these and still obtain a good model. This is elaborated in Section 7 on page 47.

- The transition from the generator to the power grid, is seen as flawless.

  - It is not covered since it is not the project scope , the transition is not seen as important and therefore not modeled.

- The wind profile is seen as static for each time instance.

  - Though a real wind profile contains various wind velocity directions and turbulences, a horizontal wind as described in Section 3 on page 25, is noted sufficient for exciting the turbine with repetitive changes.

- The dynamics of the sensors are seen as fast enough for the system, and are thus not modeled.

On behalf of the investigated turbine dynamics and environmental impacts, a wind turbine model is derived. Following the models are introduced in one state space representation, for later control purpose.

6 COMBINED MODEL

The state space is set up by combining the linear models developed in Part II on page 21 and Appendix C on page 157. These equations are implemented in the general form of a state space model which is considered as:

$$\begin{aligned} \dot{x}(t) &= Ax(t) + Bu(t) + B_{\mathrm{d}}d(t) \\ y(t) &= Cx(t) \end{aligned} \tag{6.1}$$

Where:

A	is the state matrix
B	is the input matrix
C	is the output matrix
$x(t)$	is the state space vector
$u(t)$	is the input vector
$d(t)$	is the unknown input/disturbance vector
$y(t)$	is the output vector

A, B and B_{d} matrices contain the informations given by the equations derived in Section B on page 151 to Section 5 on page 37. C is the output matrix, which determines the output of the system.

The operating points for linearising the parameters are noted with subscript $_0$, as:

$V_{i,0}$	is the operating point for the wind velocity on blade $i = 1,\ 2,\ 3$
$\theta_{\mathrm{p}i,0}$	is the operating point for the pitch of blade $i = 1,\ 2,\ 3$
$\omega_{\mathrm{r},0}$	is the operating point with respect to the angular velocity of the rotor

$Ax(t)$ is given as:

$$
\begin{bmatrix}
\dot{\omega}_\mathrm{r}(t) \\ \dot{\omega}_\mathrm{g}(t) \\ \Delta\dot{\Omega}(t) \\ \dot{T}_g(t) \\ \dot{x}_\mathrm{t}(t) \\ \ddot{x}_\mathrm{t}(t) \\ \dot{x}_{\mathrm{b}1}(t) \\ \ddot{x}_{\mathrm{b}1}(t) \\ \dot{x}_{\mathrm{b}2}(t) \\ \ddot{x}_{\mathrm{b}2}(t) \\ \dot{x}_{\mathrm{b}3}(t) \\ \ddot{x}_{\mathrm{b}3}(t) \\ \dot{\theta}_{\mathrm{p}1}(t) \\ \dot{\theta}_{\mathrm{p}2}(t) \\ \dot{\theta}_{\mathrm{p}3}(t)
\end{bmatrix}
=
\begin{bmatrix}
\mathrm{a}_{1,1} & \frac{B_\mathrm{s}}{N_\mathrm{g}J_\mathrm{r}} & -\frac{K_\mathrm{s}}{J_\mathrm{r}} & 0 & 0 & \mathrm{a}_{1,6} & 0 & \mathrm{a}_{1,8} & 0 & \mathrm{a}_{1,10} & 0 & \mathrm{a}_{1,12} & \mathrm{a}_{1,13} & \mathrm{a}_{1,14} & \mathrm{a}_{1,15} \\
\frac{B_\mathrm{s}}{N_\mathrm{g}J_\mathrm{g}} & \mathrm{a}_{2,2} & \frac{K_\mathrm{s}}{N_\mathrm{g}J_\mathrm{g}} & -\frac{1}{J_\mathrm{g}} & 0 & 0 & 0 & 0 & 0 & 0 & 0 & 0 & 0 & 0 & 0 \\
1 & -\frac{1}{N_\mathrm{g}} & 0 & 0 & 0 & 0 & 0 & 0 & 0 & 0 & 0 & 0 & 0 & 0 & 0 \\
0 & 0 & 0 & -\frac{1}{\tau_\mathrm{T}} & 0 & 0 & 0 & 0 & 0 & 0 & 0 & 0 & 0 & 0 & 0 \\
0 & 0 & 0 & 0 & 1 & 0 & 0 & 0 & 0 & 0 & 0 & 0 & 0 & 0 & 0 \\
0 & 0 & 0 & 0 & \mathrm{a}_{6,5} & \mathrm{a}_{6,6} & -\frac{K_{\mathrm{b}1}}{M_\mathrm{t}} & \mathrm{a}_{6,8} & -\frac{K_{\mathrm{b}2}}{M_\mathrm{t}} & \mathrm{a}_{6,10} & -\frac{K_{\mathrm{b}3}}{M_\mathrm{t}} & \mathrm{a}_{6,12} & \mathrm{a}_{6,13} & \mathrm{a}_{6,14} & \mathrm{a}_{6,15} \\
0 & 0 & 0 & 0 & 0 & 0 & 0 & 1 & 0 & 0 & 0 & 0 & 0 & 0 & 0 \\
0 & 0 & 0 & 0 & \frac{K_{\mathrm{b}1}}{M_{\mathrm{b}1}} & \frac{B_{\mathrm{b}1}}{M_{\mathrm{b}1}} & -\frac{K_{\mathrm{b}1}}{M_{\mathrm{b}1}} & -\frac{B_{\mathrm{b}1}}{M_{\mathrm{b}1}} & 0 & 0 & 0 & 0 & \mathrm{a}_{8,13} & 0 & 0 \\
0 & 0 & 0 & 0 & 0 & 0 & 0 & 0 & 1 & 0 & 0 & 0 & 0 & 0 & 0 \\
0 & 0 & 0 & 0 & \frac{K_{\mathrm{b}2}}{M_{\mathrm{b}2}} & \frac{B_{\mathrm{b}2}}{M_{\mathrm{b}2}} & 0 & 0 & -\frac{K_{\mathrm{b}2}}{M_{\mathrm{b}2}} & -\frac{B_{\mathrm{b}2}}{M_{\mathrm{b}2}} & 0 & 0 & 0 & \mathrm{a}_{10,14} & 0 \\
0 & 0 & 0 & 0 & 0 & 0 & 0 & 0 & 0 & 0 & 0 & 1 & 0 & 0 & 0 \\
0 & 0 & 0 & 0 & \frac{K_{\mathrm{b}3}}{M_{\mathrm{b}3}} & \frac{B_{\mathrm{b}3}}{M_{\mathrm{b}3}} & 0 & 0 & 0 & 0 & -\frac{K_{\mathrm{b}3}}{M_{\mathrm{b}3}} & -\frac{B_{\mathrm{b}3}}{M_{\mathrm{b}3}} & 0 & 0 & \mathrm{a}_{12,15} \\
0 & 0 & 0 & 0 & 0 & 0 & 0 & 0 & 0 & 0 & 0 & 0 & -\frac{1}{\tau_\theta} & 0 & 0 \\
0 & 0 & 0 & 0 & 0 & 0 & 0 & 0 & 0 & 0 & 0 & 0 & 0 & -\frac{1}{\tau_\theta} & 0 \\
0 & 0 & 0 & 0 & 0 & 0 & 0 & 0 & 0 & 0 & 0 & 0 & 0 & 0 & -\frac{1}{\tau_\theta}
\end{bmatrix}
\begin{bmatrix}
\omega_\mathrm{r}(t) \\ \omega_\mathrm{g}(t) \\ \Delta\Omega(t) \\ T_g(t) \\ x_\mathrm{t}(t) \\ \dot{x}_\mathrm{t}(t) \\ x_{\mathrm{b}1}(t) \\ \dot{x}_{\mathrm{b}1}(t) \\ x_{\mathrm{b}2}(t) \\ \dot{x}_{\mathrm{b}2}(t) \\ x_{\mathrm{b}3}(t) \\ \dot{x}_{\mathrm{b}3}(t) \\ \theta_{\mathrm{p}1}(t) \\ \theta_{\mathrm{p}2}(t) \\ \theta_{\mathrm{p}3}(t)
\end{bmatrix}
\tag{6.2}
$$

$$
\begin{aligned}
\mathrm{a}_{1,1} &= -\left(\frac{B_\mathrm{s}+B_\mathrm{r}}{J_\mathrm{r}}\right) + \frac{1}{J_\mathrm{r}}\left.\frac{\partial F_\mathrm{Q}}{\partial \omega_\mathrm{r}}\right|_{\omega_{\mathrm{r},0}} & \mathrm{a}_{1,6} &= -\frac{1}{J_\mathrm{r}}\cdot\left(\left.\frac{\partial F_\mathrm{Q}}{\partial V_1}\right|_{V_{1,0}} + \left.\frac{\partial F_\mathrm{Q}}{\partial V_2}\right|_{V_{2,0}} + \left.\frac{\partial F_\mathrm{Q}}{\partial V_3}\right|_{V_{3,0}}\right)\\
\mathrm{a}_{1,8} &= \frac{1}{J_\mathrm{r}}\left.\frac{\partial F_\mathrm{Q}}{\partial V_1}\right|_{V_{1,0}} & \mathrm{a}_{1,10} &= \frac{1}{J_\mathrm{r}}\left.\frac{\partial F_\mathrm{Q}}{\partial V_2}\right|_{V_{2,0}}\\
\mathrm{a}_{1,12} &= \frac{1}{J_\mathrm{r}}\left.\frac{\partial F_\mathrm{Q}}{\partial V_3}\right|_{V_{3,0}} & \mathrm{a}_{1,13} &= \frac{1}{J_\mathrm{r}}\left.\frac{\partial F_\mathrm{Q}}{\partial \theta_{\mathrm{p}1}}\right|_{\theta_{\mathrm{p}1,0}}\\
\mathrm{a}_{1,14} &= \frac{1}{J_\mathrm{r}}\left.\frac{\partial F_\mathrm{Q}}{\partial \theta_{\mathrm{p}2}}\right|_{\theta_{\mathrm{p}2,0}} & \mathrm{a}_{1,15} &= \frac{1}{J_\mathrm{r}}\left.\frac{\partial F_\mathrm{Q}}{\partial \theta_{\mathrm{p}3}}\right|_{\theta_{\mathrm{p}3,0}}\\
\mathrm{a}_{2,2} &= -\left(\frac{B_\mathrm{s}+B_\mathrm{g}N_\mathrm{g}^2}{N_\mathrm{g}^2 J_\mathrm{g}}\right) & \mathrm{a}_{6,5} &= \frac{-K_\mathrm{t}+K_{\mathrm{b}1}+K_{\mathrm{b}2}+K_{\mathrm{b}3}}{M_\mathrm{t}}\\
\mathrm{a}_{6,6} &= \frac{-B_\mathrm{t}+B_{\mathrm{b}1}+B_{\mathrm{b}2}+B_{\mathrm{b}3}}{M_\mathrm{t}} & \mathrm{a}_{6,8} &= -\frac{B_{\mathrm{b}1}}{M_\mathrm{t}} - \frac{1}{M_\mathrm{t}}\left.\frac{\partial F_{\mathrm{T},\,\mathrm{b}1}}{\partial V_1}\right|_{V_{1,0}}\\
\mathrm{a}_{6,10} &= -\frac{B_{\mathrm{b}2}}{M_\mathrm{t}} - \frac{1}{M_\mathrm{t}}\left.\frac{\partial F_{\mathrm{T},\,\mathrm{b}2}}{\partial V_2}\right|_{V_{2,0}} & \mathrm{a}_{6,12} &= -\frac{B_{\mathrm{b}3}}{M_\mathrm{t}} - \frac{1}{M_\mathrm{t}}\left.\frac{\partial F_{\mathrm{T},\,\mathrm{b}3}}{\partial V_3}\right|_{V_{3,0}}\\
\mathrm{a}_{6,13} &= \frac{1}{M_\mathrm{t}}\left.\frac{\partial F_{\mathrm{T},\mathrm{b}1}}{\partial \theta_{p1}}\right|_{\theta_{p1,0}} & \mathrm{a}_{6,14} &= \frac{1}{M_\mathrm{t}}\left.\frac{\partial F_{\mathrm{T},\mathrm{b}2}}{\partial \theta_{p2}}\right|_{\theta_{p2,0}}\\
\mathrm{a}_{6,15} &= \frac{1}{M_\mathrm{t}}\left.\frac{\partial F_{\mathrm{T},\mathrm{b}3}}{\partial \theta_{p3}}\right|_{\theta_{p3,0}} & \mathrm{a}_{8,13} &= \frac{1}{M_{\mathrm{b}1}}\left.\frac{\partial F_{\mathrm{T},\mathrm{b}1}}{\partial \theta_{\mathrm{p}1}}\right|_{\theta_{\mathrm{p}1,0}}\\
\mathrm{a}_{10,14} &= \frac{1}{M_{\mathrm{b}2}}\left.\frac{\partial F_{\mathrm{T},\mathrm{b}2}}{\partial \theta_{\mathrm{p}2}}\right|_{\theta_{\mathrm{p}2,0}} & \mathrm{a}_{12,15} &= \frac{1}{M_{\mathrm{b}3}}\left.\frac{\partial F_{\mathrm{T},\mathrm{b}3}}{\partial \theta_{\mathrm{p}3}}\right|_{\theta_{\mathrm{p}3,0}}
\end{aligned}
$$

$$
Bu(t) = \begin{bmatrix}
0 & 0 & 0 & \frac{1}{\tau_\mathrm{t}} & 0 & 0 & 0 & 0 & 0 & 0 & 0 & 0 & 0 & 0 & 0\\
0 & 0 & 0 & 0 & 0 & 0 & 0 & 0 & 0 & 0 & 0 & 0 & \frac{1}{\tau_\theta} & 0 & 0\\
0 & 0 & 0 & 0 & 0 & 0 & 0 & 0 & 0 & 0 & 0 & 0 & 0 & \frac{1}{\tau_\theta} & 0\\
0 & 0 & 0 & 0 & 0 & 0 & 0 & 0 & 0 & 0 & 0 & 0 & 0 & 0 & \frac{1}{\tau_\theta}
\end{bmatrix}^T
\begin{bmatrix}
T_{\mathrm{g,ref}}(t)\\ \theta_{\mathrm{p}1}(t)\\ \theta_{\mathrm{p}2}(t)\\ \theta_{\mathrm{p}3}(t)
\end{bmatrix}
$$

$$
B_\mathrm{d} d(t) = \begin{bmatrix}
\frac{1}{J_\mathrm{r}}\left.\frac{\partial F_\mathrm{Q}}{\partial V_1}\right|_{V_{1,0}} & \frac{1}{J_\mathrm{r}}\left.\frac{\partial F_\mathrm{Q}}{\partial \mathrm{V}_2}\right|_{V_{2,0}} & \frac{1}{J_\mathrm{r}}\left.\frac{\partial F_\mathrm{Q}}{\partial \mathrm{V}_3}\right|_{V_{3,0}}\\
0 & 0 & 0\\
0 & 0 & 0\\
0 & 0 & 0\\
0 & 0 & 0\\
\frac{1}{M_\mathrm{t}}\left.\frac{\partial F_{\mathrm{T},\mathrm{b}1}}{\partial \mathrm{V}_1}\right|_{V_{1,0}} & \frac{1}{M_\mathrm{t}}\left.\frac{\partial F_{\mathrm{T},\mathrm{b}2}}{\partial \mathrm{V}_2}\right|_{V_{2,0}} & \frac{1}{M_\mathrm{t}}\left.\frac{\partial F_{\mathrm{T},\mathrm{b}3}}{\partial \mathrm{V}_3}\right|_{V_{3,0}}\\
0 & 0 & 0\\
\frac{1}{M_{\mathrm{b}1}}\left.\frac{\partial F_{\mathrm{T},\mathrm{b}1}}{\partial \mathrm{V}_1}\right|_{V_{1,0}} & 0 & 0\\
0 & 0 & 0\\
0 & \frac{1}{M_{\mathrm{b}2}}\left.\frac{\partial F_{\mathrm{T},\mathrm{b}2}}{\partial \mathrm{V}_2}\right|_{V_{2,0}} & 0\\
0 & 0 & 0\\
0 & 0 & \frac{1}{M_{\mathrm{b}3}}\left.\frac{\partial F_{\mathrm{T},\mathrm{b}3}}{\partial \mathrm{V}_3}\right|_{V_{3,0}}
\end{bmatrix}
\begin{bmatrix}
\mathrm{V}_1\\ \mathrm{V}_2\\ \mathrm{V}_3
\end{bmatrix}
$$

The output of the model is composed of:

$$
\begin{bmatrix}
\omega_\mathrm{g}(t) & T_\mathrm{g}(t) & x_\mathrm{t}(t) & x_{\mathrm{b}1}(t) & x_{\mathrm{b}2}(t) & x_{\mathrm{b}3}(t) & \theta_{\mathrm{p}1}(t) & \theta_{\mathrm{p}2}(t) & \theta_{\mathrm{p}3}(t)
\end{bmatrix}^T \tag{6.3}
$$

7 Model Validation

To verify the dynamics of the combined linear model, is compared to the nonlinear NREL 5 MW turbine. This is done by affecting the two models with the same step, and comparing the dynamics of the outputs, which are:

- Angular velocity of the generator.
- Tower dynamics.
- Blade dynamics.

Both models are run without control to ensure no interference from such to affect the verification. The control model, with the sample time of 0.0125 s, has the following operating points:

- Wind velocity at 18 m/s.
- Angular velocity of the generator 122.9 rad/s.
- Tower displacement is 0.09 m.
- Blade displacement is 0.65 m.
- Torque is 43050 Nm.

The input is initiated at zero and is affected by a step of one, as noted in Figure 7.1(a). The nonlinear FAST model is run at 18 m/s and is also affected by a step of one to 19 m/s. The parameters for the control model are matched with those given for the NREL model. The input and outputs of the FAST model are normalised, for comparison.

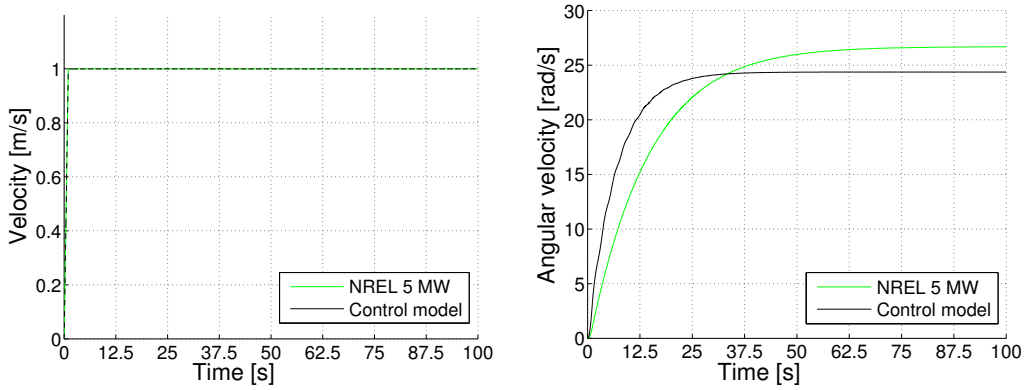

(a) Input step for the control model and the NREL 5 MW model.

(b) Comparison of the angular velocity of the rotor.

Figure 7.1: The input of the parameter estimation and the dynamics of the angular velocity of the rotor.

Following the comparison of the tower and blade dynamics are shown.

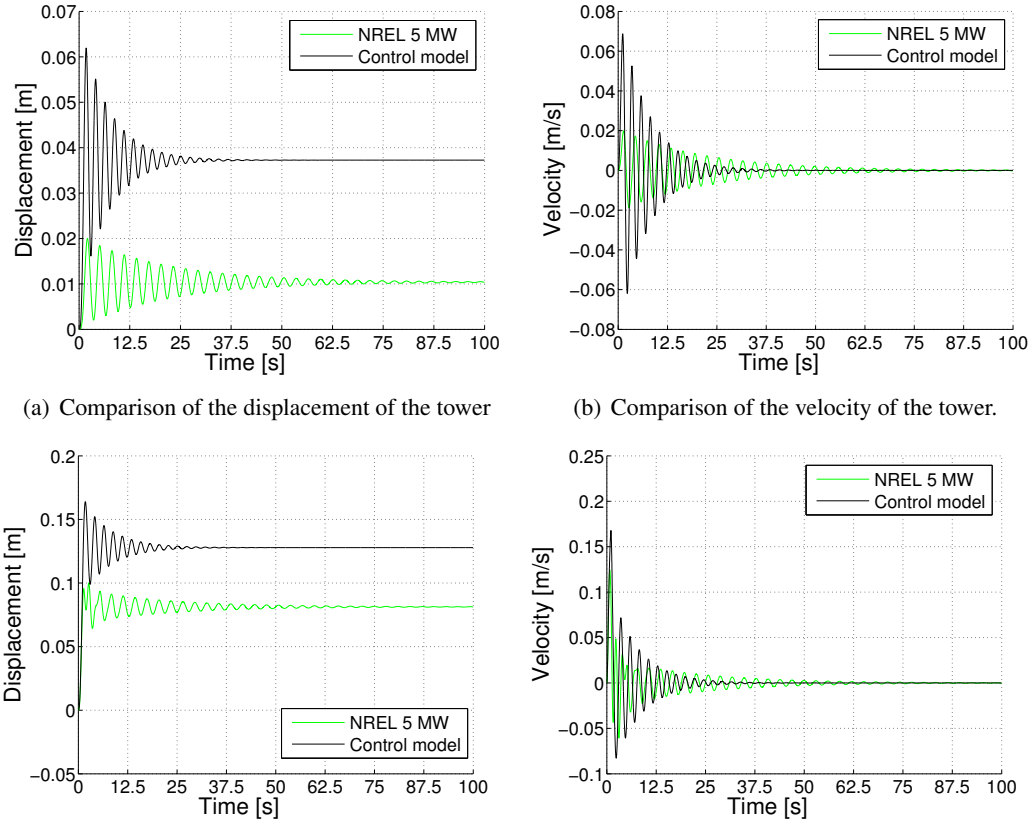

(a) Comparison of the displacement of the tower

(b) Comparison of the velocity of the tower.

(c) Comparison of the displacement of the blades.

(d) Comparison of the velocity of one of the blades.

Figure 7.2: Dynamics of the tower and blade.

When comparing the linearised control model to the nonlinear FAST model, displayed in Figure 7.1 and 7.2, it is clearly noted that both the dynamics and steady states are off, though the steady states for the velocity of the tower and blade are matched, as expected. With thought of control purpose, it is important to have matching dynamics of the system used for control purposes. Thus parameter estimation using *SENSTOOLS* (further elaborated in Appendix D.3 on page 164) with respect to the control model, is performed. *SENSTOOLS* iterates from an initial guess and computes the optimal parameter for matching dynamics of the FAST turbine. The initial guess is made with respect to the NREL FAST model, noted in the following table:

Parameter	Description	Guess	Estimated	Unit
M_{t}	Mass of the tower	3.4746e5	4.1886e6	[Kg]
K_{t}	Stiffness of the tower	1.4400e6	1.8412e7	[N/m]
B_{t}	Damping of the tower	1.4147e4	2.6859e5	[Nm/(rad/s)]
$M_{\mathrm{b}i}$	Mass of one blade	1.7740e4	2.4615e4	[Kg]
$K_{\mathrm{b}i}$	Stiffness of one blade	3.4248e5	4.5684e5	[N/m]
$B_{\mathrm{b}i}$	Damping of one blade	1.0133e5	2.1225e4	[Nm/(rad/s)]
J_{r}	Inertia of the rotor	3.5444e7	7.5321e7	[Kg·m^2]

Through iterations, new parameters are estimated, as noted in the above table. By using these parameters, the dynamics of the angular velocity, tower and blade are depicted in Figure 7.3 to Figure 7.5.

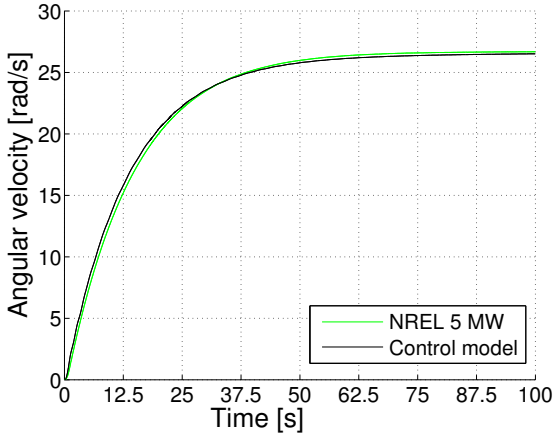

Figure 7.3: Angular velocity of the generator as a result of *SENSTOOLS* parameter estimation.

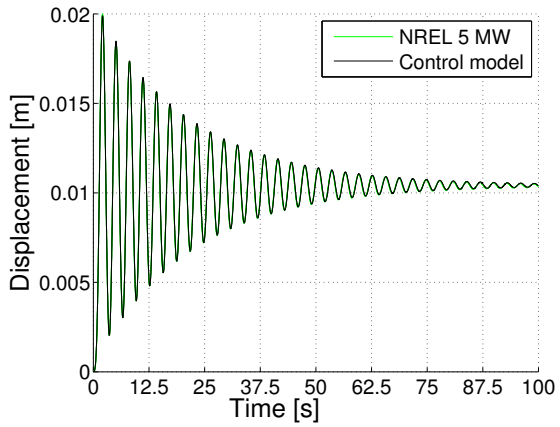

(a) The displacement of the tower with the estimated parameters.

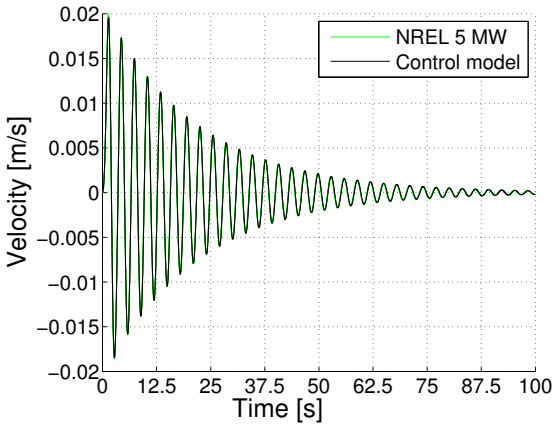

(b) The velocity of the tower with the estimated parameters.

Figure 7.4: Comparison of the tower dynamics with the estimated parameters.

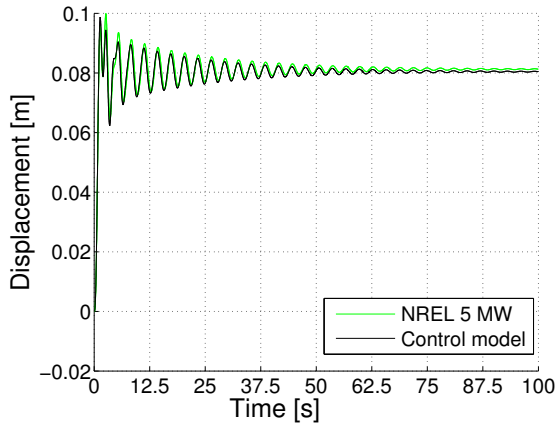

(a) The displacement of the blade with the estimated parameters.

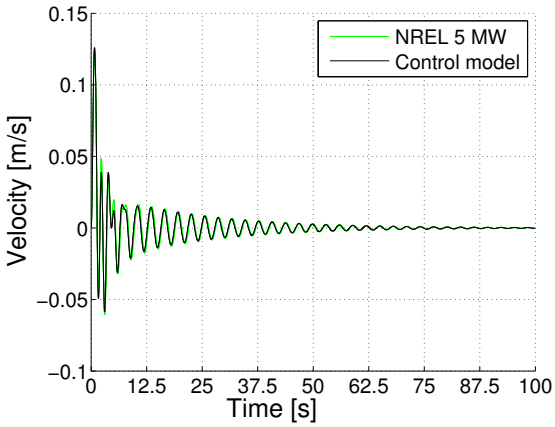

(b) The velocity of the blade with the estimated parameters.

Figure 7.5: Comparison of the blade dynamics with the estimated parameters.

It is noted that the dynamics in Figure 7.4 and Figure 7.5, are well kept. According to the project scope, the turbine should be able to operate in *Region 3*, thus additional investigation in how the dynamics of the linearised model from 12 m/s to 24 m/s, is performed. The same approach as for finding the parameters for one step is used. The deviation of the dynamics is expected to increase when moving away from the linearisation point. To get the best fit, the linearisation point is chosen as the median of the wind velocity of *Region 3*, which is at 18 m/s. The input steps are noted in Figure 7.6(a), where the input for the FAST model is normalised.

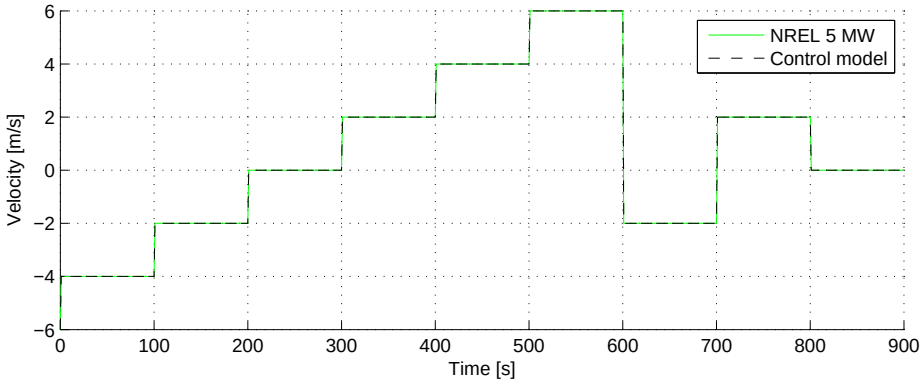

(a) Input for the verification of the control model from 12 m/s to 24 m/s, normalised at 18 m/s.

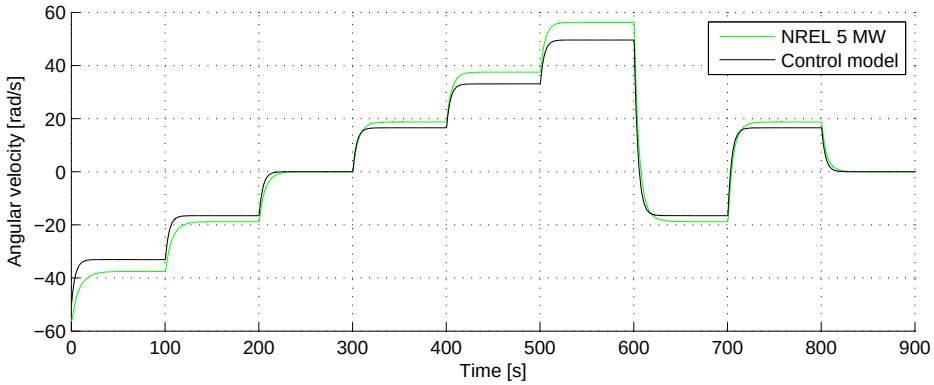

(b) The angular velocity of the generator in *Region 3*.

Figure 7.6: Input and resulting angular velocity

As noted in Figure 7.6(b) the angular velocity of the generator deviates as soon as the input differs from the linearised point, as expected. The difference in amplitude noted in Figure 7.6(b) is caused by the linearised pitch angle of 14.92°. Through tests it is noted that it is possible to get a very close match for either the region from 18 m/s and above or below. However, a trade-off is made to obtain the best model for the entire region, noted in Figure 7.6(b). This may of course have some effect when implementing a controller derived for the linearised model. The controller may not drive the given signal to the same steady state value when using it on the NREL 5 MW wind turbine.
The dynamics for the tower and blades in *Region 3*, are presented in Figure 7.7.

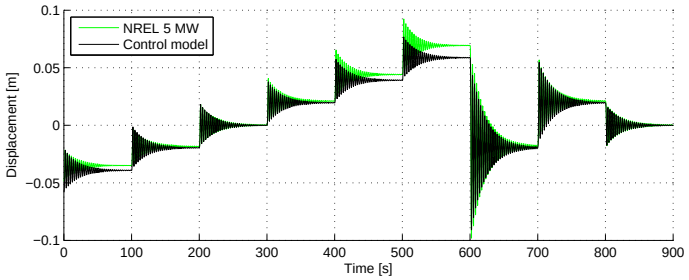

(a) The displacement of the tower for *Region 3*.

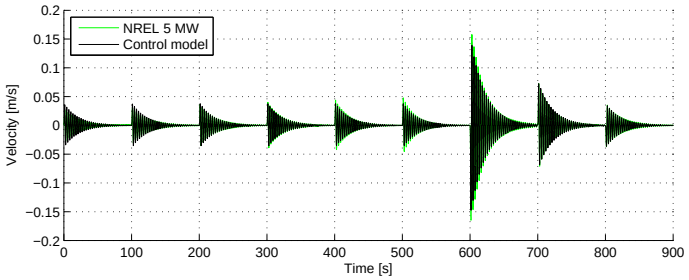

(b) The velocity of the tower for *Region 3*.

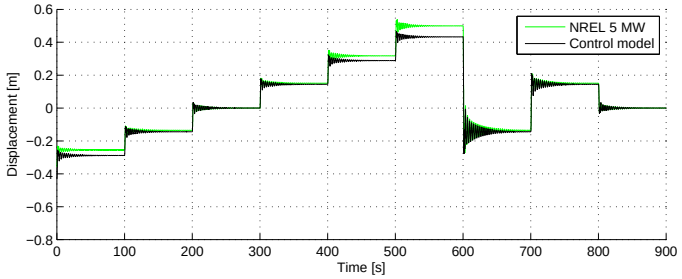

(c) The displacement of the blade for *Region 3*.

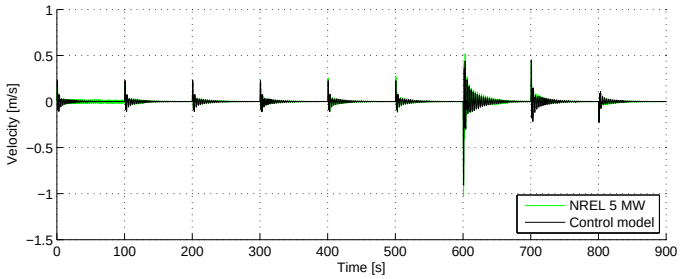

(d) The velocity of the blade for *Region 3*.

Figure 7.7: Tower and blade dynamics for wind velocities from 12 to 24 m/s.

As expected, and noted in Figure 7.7, the steady states are deviating as the dynamics differ from the linearisation point, compared to the those of the nonlinear FAST model. The dynamics are kept to a certain extent, which is the best approximation, with the derived linearised model. The new parameters take their initial guess in the parameters estimated for the one step model.

Parameter	Description	Guess	Estimated	Unit
M_t	Mass of the tower	4.1886e6	1.0893e7	[Kg]
K_t	Stiffness of the tower	1.8412e7	4.8135e7	[N/m]
B_t	Damping of the tower	2.6859e5	7.1574e5	[Nm/(rad/s)]
M_{bi}	Mass of one blade	2.4615e4	6.8464e4	[Kg]
K_{bi}	Stiffness of one blade	4.5684e5	1.2598e6	[N/m]
B_{bi}	Damping of one blade	2.1225e4	5.5937e4	[Nm/(rad/s)]
J_r	Inertia of the rotor	7.5321e7	7.2132e7	[Kg·m^2]

These parameters are implemented for the model and used subsequently. Though the model did not seem to match the nonlinear NREL 5 MW wind turbine to the full extend, it would be interesting to investigate how it behaves in the frequency domain, which is performed following.

7.1 Power Spectrum Density Comparison

It is proven that the linearised model (control model), and the nonlinear FAST 5 MW model do not share full dynamics, thus it is in interest to investigate their dynamic behavior in the frequency domain. It is investigated by power spectrum density. It is expected that the dynamics, as in the time domain, do not match completely. The natural frequency of the states, noted by NREL FAST 5 MW wind turbine, is depicted by a vertical blue line in the following figures. The power spectrum density's are made with respect to the outputs noted in Figure 7.6(b) to Figure 7.7. Figure 7.8 shows the power spectrum density of the angular velocity of the generator.

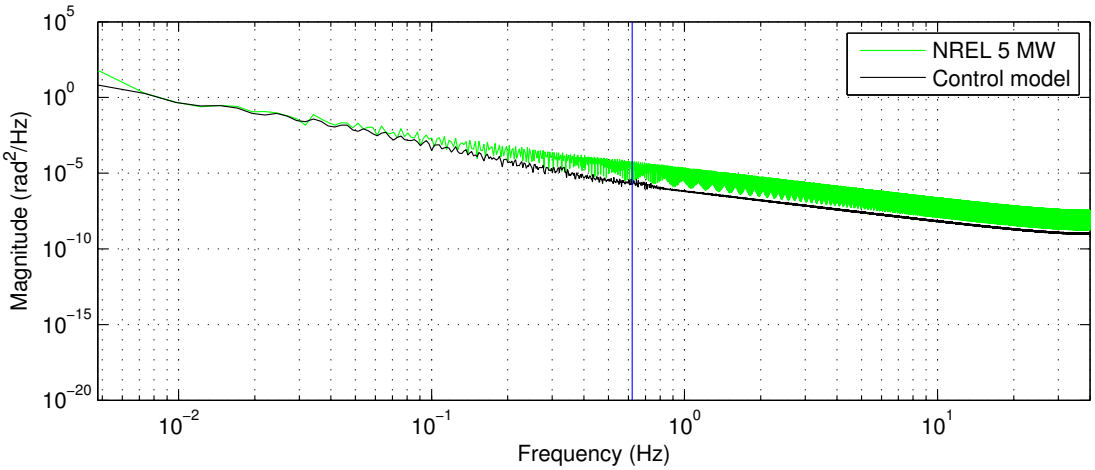

Figure 7.8: The power spectrum density for the angular velocity of the generator for the linear control model compared to the nonlinear NREL model.

It is noted that the NREL model through the whole frequency spectrum has higher dynamics and magnitude compared to the control model. Unmodelled dynamics may be the reason of missing dynamics for the control model. Thus, by implementing a controller, designed for the presented model on the NREL model, may result in different behavior.

The following figures show the displacement of the tower, Figure 7.9(a), and the velocity of the tower, 7.9(b).

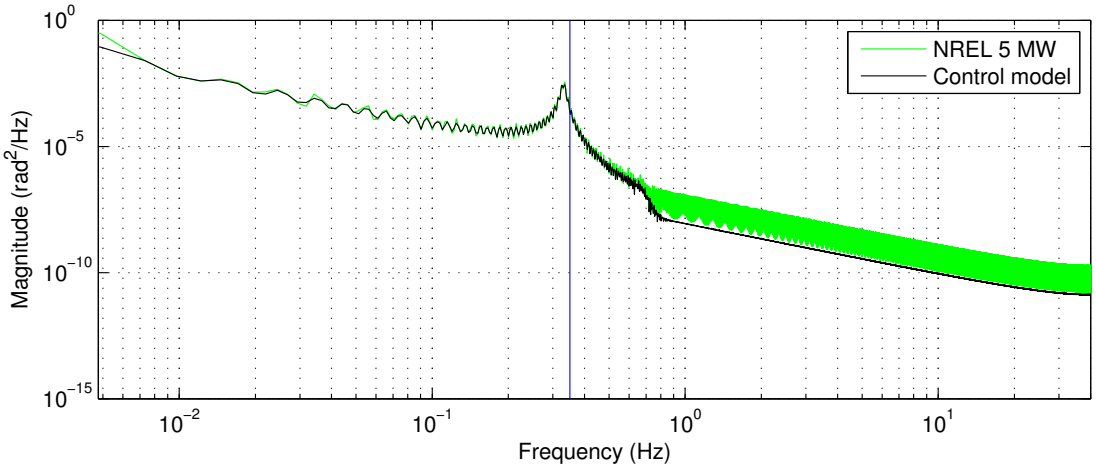

(a) The power spectrum density of the tower displacement of the linear control model compared to the nonlinear FAST model.

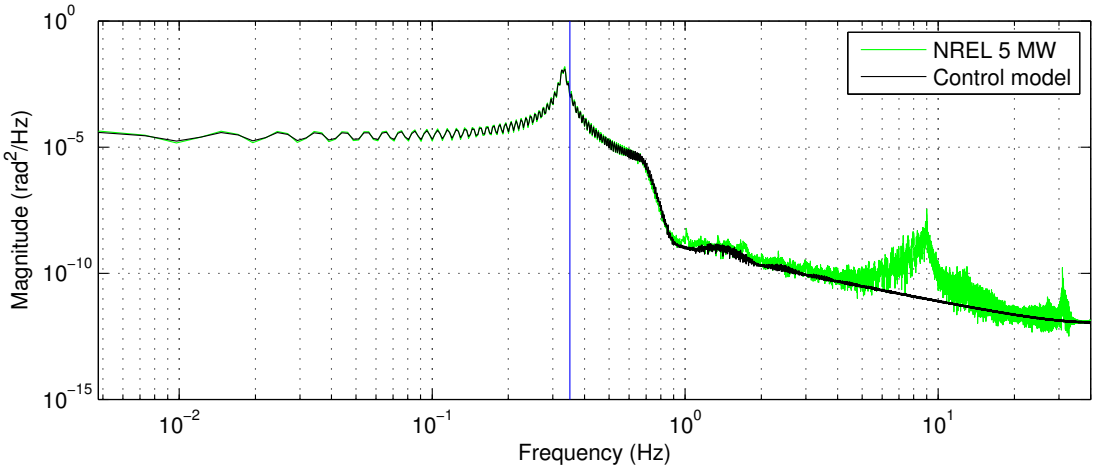

(b) The power spectrum density of the tower velocity of the linear control model compared to the nonlinear FAST model.

Figure 7.9: The power spectrum density of the tower dynamics.

The dynamics of the tower displacement match until approximately 0.5 Hz. This is accepted because the natural frequency of the tower for-aft displacement given by the NREL model is given as 0.32 Hz, thus the fore-aft displacement of the tower is accepted. The same is present when looking at the power spectrum density for the tower velocity in Figure 7.9(b). After 1 Hz, the dynamics are starting to differ. This includes the 0.32 Hz thus the blade velocity is within the limit, and is accepted as an acceptable fit.

The power spectrum density of the blade displacement, Figure 7.10(a), and the blade velocity, Figure 7.10(b) are shown following.

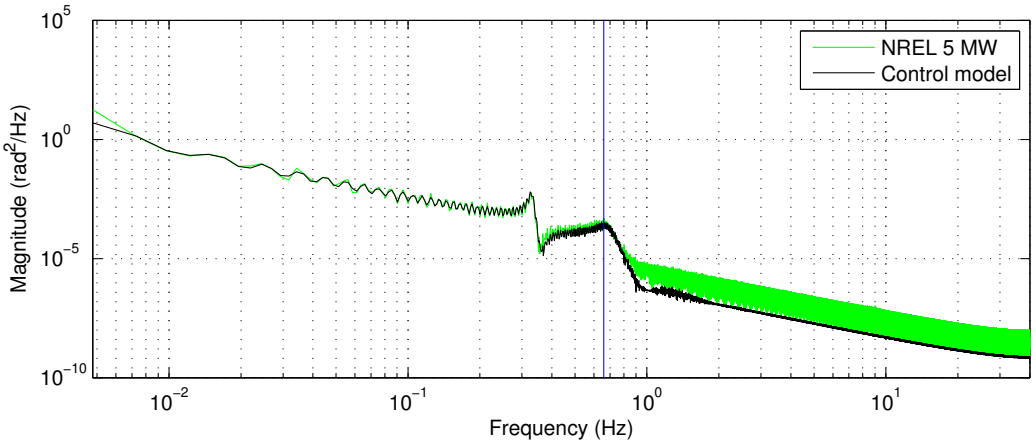

(a) The power spectrum density of the blade displacement of the control model compared to the FAST model.

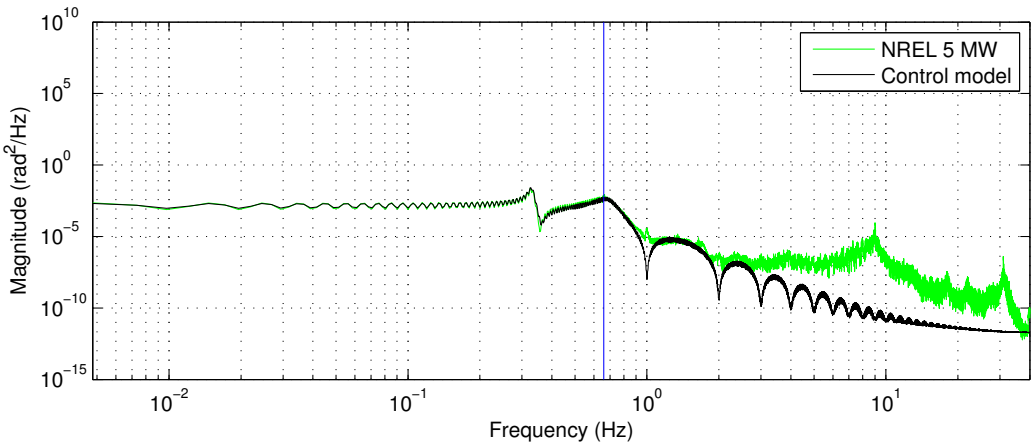

(b) The power spectrum density of the blade velocity of the control model compared to the FAST model.

Figure 7.10: The power spectrum density of the blades.

The natural frequency for the blade fore-aft is given as 0.66 Hz, and it is noted that the frequencies for both the blade displacement and the blade velocity, as seen in Figure 7.10 match very well.

7.1.1 Conclusion

A comparison of the nonlinear FAST NREL 5 MW wind turbine and the derived linear control model, with the same parameters as for the FAST model, was performed. This showed some differences, which lead to parameter estimation using *SENSTOOLS*. The resulting model, with the new parameters, has been inspected using time and frequency domain, where it is noted that the resulting model shows good resemblance to the FAST model, until the natural frequencies for the tower and the blades respectively. Due to the fact that not all the dynamics have been modeled, the angular velocity of the generator does not fully resemble the FAST model. This means that the FAST model is more sensitive to the changes e.g. in wind, than the control model. Thus, when implementing a controller designed for the linearised control model on the nonlinear FAST model, the results may not be the same. This is also present, when considering the frequency in which the controller operates. If the controller is too fast, it may enter the region above the natural frequency of the given structure, where the models do not resemble as well.

8 System Analysis

The system analysis is performed to determine the open-loop stability, controllability and observability of the linearised control model derived in Chapter 6 on page 43. By investigating these subjects a good understanding of the system is given.

8.1 Stability

When determining the stability of the system, the Routh Hurwitz theorem is investigated. It states that if, and only if, the eigenvalues of the state matrix A are strictly in the left half plane of the s-plane, $\mathrm{Re}(\lambda_i) < 0$, the open-loop system is stable [Franklin et al., 2006, p.131]. By using the `MATLAB eig` function, the eigenvalues are found and noted in Appendix E on page 167. It is noted that the Hurwitz theorem holds, thus the system is open-loop stable.

8.2 Controllability and Observability

Due to the fact that the system is open loop stable, it is possible to investigate the gramians for the continuous time system, by solving the two gramian equations stated by [Antoulas, 2005] and [Franklin et al., 2006, p.850] by solving the two Lyapunov equations:

$$AW_\mathrm{c} + W_\mathrm{c}A^T = -BB^T \tag{8.1}$$

$$W_\mathrm{o}A^T + AW_\mathrm{o} = -C^TC \tag{8.2}$$

Where A, B, C, are the: state matrix, input matrix and output matrix respectively, from the linearised state space from Section 6 on page 43. W_c and W_o are the controllability and observability gramians.

If and only if the observability and controllability gramians have full rank respectively, then the system is full controllable and observable. The rank of the controllability gramian is found to be 15, which is the same value as the size of the A-matrix of the linear control model, thus the system is fully controllable. The rank of the observability gramian is of order 15, thus the system is fully observable as well.

8.3 Discretization

The *control model* is discretised to resemble the information rate of the sensors. This is done by using Zero-Order Hold, since it is one of the most common methods for converting continuous time signals to the discrete domain. The sampling rate is set with respect to the NREL FAST 5 MW model at 0.0125 s [Jonkman et al., 2009]. To verify the resemblance of the continuous and the discretised linear system, two bode plots are investigated with respect to the states used for later control purpose. These input-output relations are the torque reference as input, and the torque output, noted in Figure 8.1, and the pitch angle as input and the angular velocity of the generator as output, noted in Figure 8.2.

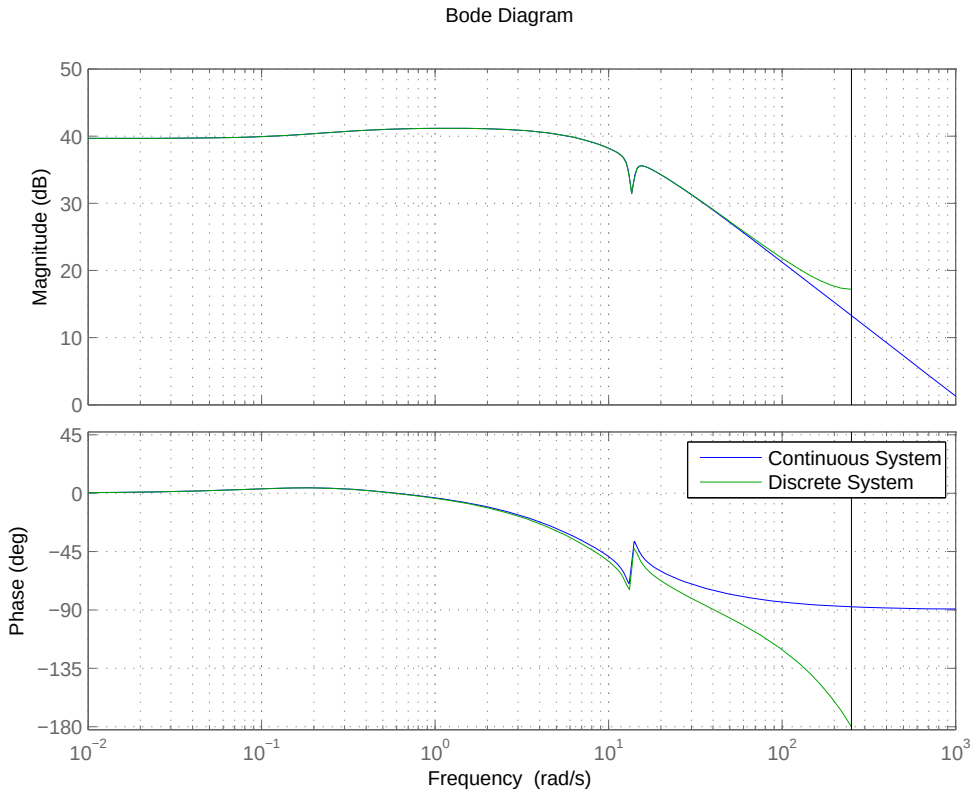

Figure 8.1: Bode Diagram for comparison of the continuous and discretised control model, having the torque reference as input and the torque as output.

It is noted in Figure 8.1, that the frequency response of the discretised and continuous input output relation is the same until the frequency of approximately 14 rad/s is reached. It is further noted that because the magnitude is above 0 dB in the whole frequency spectra, every input is amplified, with respect to the input output relation from the torque reference as input to the torque as output.

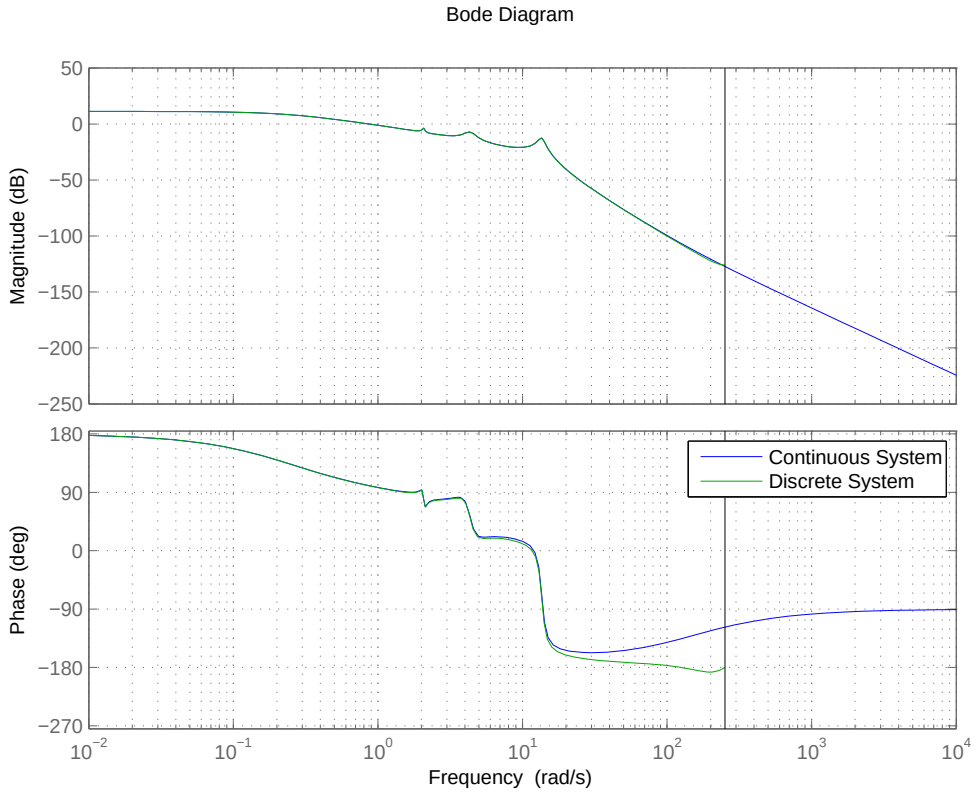

Figure 8.2: Bode Diagram for comparison of the continuous and discretized control model. Having the pitch angle of one blade as input, and the angular velocity of the generator as output.

It is noted in Figure 8.2, that the sampling time of 0.0125 s does not corrupt the model until a frequency of approximately 11 rad/s. This is accepted for further control purpose.

It is concluded that the model is open loop stable, fully controllable and observable, resulting that it is suitable for control purposes, thus leading to the next part. In the following part the control strategies are presented and implemented on the linearised model derived in Chapter 6 on page 43.

Part III

Control and Implementation

This part concerns the design of a controller for the continuous linearised wind turbine model, derived in Part II. As mentioned in the introduction, Section 1.5 on page 12, the project scope is to minimise the repetitive strains, that are affecting the performance of the wind turbine negatively, and the factors which can lead to an early degradation of its components, when operating in *Region 3*. This is further elaborated in the following chapter, where the main problems are presented with appertaining reasons for the control need. Three control approaches are investigated and implemented. Note that the controller strategies are implemented in discrete-time on the continuous linearised model, for testing. The model is further affected with sensor noise, elaborated in Table D.3 on page 166. Zero-Order Hold is used for discretisation. The first approach involves the general control scheme for collective pitch control, as controlling the angular velocity of the generator by means of collective pitch and stabilising the output power by means of reducing or increasing the generator torque. The following two control schemes are for individual pitch control of wind turbines. These schemes are the multi-bladed coordinate transformation, and the repetitive control scheme. When deriving the repetitive control scheme, the discrete time linearised model is used. In the final chapter, a comparison of the two repetitive control schemes and the collective control scheme is given, with a conclusion on their performances. This leads to the acceptance test in Chapter 14.1 on page 123, where the controllers are implemented on the nonlinear FAST 5 MW wind turbine, and the results are elaborated upon.

9 CONTROL INTRODUCTION

The main purpose for implementing control algorithms on wind turbines, is to drive the system to the desired reference values: achieve maximal power output and keep the angular velocity of the generator constant. In addition, the control strategy should ensure minimum wear of the wind turbines structure and mechanical parts. By reducing the loads on the components of the turbine, the damage caused by fatigue of the mechanical parts, is diminished, thus prolonging its lifetime. The mechanical loads that influences the system are split into two types: static loads, which are the result of the interaction between the turbine and the mean wind velocity, and dynamic loads, which are induced by the spatial and temporal distribution of the wind velocity within the area swept by the rotor. The dynamic loads are also present in the form of transient loads (low frequency), caused by turbulence and gusts, or cyclic loads, represented as the relation between the amplitude of stress, and number of cycles a given material is able to withstand before failure occurs. Though it should also be noted, that too severe pitch actuation reduces the lifespan of the actuators as well.

The control scheme, in *Region 3*, is often designed with respect to pitch control, changing the pitch angle with respect to the wind velocity, by pitch to feather, when wind is increased. This is done to obtain the optimal pitch angle, with respect to the wind velocity, resulting in the desired rotor speed, thus leading to a mechanical power output by affecting the angular velocity of the generator with a counter torque. In this scheme, the torque control is added, to eliminate the minor disturbances, which the pitch actuation is not able to accomplish, thus resulting in a more steady power output. Figure 9.1 shows the overall wind turbine control system, with indicators and how these systems affect each other.

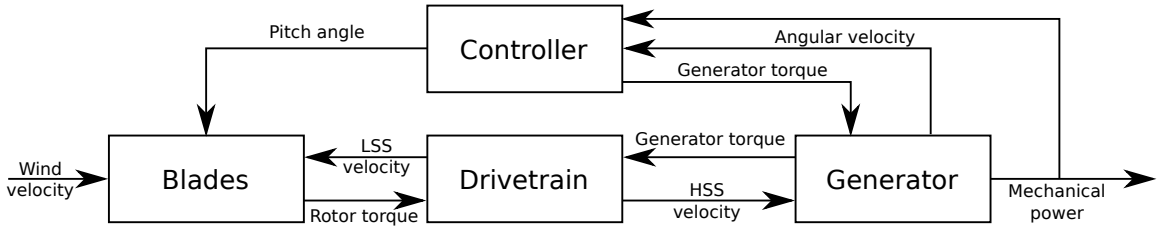

Figure 9.1: The overall wind turbine control scheme with the input signals used for control, angular velocity of the generator and the mechanical power. Further output signals from the controller used for the given actuators, the pitch angle and the generator torque, are noted.

The design of the controller is done with respect to the predefined criteria, set with respect to the overall requirements, described in the Introduction Chapter 2 on page 15, and the operating values for the NREL 5 MW wind turbine in the above rated region presented in Table D.2 on page 163.

1. The angular velocity of the generator is kept constant, at a rated value of 122.9 rad/s, and allowed to deviate $\pm 1\%$.

2. The power output from the wind turbine is kept constant, at a rated value of 5 MW, and allowed to deviate $\pm 1\%$.

3. Minimise the loads occurring on the blades, tower and drivetrain, caused by the repetitive nature of the wind affecting the turbine, with respect to the base line controller of the FAST NREL 5 MW wind turbine.

The deviation limits of $\pm 1\%$, for the angular velocity and the power output, are set as reference only. The limitations regarding the performance of the controllers have been presented with appertaining reasons for control necessity, leading to the control design.

10 KALMAN FILTER

As the noise from the sensors, stated in Table D.3 on page 166, are present in the system, a Kalman filter is implemented for noise filtering and used as estimator for the unmeasured states of the continuous-time linear state-space model, presented in Chapter 6 on page 43. It is of interest to obtain an estimated value of these states ($\Delta\Omega$, $\dot{x}_{\mathrm{t}}$ and $\dot{x}_{\mathrm{b}i}$). This information is further required in order to implement the repetitive control algorithm presented in Section 13.2 on page 92. It is noted that the same output as used for the matrix C of the linear state space model, is also used as the measurable outputs for the nonlinear NREL FAST 5 MW wind turbine. The continuous linear control model is corrupted by noise and rewritten as:

$$\begin{cases} \dot{x}(t) &= Ax(t) + Bu(t) + B_{\mathrm{d}}d(t) \\ y(t) &= Cx(t) + \eta(t) \end{cases} \tag{10.1}$$

where

$\eta(t)$ is white Gaussian noise for the sensors, $\mathcal{N}(0,\sigma)$

In order to design the Kalman filter for the continuous time linear state space system, the discretisation using a Zero-Order Hold method is performed, thus obtaining:

$$\begin{cases} x_{k+1} &= Ax_k + Bu_k + B_{\mathrm{d}}d_k \\ y_k &= Cx_k + \eta_k \end{cases} \tag{10.2}$$

It is noted that it is also of interest to estimate the winds affecting the blades, thus three new states are augmented to the state space model corresponding to the wind velocities on each blade $V1$, $V2$ and $V3$. Following the augmentation is presented with the resulting state space, used to estimate the states and the disturbances.

$$\begin{cases} \begin{bmatrix} x_{k+1} \\ \boldsymbol{V1}_{k+1} \\ \boldsymbol{V2}_{k+1} \\ \boldsymbol{V3}_{k+1} \end{bmatrix} &= \underbrace{A_{\mathrm{KF}} \begin{bmatrix} x_k \\ \boldsymbol{V1}_k \\ \boldsymbol{V2}_k \\ \boldsymbol{V3}_k \end{bmatrix}}_{f_k} + B_{\mathrm{KF}}u_k \\ y_k &= \underbrace{C_{\mathrm{KF}} \begin{bmatrix} x_k \\ \boldsymbol{V1}_k \\ \boldsymbol{V2}_k \\ \boldsymbol{V3}_k \end{bmatrix}}_{g_k} \end{cases} \tag{10.3}$$

Where:

$$A_{\mathrm{KF}} = \begin{bmatrix} A & B_{\mathrm{d}} \\ 0 & I_3 \end{bmatrix} \quad B_{\mathrm{KF}} = \begin{bmatrix} B_{\mathrm{d}} \\ 0 \end{bmatrix} \quad C_{\mathrm{KF}} = I_{18} \tag{10.4}$$

The output matrix, C_{KF}, of state space model, used in the Kalman filter, is chosen as an identity matrix with the size corresponding to the number of states in the system, which is 15, and the 3 new states, corresponding to the wind disturbances affecting the system.

The linear discrete time Kalman filter performances are proven as optimal state estimator by [Haykin, 2001, p.1-10] and [Ogata, 1987, p.878-881]. Thus in the following, the used Kalman filter design is presented.

The initial conditions are defined as the expected value E[·] :

$$\begin{aligned} \hat{x}_0 &= \mathrm{E}[x_o] \\ \Sigma_0 &= \mathrm{E}\left[(x_0 - \mathrm{E}[x_0])(x_0 - \mathrm{E}[x_0])^T\right] \end{aligned}$$

The Kalman filter is divided into two steps: **prediction** and **update**. The prediction step consists of state prediction, states covariance prediction and measurement prediction. The update step consists of measurement covariance prediction, Kalman gain computation, state estimate update and state covariance update. The equations corresponding to the steps are presented following:

PREDICTION STEP

$$\begin{aligned} \hat{x}_{k|k-1} &= A_{\mathrm{KF}}\hat{x}_{k-1|k-1} + B_{\mathrm{KF}}u_{k-1} \\ \Sigma_{k|k-1} &= A_{\mathrm{KF}}\Sigma_{k-1|k-1}A_{\mathrm{KF}}^T + Q_{\mathrm{KF}} \\ \hat{y}_k &= C_{\mathrm{KF}}\hat{x}_{k|k-1} \end{aligned}$$

UPDATE STEP

$$\begin{aligned} K_{\mathrm{KF}} &= \Sigma_{k|k-1}C_{\mathrm{KF}}^T(C_{\mathrm{KF}}\Sigma_{k|k-1}C_{\mathrm{KF}}^T + R_{\mathrm{KF}})^{-1} \\ \hat{x}_{k|k} &= \hat{x}_{k|k-1} + K_{\mathrm{KF}}(y_k - \hat{y}_k) \\ \Sigma_{k|k} &= (I - K_{\mathrm{KF}}C_{\mathrm{KF}})\Sigma_{k|k-1} \end{aligned}$$

Where

$\hat{x}_{k\|k-1}$	is the apriori state estimate.
$\hat{x}_{k-1\|k-1}$	is the aposteriori state estimate.
y_k	is the measurement of the systems sensors.
$\hat{y}_k$	is the estimate of the measurement.
A_{KF}	is the discretised augmented state matrix.
B_{KF}	is the discretised augmented input matrix.
C_{KF}	is the discretised augmented output matrix.
$\Sigma_{k\|k-1}$	is the uncertainty of the estimated state covariance propagation.
$\Sigma_{k-1\|k-1}$	is the updated uncertainty of the covariance propagation.
Q_{KF}	is the state covariance matrix of the Kalman Filter.
R_{KF}	is the measurement covariance matrix of the Kalman Filter.
K_{KF}	is the Kalman gain matrix.

The Kalman filter has two covariance matrices, Q_{KF} and R_{KF}. When $Q_{\mathrm{KF}} > R_{\mathrm{KF}}$, it indicates that the model is more trusted, though if $Q_{\mathrm{KF}} < R_{\mathrm{KF}}$, indicates that the estimates are more trusted. The overall scheme of the Kalman filter is illustrated in Figure 10.1.

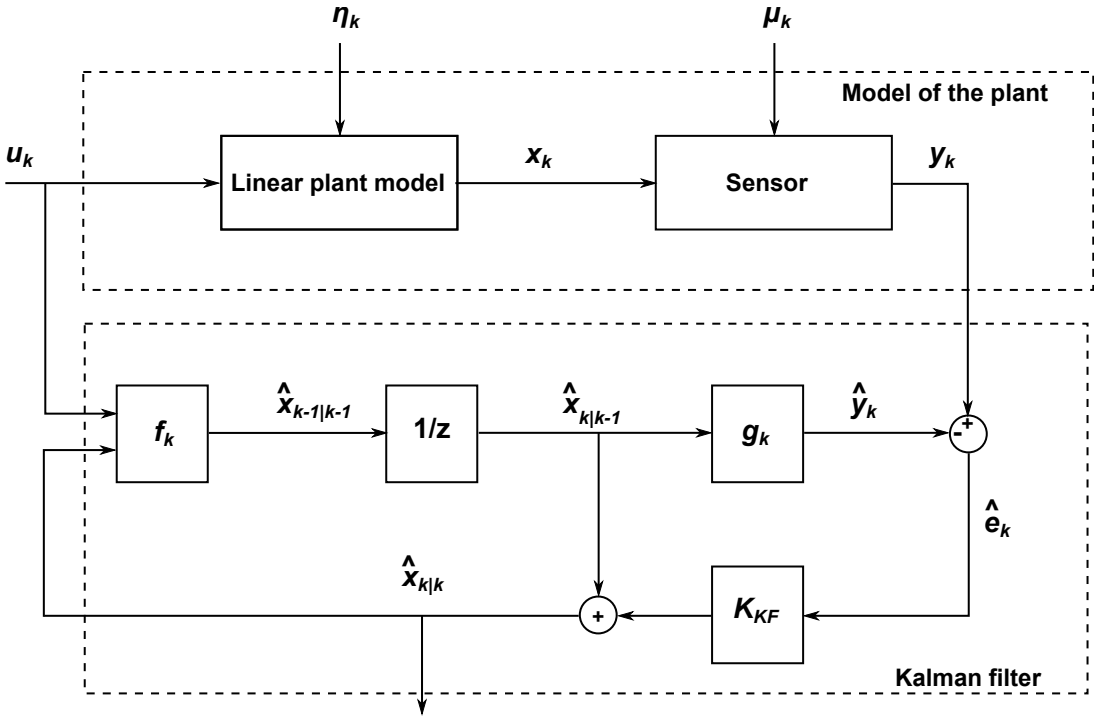

Figure 10.1: Block diagram of a Kalman filter in discrete time.

The output covariance matrix (covariance of the sampled sensor data and true state), R_{KF} is designed with respect to the noise affecting the sensors presented in Appendix D.4 on page 165. For the implementation however, a zero mean white Gaussian noise process, μ_k, is used, with the power corresponding to the ones presented in Appendix D.4 on page 165. The state covariance matrix (covariance between plant and model), Q_{KF}, is considered a tuning parameter. When tuning the state covariance matrix, it is noted that small values lead to slow convergence towards the true states, while large values increase the Kalman gain, resulting in a more sensitive filter. Consequently a compromise needs to be made, in order to obtain proper estimates. The entries of the Q_{KF}, are shown, with the appertaining states.

$$\begin{aligned} Q_{\mathrm{KF}} = diag[&100 \;\; 0.001 \;\; 0.000001 \;\; 0.1 \;\; 0.001 \;\; 10 \;\; 0.001 \;\; 100 \;\; 0.001 \;\; 100 \\ &0.001 \;\; 100 \;\; 0.001 \;\; 0.001 \;\; 0.001 \;\; 100000 \;\; 100000 \;\; 100000] \end{aligned} \tag{10.5}$$

$$\begin{aligned} x_k = [&\omega_g \;\; \omega_r \;\; \Delta\Omega \;\; T_{\mathrm{g}} \;\; x_{\mathrm{t}} \;\; \dot{x}_{\mathrm{t}} \;\; x_{\mathrm{b1}} \;\; \dot{x}_{\mathrm{b1}} \;\; x_{\mathrm{b2}} \;\; \dot{x}_{\mathrm{b2}} \\ &x_{\mathrm{b3}} \;\; \dot{x}_{\mathrm{b3}} \;\; \theta_{\mathrm{p1}} \;\; \theta_{\mathrm{p2}} \;\; \theta_{\mathrm{p3}} \;\; V1 \;\; V2 \;\; V3] \end{aligned} \tag{10.6}$$

The values in the state covariance matrix are relative to the value of the variable. In the case of the first element from Equation 10.5, corresponding to the angular velocity of the rotor (rated value $\omega_r = 1.267$ rad/s), it is noted that the value is high. The second element, corresponding to $\omega_g = 122.9$, has a small value. The reason for these differences are the fact that the angular velocity of the generator, and the one of the rotor, are connected through the drive train. Meaning that ω_g is measured, thus the measurement is considered certain. By doing so, ω_r is allowed to be updated based on the measurements instead of the model. The same is true in the case of the velocities of the tower and blades, which are set as high values

in order to allow the Kalman estimator to use the available measurements in order to estimate the states instead of relying on the model. The last three elements in the Q_{KF} are used for estimation of the states corresponding to the wind disturbances affecting each individual blades. The values are large, due to the fact that the designed wind model is not trusted, as it is a simple model. Thus a high weight is set on the measurements compared to the model. By using the measurements, the wind disturbances are estimated quite well, dependent on how good the measurements are and the level of noise present.
The results of the Kalman state estimator are presented following. In order to determine the accuracy of the estimation, the error between the estimated states and the true states is investigated and presented in Figure 10.2

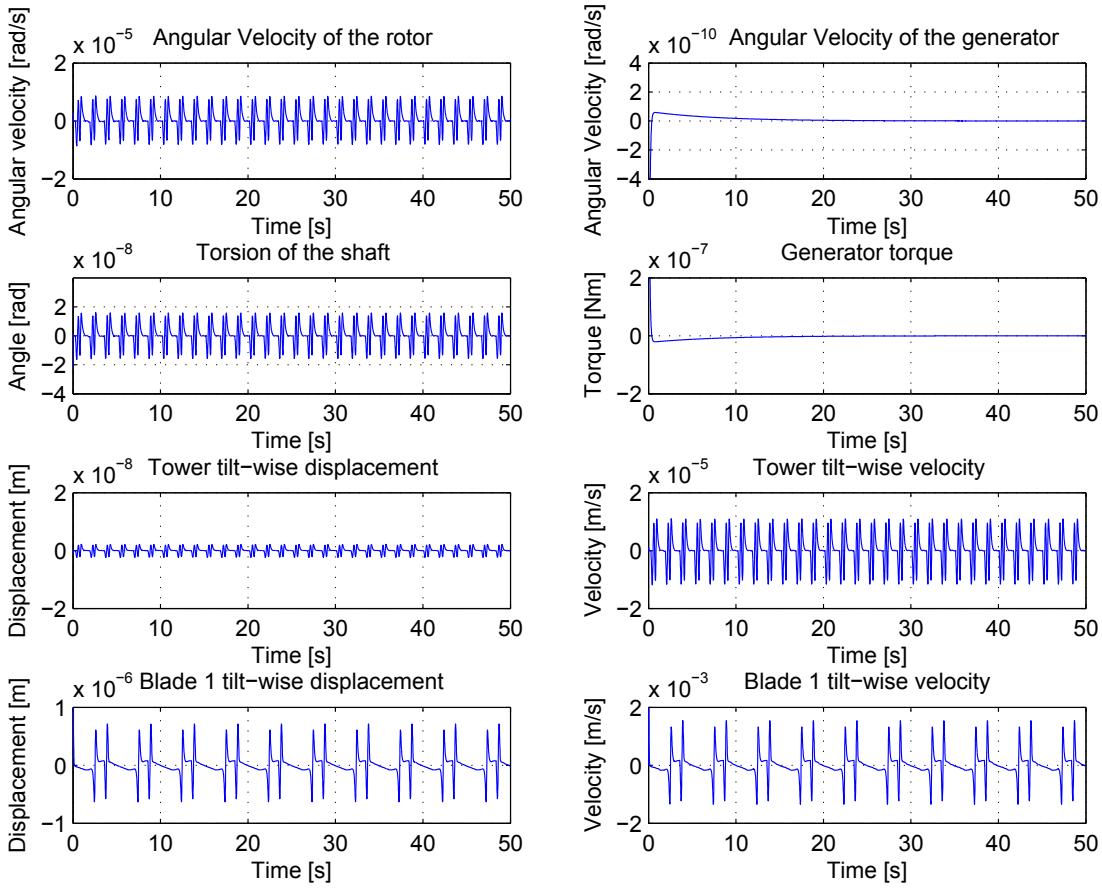

Figure 10.2: Error between the true states of the linear continuous model and the estimated states using Kalman estimator.

The error between the true wind and the estimation of the wind is presented in Figure 10.3.

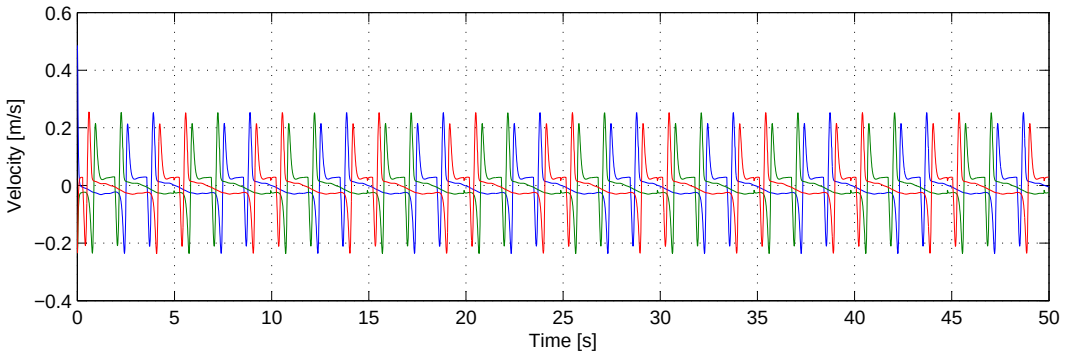

Figure 10.3: Error between the true value of the disturbance (wind velocity) and the estimated disturbance (wind velocity) using Kalman estimator.

Based on the results in the Figures 10.2 and 10.3, the designed Kalman state estimator is capable of estimating the states in presence of sensor noise. Moreover, by augmenting the state space with states corresponding to the disturbances (wind velocities) affecting the system, the Kalman estimator is able to estimate these as well. Even though these estimates are not very accurate, it is considered sufficient.

Throughout the report the Kalman filter is used with respect to this chapter. Following the collective pitch control is elaborated.

11 Collective Pitch Control

In order to keep the angular velocity of the rotor, and the power output at the desired reference values, defined on Page 66, two PI controllers are designed. These are later used in a more complex control scheme where the stabilised closed loop system is needed. The derivation of the PI controllers are explained following. The results are illustrated by figures, generated with respect to the operating value of the given state, though the linearised control model, presented in Chapter 6 on page 43, is operating with small signals.

11.1 Derivation and Implementation

The overall control scheme is depicted in Figure 11.1.

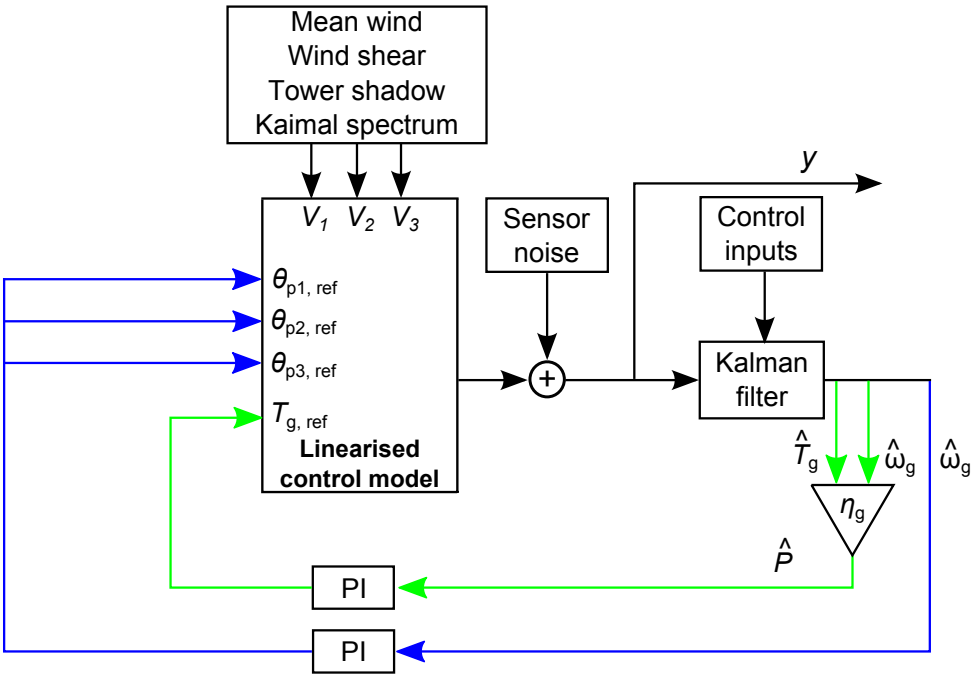

Figure 11.1: Control strategy, using the linearised control model, for controlling the power output, noted by the green line, and the angular velocity, noted by the blue line. The Kalman estimator is used to estimate the states. Its inputs are the control inputs and outputs of the linearised control model.

The wind profile is derived in Chapter 3 on page 25, is composed of wind shear, tower shadow, wake and turbulence. Figure 11.2 displays the linearised wind velocity (at 18 m/s) on each blade. This profile is used throughout the following simulations.

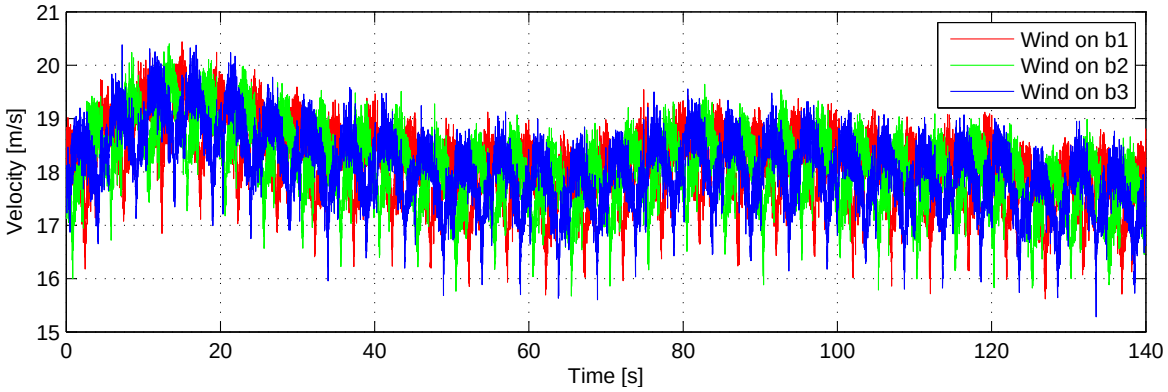

(a) Wind model composed of wind shear, tower shadow, wake and Kaimal filter, used throughout the simulations.

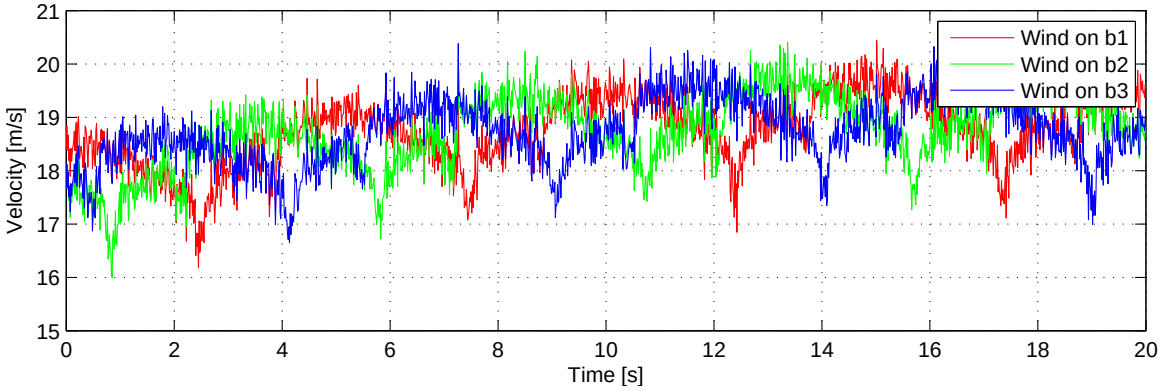

(b) A time-period from 0-20 s of the wind model used throughout the simulations.

Figure 11.2: Wind profile for the collective pitch controller.

Power Control

The feedback loop depicted green, in Figure 11.1, contains the PI controller that maintains the power output constant at 5 MW. The power, $P(t)$, is calculated by multiplying the torque of the generator, $T_g(t)$, with the angular velocity of the generator and with a loss factor η_g. The signal is fed through the PI controller and used as the control input for the torque reference, $T_{g,\,ref}(t)$, in the linearised control model. The controller is designed as a slow controller to avoid overshoots, and thus severe fluctuations. The PI controller has a high integral effect, in order to keep the power constant with respect to the reference value. The proportional gain is small compared to it, though still present in order to drive the deviation of the generator torque to the reference value. The PI gains are derived according to Ziegler-Nichols method, and fine tuned by using Table F.2 on page 171. For further explained see Appendix F on page 169. The derived gains are for $K_p = -0.013$ and for $K_i = -0.13$. Note that the negative gains are due to the physical interpretation: as the output power increases, the generator torque has to be decreased to keep the output power constant and vice-versa.

The closed loop result of the power output is presented in Figure 11.3.

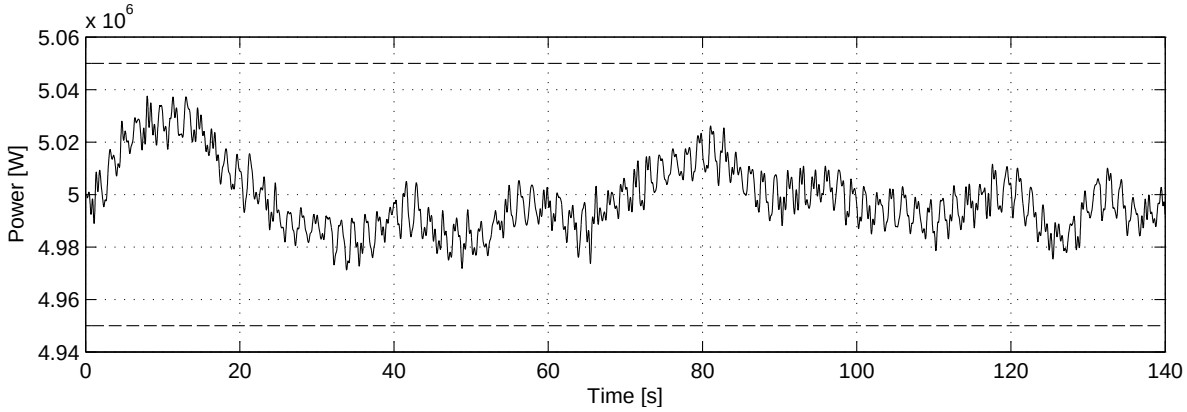

Figure 11.3: Power output of the linearised model controlled by the implemented PI controller. The stippled lines are the boundaries for the $\pm 1\%$, of the operating value of 5 MW.

It is noted that boundaries of $\pm 1\%$ are kept, thus this controller is accepted for further use.

Angular Velocity Control

The angular velocity of the generator, $\omega_g(t)$, is controlled by a PI controller with respect to the pitch angles, $\theta_{p1,\,ref}(t)$, $\theta_{p2,\,ref}(t)$, $\theta_{p3,\,ref}(t)$, corresponding to the respective blades. This scheme is presented by a feedback loop depicted with blue in Figure 11.1. Note that only one control signal is fed to the pitch actuators in the linearised control model, thus this scheme is collective pitch control. By changing the pitch angles, the lift and drag coefficients are altered, which then results in a change in the angular velocity of the generator. The derivation of the controller is elaborated in Appendix F on page 169. The result is presented in Figure 11.4.

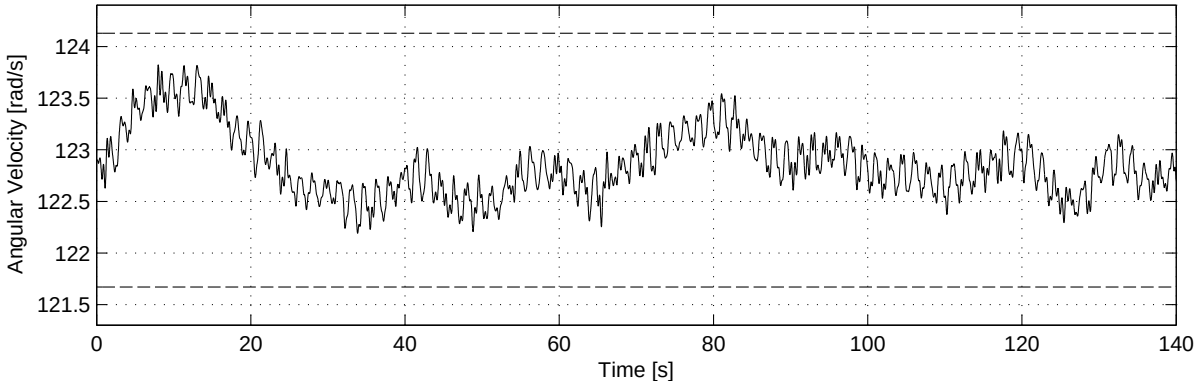

Figure 11.4: Angular velocity of the generator, controlled by a PI controller on the linearised model. The stippled lines are the boundaries of the $\pm 1\%$, for the operating value of 122.9 rad/s.

The PI controller is able to maintain an acceptable steady angular velocity, though the signal from the pitch actuators, presented in Figure 11.5, is similar to the effect, which the wind has on the angular velocity.

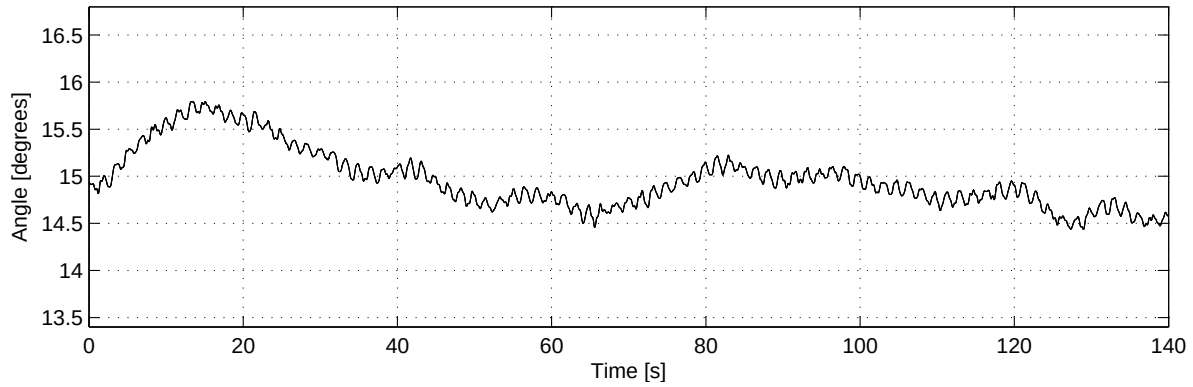

Figure 11.5: Control effort of the implemented collective pitch control strategy on the linearised model.

The gains of the PI controller are $K_\mathrm{p} = 0.01$ and $K_\mathrm{i} = 1.15e-03$. Note the gains of the PI controller are positive, which leads to a physical interpretation: at an increase in the wind velocity, the angular velocity of the generator increases and vice-versa. Thus, in order to compensate for this, the pitch angle has to increase, to drive the angular velocity of the generator to the reference value. This pitch action gives the following blade displacement, noted in Figure 11.6.

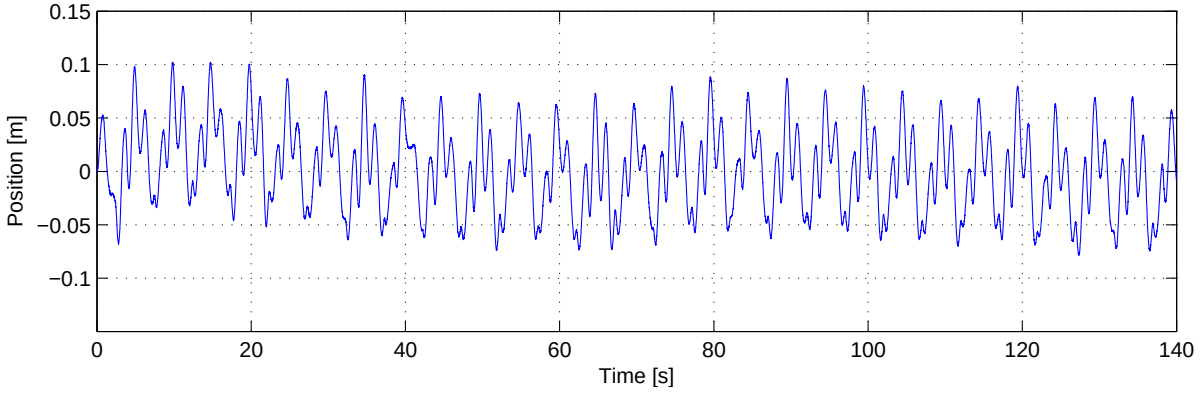

Figure 11.6: Displacement of blade one, by using collective pitch control strategy on the linearised model.

The displacement of blade one, is oscillating according to the wind disturbances and because of the effect the wind has on blade two and three. Without the pitch control the displacement and oscillation would be more severe. Furthermore, a repetitive behavior of the response is noted, caused by wind disturbance.

11.2 Conclusion

The mechanical power output of the linearised model, is driven to the reference value of 5 MW and kept constant without violating the boundaries of $\pm 1\%$, although it is affected by turbulence, tower shadow, wake and wind shear. The same boundaries are kept regarding the angular velocity of the generator. As noted in Figure 11.4 and 11.6, the repetitiveness present in the wind disturbance, induces an oscillatory behavior on the angular velocity of the generator, the power and the blade displacement. In order to treat the repetitiveness, and minimise the deviation from the reference point, two approaches are presented. One in the following Chapter 12 on page 79 and one in the consecutive Chapter 13 on page 91. These

approaches have to fulfill the following requirement, corresponding to the requirement stated in Chapter 2 on page 15.

Minimise the fatigue on the wind turbine components by means of individual pitching.

This is done by designing a second controller which is implemented in addition to the collective pitch controller. Its purpose is to minimises the loads on the turbine due to the tilt-wise motion. As the source of the loads is the repetitive nature of the wind acting on the blades, an individual pitch controller is designed for reducing the loads on the blades. This is further elaborated in the following chapter.

12 Individual Pitch Control by Multi-bladed Coordinate Transformation

The turbine captures wind by pitching the blades with respect to a given wind velocity, which causes the blades to bend in a flap-wise motion. This motion is called the blade displacement. The displacement of the blades are considered measurable, by means of strain gauge sensors. These determine the actual flap-wise position of each individual blade. As the blade moments are of interest in the control design, the blade moments are calculated as follows, [Benenson et al., 2002, p.161]:

$$F_{\mathrm{b},i} = K_{\mathrm{b},i} \cdot x_{\mathrm{b}i} \qquad [N] \quad (12.1)$$

$$M_{\mathrm{b},i} = F_{\mathrm{b},i} \cdot L_{\mathrm{b},i} \qquad [Nm] \quad (12.2)$$

where

$F_{\mathrm{b},i}$	is the force of thrust on blade $i = 1,\ 2,\ 3$	[N]
$M_{\mathrm{b},i}$	is the moment of blade $i = 1,\ 2,\ 3$	[Nm]
$K_{\mathrm{b},i}$	is the stiffness of blade $i = 1,\ 2,\ 3$	[Nm]
$x_{\mathrm{b}i}$	is the displacement of blade $i = 1,\ 2,\ 3$	[m]
$L_{\mathrm{b},i}$	is the length of blade $i = 1,\ 2,\ 3$	[m]

The loads, which the blade bending moments encounters, are often noted by P. The 1P loads are iterated through the structure and mechanical part of the turbine, as 3P loads. In other words, the 1P frequency, once per revolution component of the blade loads, occurs corresponding to each single blade. Due to the fact that the blades are phase shift by 120 degrees, then, e.g. the tower, encounters 3P, 6P, ... harmonics. Note that the 1P frequency has the harmonics of the frequencies 2P, 3P, 4P and so on, while e.g. the structure of the turbine, has 3P frequency with the corresponding harmonics of 6P, 9P and so on. These frequencies may lead to rapid degradation or even be the cause of the destruction of the turbine, if not treated. Thus the controller should be able to reduce the transient bending of the blades, which then results in a reduced oscillating behavior. The collective pitch controller, presented in Chapter 11 on page 73, has the purpose of stabilising the angular velocity of the generator, which encounters the 3P frequency along with the 6P, 9P ... harmonics. As the collective pitch controller is not able to handle the 1P frequencies, caused by the individual blades, a new approach is proposed.

Throughout the rotational movement of the blades, these experience individual loads, thus it is of interest to find a transformation to a fixed frame, where the loads that the blades encounter are combined. However, for this it is not sufficient to add together the loads on each of the blade as they are asymmetric and the blades have a phase shift of 120 degrees. Consequently, a geometric transformation is used to project

the loads from the rotating frame to a fixed frame.

This is done by means of the multi-bladed coordinate transformation, also known as the Coleman transformation. These terms are used interchangeably in the following sections. The approach was initially introduced by [Park, 1929] as d-q axis transformation for three-phase electrical machine theory, later used in helicopter theory by Coleman [Coleman and Feingold, 1957] and as well for wind turbines by [Bossanyi et al., 2005], [Bossanyi, 2002], [Lackner and van Kuik, 2009] and [Jelavic et al., 2010].

12.1 Deriving the Coleman Transformation Scheme

According to [Prinsen, 2011], the *rotating frame of reference* is expressed in *fixed frame of reference*, by means of the degrees of freedom, which are the q (bending moments), of the blades in *rotating frame*. In the case of a three-bladed turbine this is given by:

$$q_{\text{avg}} = \frac{1}{3}\sum_{i=1}^{3} M_{\text{b},i} \quad [\cdot] \quad (12.3)$$

$$q_{\text{tilt}} = \frac{2}{3}\sum_{i=1}^{3} M_{\text{b},i}\cos n\psi_i \quad [\cdot] \quad (12.4)$$

$$q_{\text{yaw}} = \frac{2}{3}\sum_{i=1}^{3} M_{\text{b},i}\sin n\psi_i \quad [\cdot] \quad (12.5)$$

where

ψ_i	is the azimuth angle of blade $i = 1,\ 2,\ 3$
n	represents the harmonic (rotational frequency) for which the transformation is performed
q_{avg}	is the *fixed frame of reference* degree of freedom for average blade moment
q_{tilt}	is the *fixed frame of reference* degree of freedom for tilt-wise blade moment
q_{yaw}	is the *fixed frame of reference* degree of freedom for yaw-wise blade moment

By performing a 1P coordinate transformation, the projection of the *rotating frame of reference* on the *fixed frame of reference* of reference (fixed turbine structure) is obtained. For further elaboration on the Coleman transformation, a second frame at the tower base is entered, called the *fixed frame of reference*. Note that this frame is not a part of the physical turbine, it is for illustrative purposes only. In Figure 12.1 the two frames are depicted. One with red, for the *rotating frame of reference* of reference, and one blue, for the *fixed frame of reference* of reference. The blade moments, $M_{\text{b}i}$, are transferred to the *fixed frame of reference*, by projecting the loads from the *rotating frame of reference*, to the *fixed frame of reference*.

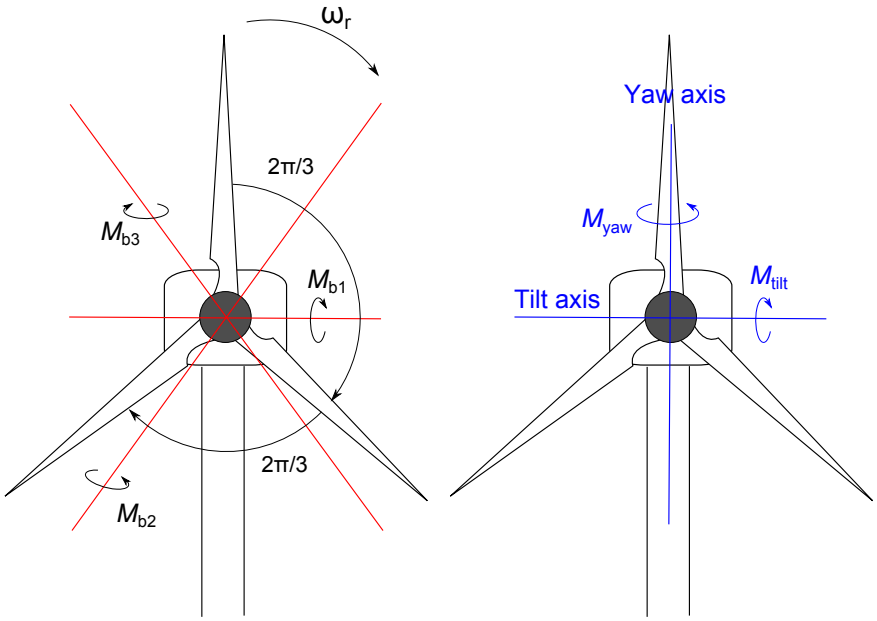

(a) *Rotating frame* of reference. (b) *Fixed frame* of reference.

Figure 12.1: Coleman transformation from *rotating frame* of reference (red) to *fixed frame* of reference (blue)

For a better understanding of the loads transfer from *rotating frame* to the *fixed frame*, the harmonics of the blade moment are examined in the case of 1P loads component in the blade bending moment. The 1P blades load in the *rotating frame* are transfered as 0P component to the *fixed frame*, meaning that the blade moments that are fluctuating with a constant amplitude at 1P frequency are transformed to 0P moments around the tilt and yaw axis in the *fixed frame*. Moreover, the 2P loads in the *rotating frame* are transfered as 3P loads in the *fixed frame*. As the controllers for the 1P algorithm are not capable of actuating based on these frequencies, a filter has to be used to filter out the undesired 3P frequencies.

Following, a schematic in Figure 12.2 is presented, with the appertaining equations required.

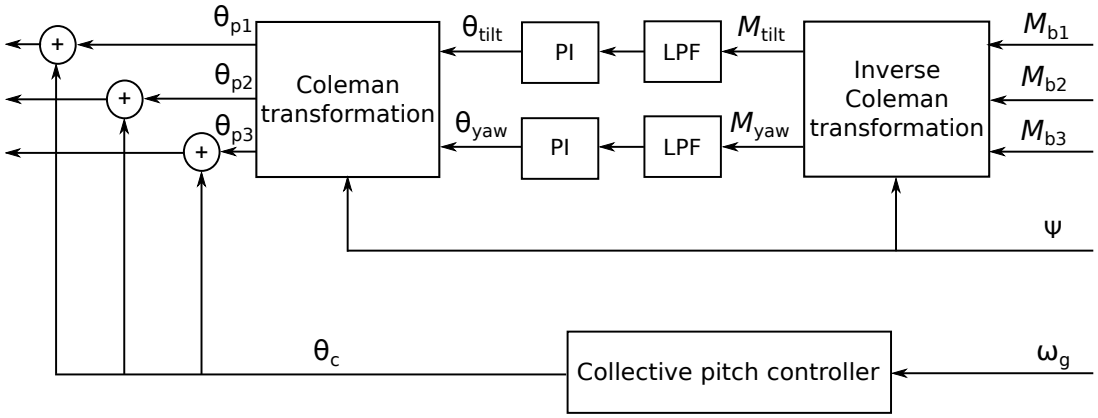

Figure 12.2: Individual pitch control approach by using Coleman and inverse Coleman transformation including two PI controllers and two low pass filters (LPF).

The inputs of the inverse Coleman transformation are the moment of each blade, noted in Equation 12.6,

according to [Jelavic et al., 2010].

$$\begin{bmatrix} M_{\text{tilt}}(t) \\ M_{\text{yaw}}(t) \end{bmatrix} = \left(\frac{2}{3}\right) \begin{bmatrix} \cos(\psi(t)) & \cos\left(\psi(t)+\frac{2\pi}{3}\right) & \cos\left(\psi(t)+\frac{4\pi}{3}\right) \\ \sin(\psi(t)) & \sin\left(\psi(t)+\frac{2\pi}{3}\right) & \sin\left(\psi(t)+\frac{4\pi}{3}\right) \end{bmatrix} \begin{bmatrix} M_{\text{b1}}(t) \\ M_{\text{b2}}(t) \\ M_{\text{b3}}(t) \end{bmatrix} \quad [\text{Nm}] \quad (12.6)$$

where:

$M_{\text{tilt}}(t)$	is the tilt-wise result of the inverse Coleman transformation	[Nm]
$M_{\text{yaw}}(t)$	is the yaw-wise result of the inverse Coleman transformation	[Nm]
$\psi(t)$	is the azimuth angle of blade 1 with respect to the upright position, zero rad	[°]
$M_{\text{b1}}(t)$	is the moment on blade 1	[Nm]
$M_{\text{b2}}(t)$	is the moment on blade 2	[Nm]
$M_{\text{b3}}(t)$	is the moment on blade 3	[Nm]

To further minimise the undesired P harmonics, a low pass filter is introduced. The signal is then controlled by a PI controller, and transferred back to the *rotating frame of reference* via the Coleman transformation. These outputs of the Coleman transformation are the corresponding individual pitch angles, which are used to compensate for the undesired loads on the blades. The resulting individual pitch control signals are added to the collective pitch control signal, that compensating for the 1P frequency, which the collective pitch controller is not able to remove. The Coleman transformation from the *fixed frame of reference*, to the *rotating frame of reference* is given by, [Jelavic et al., 2010]:

$$\begin{bmatrix} \theta_{\text{p1}}(t) \\ \theta_{\text{p2}}(t) \\ \theta_{\text{p3}}(t) \end{bmatrix} = \begin{bmatrix} \cos(\psi(t)) & \sin(\psi(t)) \\ \cos\left(\psi(t)+\frac{2\pi}{3}\right) & \sin\left(\psi(t)+\frac{2\pi}{3}\right) \\ \cos\left(\psi(t)+\frac{4\pi}{3}\right) & \sin\left(\psi(t)+\frac{4\pi}{3}\right) \end{bmatrix} \begin{bmatrix} \theta_{\text{tilt}}(t) \\ \theta_{\text{yaw}}(t) \end{bmatrix} \quad [^\circ] \quad (12.7)$$

where

$\theta_{\text{p1}}(t)$	is the resulting pitch angle for blade 1 after the Coleman transformation	[°]
$\theta_{\text{p2}}(t)$	is the resulting pitch angle for blade 2 after the Coleman transformation	[°]
$\theta_{\text{p3}}(t)$	is the resulting pitch angle for blade 3 after the Coleman transformation	[°]
$\psi(t)$	is the azimuth angle of blade 1 with respect to the upright position, zero rad	[°]
$\theta_{\text{tilt}}(t)$	is the result of the low pass filtered signal through the PI controller, tilt-wise	[°]
$\theta_{\text{yaw}}(t)$	is the result of the low pass filtered signal through the PI controller, yaw-wise	[°]

By using the multi-bladed coordinate transformation, the 1P asymmetric loads on each blade are obtained as the decoupled tilt, M_{tilt}, and yaw, M_{yaw}, terms. The control problem is then controlling as LTI SISO system, which can be accomplished by means of traditional PI controller in series with a low pass filter, noted LPF in Figure 12.2. The aim of the PI controllers used in the *fixed frame*, is to minimise M_{tilt} and M_{yaw}.

Following three requirements are made regarding the performances of the implemented Coleman transformation scheme that follows. Based on these requirements, conclusions are elaborated at the end of the section.

Initial requirements for the Coleman transformation scheme:

1. The individual pitch control signal from the designed controllers, does not interfere with the control signal of the collective pitch controller, in the absence of the 1P loads on the blades bending moment.

2. The individual pitch controller minimises only the 1P loads on the blades.

3. The individual pitch controller does not minimise the 3P loads which affect the structure and mechanism of the turbine.

12.2 Implementation of the Coleman Transformation

In Figure 12.3, the control loop for the individual pitch, is presented by a red line. For the *fixed reference frame*, the input of the controllers are the filtered tilt-wise and yaw-wise moments of the blades, respectively. The parameters, for the two PI controllers, are designed with respect to Table F.2 on page 171. By fine tuning, the following PI gains are determined, $K_{\mathrm{p}} = 4.23e-08$ and $K_{\mathrm{i}} = 1.87e-7$. Note that the small gains are due to the order of magnitude of the blades bending moment, Nm, compared to the pitch control signals, rad. In other words, the conversion of units $\frac{Nm}{rad}$. The PI controller is chosen for its integral effect that ensures a convergence of the tilt and yaw loads towards zero. Furthermore, its proportional effect decreases the steady state error and the rise time. Thus, resulting in a desired response for the system.

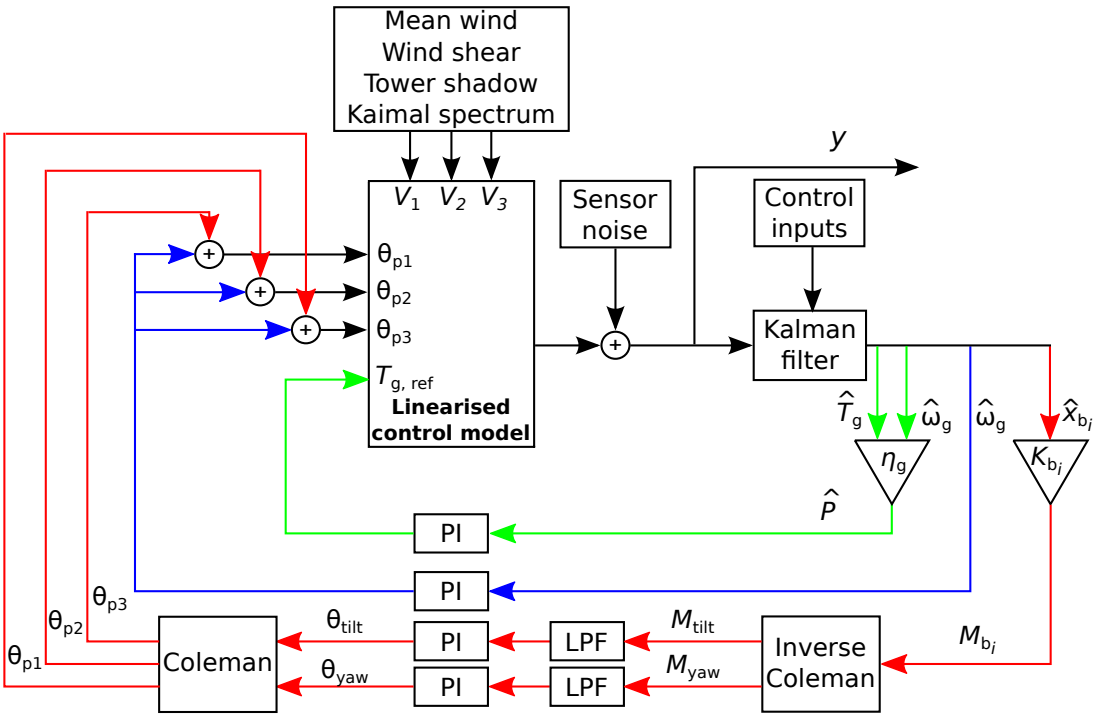

Figure 12.3: Basic control strategy with the Coleman transformation, for the small signal linearised control model.

To ensure that the individual pitch controller is decoupled from the collective pitch controller, that controls the 3P frequency, two low pass filters are used to cut off the undesired control frequencies. The goal

is to cut off every frequency higher than the 1P frequency. Based on the results of the power spectrum density of the signal, noted in Figure 12.4(a). Thus the low pass filters are chosen to be of fifth order Butterworth filters, with the cut-off frequency at 0.5 Hz. An improvement for this could be a second control loop, which would be able to handle the 2P harmonic present in the blade bending moment, though it is not considered.

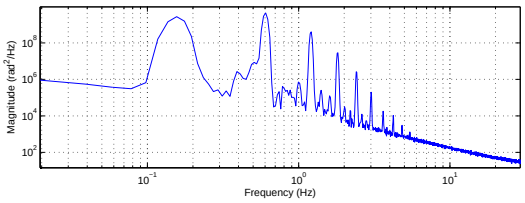

(a) Power spectrum density of the tilt-wise motion of the blades in the *fixed frame of reference* before the Butterworth filter.

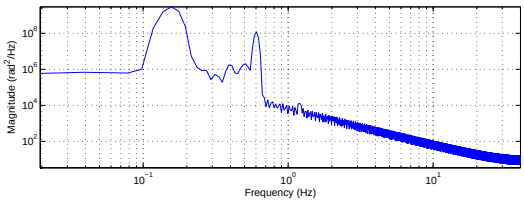

(b) Power spectrum density of the tilt-wise motion of the blades in the *fixed frame of reference* after the Butterworth filter.

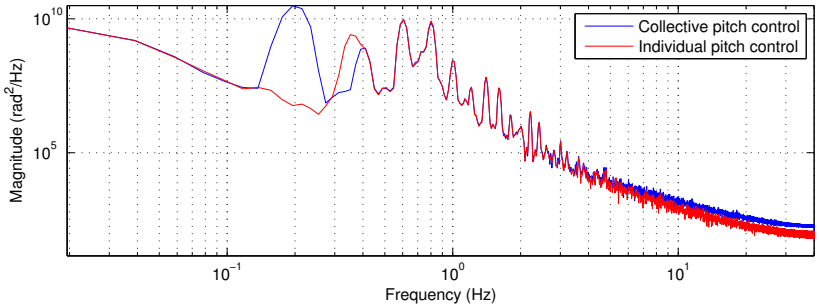

(c) Comparison of the power spectrum densities for the tilt-wise motion of the blades with respect to collective pitch control and the Coleman transformation, implemented on the linearised plant model.

Figure 12.4: Power spectrum density comparison for the Coleman transformation.

As noted in Figure 12.4(c), the 1P frequency at 0.2 Hz is minimised by the multi-bladed coordinate transformation control scheme, as desired.
In the following figures, a comparison of the performance for the individual pitch control system, and the collective pitch control system, using the plant model, is presented.

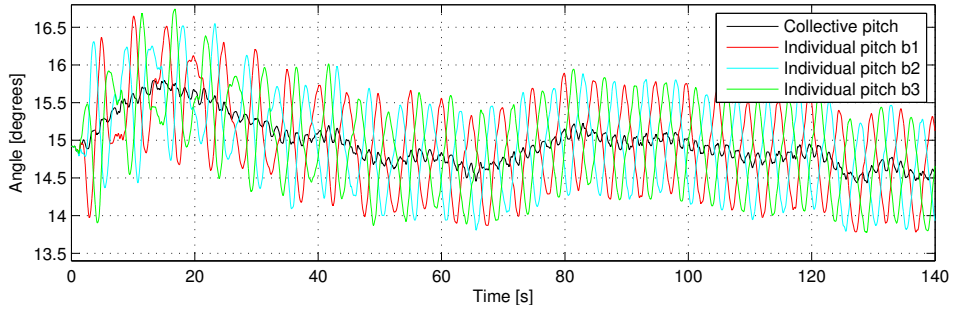

Figure 12.5: Pitch control actuation comparison between collective pitch control and Coleman transformation, implemented on the linearised model.

The comparison of the pitch actuation is displayed in Figure 12.5. It is noted that in the case of the multi-bladed coordinate transformation, the actuators are pitching individually, while in the case of the collective pitch controller, the same control effort is performed by each blade, depicted with black. When Coleman transformation is mentioned in the following, it is including the PI controllers and the low pass filter.

Figure 12.6(a) presents the angular velocity of the generator. It is noted that the Coleman transformation has no affect on it, due to the fact that the angular velocity for the collective pitch and the individual pitch scheme are equal. The same is also valid in the case of the power output presented in Figure 12.6(b) and the tower displacement presented in Figure 12.6(c).

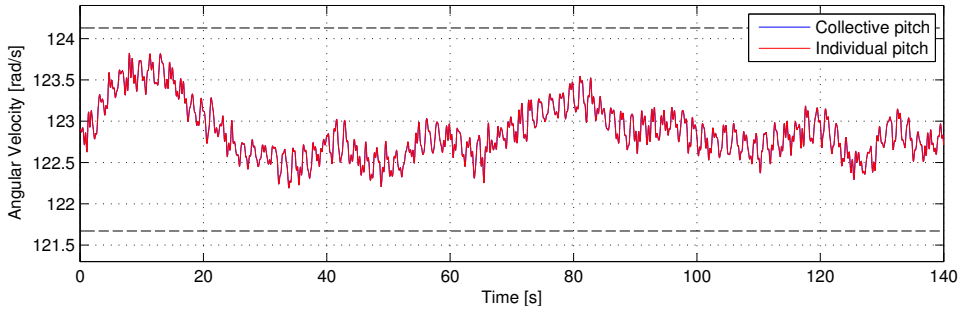

(a) Comparison of the angular velocity of the generator, for the collective pitch control scheme, and the Coleman transformation, implemented on the linearised plant model.

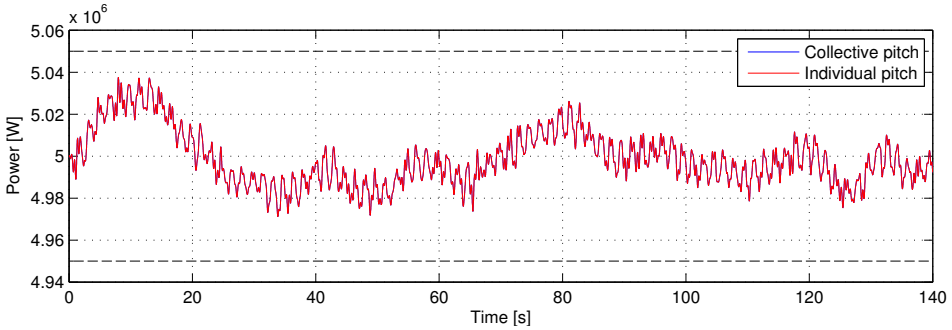

(b) Comparison of the mechanical power for the collective pitch control scheme and the Coleman transformation, implemented on the linearised plant model.

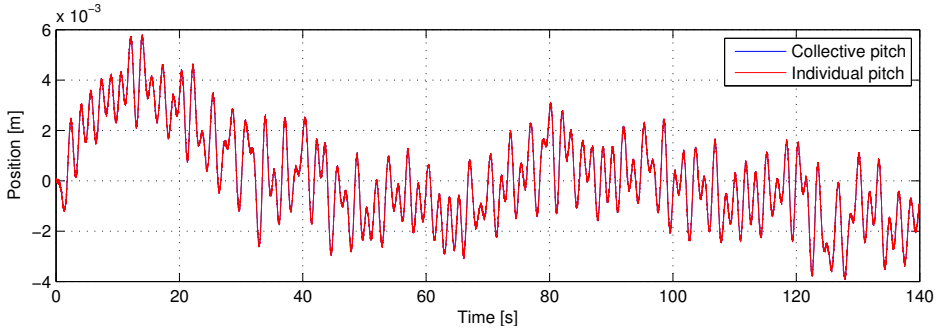

(c) Comparison of the tower displacement for the collective pitch control scheme and the Coleman transformation, implemented on the linearised plant model.

Figure 12.6: Wind turbine dynamics that are not affected by the Coleman transformation.

As noted in Figure 12.6, the multi-bladed coordinate transformation does not have any effect on the angular velocity of the rotor, the output power nor tower displacement, due to the fact that the 3P frequency corresponding to these, are eliminated when the multi-bladed coordinate transformation of the moments to the *fixed frame of reference* is performed. Thus, by using the Coleman transformation, only the 1P frequency corresponding to the individual blades is affected, as noted by the fact that the blade displacement is minimised as displayed in Figure 12.7.

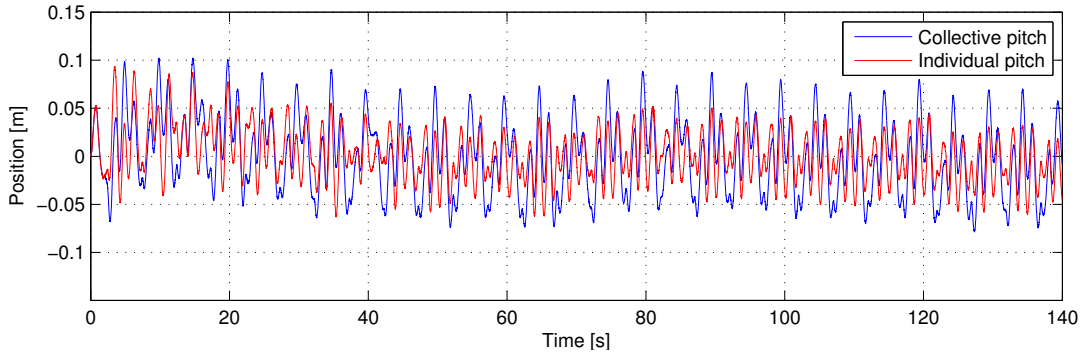

Figure 12.7: Comparison of the blade displacement for the collective pitch control and Coleman transformation, implemented on the linearised plant model.

Verification of the Coleman Transformation

In order to verify the performance of the implemented multi-bladed coordinate transformation and determine whether the requirements stated on Page 80, are accomplished, a second wind model is used. This wind model contains only the wind turbulences caused by the Kaimal filter. Thus, by having a low 1P frequency content the effect of the multi-bladed coordinate transformation for this frequency can be determined.

Figure 12.8(a) presents the wind model. Following the control signal is investigated in Figure 12.8(b), in order to determine if the Coleman transformation has any effect on it. Finally, the power spectrum density of the signal driven through the transformation module is represented in Figure 12.9, in order to determine the frequency content of the blade bending moments.
It is noted in Figure 12.8(b), that the pitch angles do not differ with respect to the individual blade. The result of the individual pitch control, with respect to the wind profile, is presented in Figure 12.8 and 12.9.

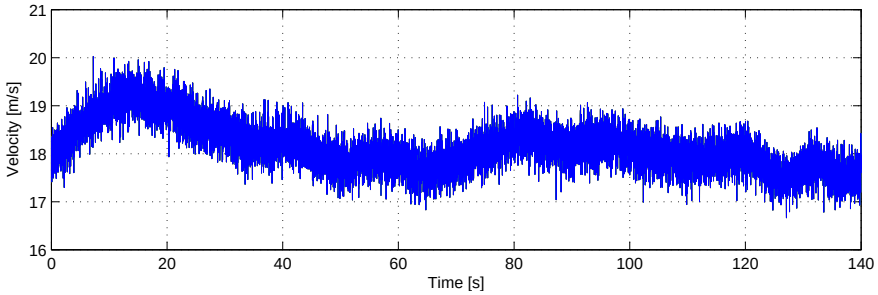

(a) Wind sequence, containing only the wind turbulence.

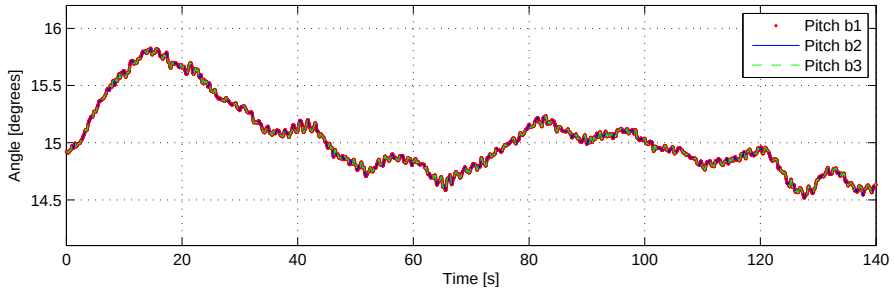

(b) Control effort of the pitch actuators, using Coleman transformation, with the wind model containing only the wind turbulence.

Figure 12.8: The pitch actuation with the given turbulent input, for the plant model.

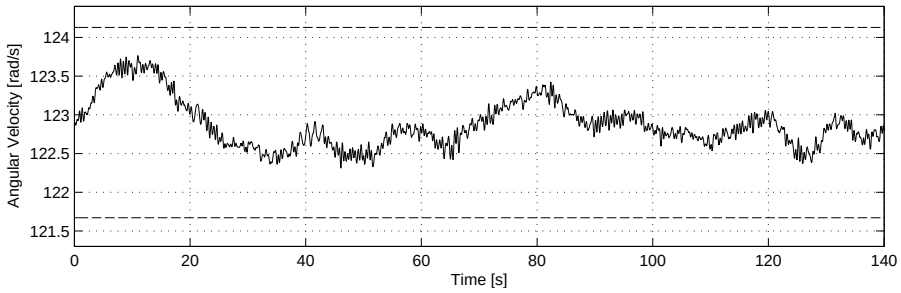

(a) Angular velocity of the generator, using Coleman transformation, with the wind model containing only the wind turbulence, by using the plant model.

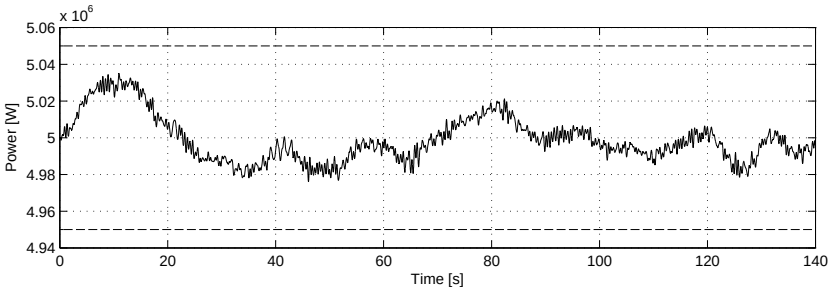

(b) Output power, using Coleman transformation, with the wind model containing only the wind turbulence, by using the plant model.

Figure 12.9: Power output and angular velocity of the generator, using the Coleman transformation of the plant model.

It is noted in Figure 12.8(b), that the pitch angles do not differ with respect to the individual blade. The result of the individual pitch control, with respect to the wind profile, is presented in Figure 12.8 and 12.9.

Figure 12.9 presents the power spectrum density of the blade moment. The magnitude of the power spectrum density is lower than the power spectrum density determined with all the elements of the wind profile (wind shear, tower shadow and wake), noted in Figure 12.4, thus less strain affects the blades.

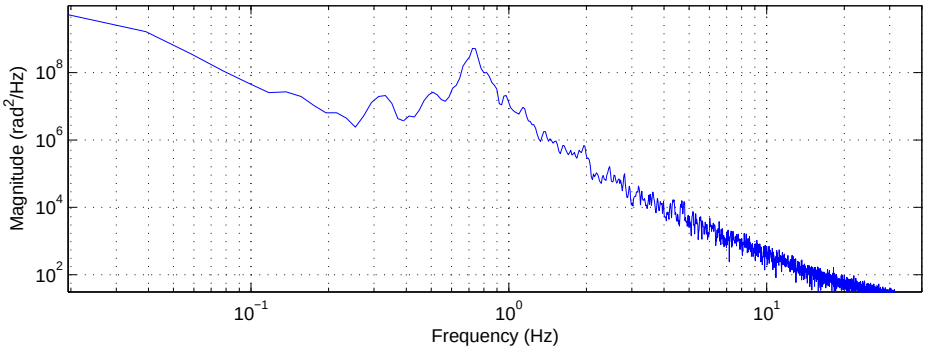

Figure 12.10: Power spectrum density of the bending moment of blade one, using Coleman transformation, with the wind model containing only the wind turbulence.

12.3 Conclusion

Based on the obtained results, by using the multi-bladed coordinate transformation, the loads on the individual blades are reduced compared to the collective pitch control. At the same time, the output power and the angular velocity of the generator are driven towards their reference values respectively, and kept in between the boundary limits of $\pm 1\%$. As displayed in Figure 12.8(b), the Coleman transformation does not interfere with the collective pitch control. This is concluded on grounds of the pitch actuation for each blade is the same, they overlay, thus no individual pitch control signals are generated. Moreover, in Figure 12.6 it is noted that the turbine structure and mechanism, affected by the 3P loads, are not influenced by the multi-bladed coordinate transformation. By considering the result in Figure 12.4(c) it is noted that the 1P loads are minimised. The requirements, noted on Page 80, are verified and successfully fulfilled by the multi-bladed coordinate transformation. Thus, the Coleman transformation is suitable for minimising the loads on the individual blades.

The multi-bladed coordinate transformation has been implemented on the linear plant model, in order to have a performance boundary for the repetitive control strategy that follows in the next chapter.

13 REPETITIVE CONTROL

This chapter presents an overview on the general steps leading to the design of the repetitive control, with respect to the following sources, [Houtzager, 2011, p.114-130], [Manish Gupta, 2005], [Wang et al., 2008] and [Lee et al., 2001]. In the first part an introduction on how the repetitive control works and an overall picture of its structure is given. By knowing the idea behind the repetitive control, an algorithm for designing a repetitive control scheme, in the case of a general linear system with the necessary assumptions, is given. Using the provided algorithm, the repetitive control is first implemented on a simpler system, namely the pitch model of the wind turbine system, in order to persuade the reader that this approach is suitable for fulfilling the project requirements. The results of the simulations are presented, and concluded upon. The second part of the chapter gives a thoroughly explanation on the repetitive control implementation on the developed linearised wind turbine model, the plant model. A series of tests are presented and performed in this implementation, in order to evaluate its performance compared to the performance of the controllers designed for the collective pitch in Chapter 11 on page 73, and the individual pitch using multi-bladed coordinate transformation in Chapter 12 on page 79. In the end, a conclusion based on the performance of the repetitive control, is given.

13.1 Repetitive Control Overview

A vast majority of engineering applications encounter periodic disturbances due to their periodic operation patterns. These periodic behaviors can either be caused by purpose, in order to stabilise the plant or maximise its performances, or occur in a natural way. An example of natural repetitive pattern induced on a system, is the kinetic energy of the wind acting as a disturbance on wind turbines. Regardless of the cause of the repetitiveness in the system, the periodicities of the processes can be treated by use of a repetitive controller. The basic structure of the repetitive controller is presented in Figure 13.1. The

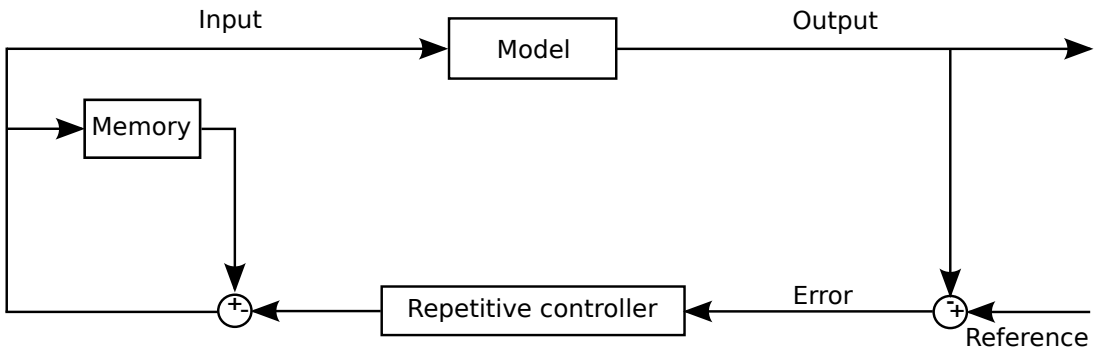

Figure 13.1: General repetitive control scheme overview.

goal of the repetitive controller is to assure asymptotic tracking of a periodic reference trajectory, or to

reject repetitive disturbances, as stated by [Shinji Hara and Nakano, 1988]. The strategy is based on the internal model principle, introduced by [Francis and Wonham, 1975].
The internal model principle presented in Appendix G on page 173 states:

The output of the controller, tracks a reference, without having any steady state error or deviation, if and only if the model of the exogenous signal generator is included in the stabilised closed-loop system used for control.

In order to design a repetitive control, the signal to be tracked or the repetitive disturbance to be rejected, has to be known in advance [Manish Gupta, 2005]. In order to fulfill this requirement, a periodic signal generator or memory loop containing this signal, is needed as depicted in Figure 13.1. By including the memory loop, the error throughout previous trials is stored, in order to calculate the input of the plant for future trials. This memory loop is based on the internal model principle, and by having a stabilised feedback system, the resulting closed loop system should asymptotically track the signal stored in the memory. It is noted that the repetitive control strategy is a frequency domain technique, thus in order to use it in time domain, with e.g. a LQR control strategy, the memory loop is used. In frequency domain the memory loop acts like an integrator, and adds the error at each sampling time, whereas in time domain the repeating error is stacked for each trial period. Furthermore, this leads to a trial by trial control technique, which can be used with the time domain LQR scheme.

In the following section, a general algorithm for designing the repetitive controller is presented, followed by an example of the implementation on the pitch system of the linearised wind turbine presented in Section 5.3 on page 39.

13.2 Repetitive Control Design

The general algorithm with assumptions and requirements follows.

Linear Discrete-Time Model of the System

Given a general linear discrete-time state space model S, shown in Equation 13.1, the repetitive control algorithm can be designed.

$$S\begin{cases} x_{k+1} &= Ax_k + Bu_k + B_\mathrm{d}d_k \\ y_k &= Cx_k + Du_k \end{cases} \tag{13.1}$$

Where

x_k	is the discrete state vector
u_k	is the discrete input vector
d_k	is the discrete disturbance vector
y_k	is the discrete output vector
A	is the discrete state matrix
B	is the discrete input matrix
B_d	is the discrete disturbance matrix
C	is the discrete output matrix
D	is the discrete feed-forward matrix
k	is the discrete time step for a given state

Stabilising the System

In order to design a repetitive control for discrete systems, the system has to be fully observable and controllable. Further, *the closed loop system has to satisfy Juri-Marden stability criterion*. In other words, the stability of the closed loop system is assured, if and only if, the poles of the discrete-time closed loop system, lie inside the unit circle in the z-plane, [Bistritz, 1996]. If that is not the case, a stabilising feedback controller has to be designed, thus the state space is augmented with the new states corresponding to the stabilising controller, [Manish Gupta, 2005]. In order to proceed with the system lifting, the period needs to be known, thus the following assumption is made:

The disturbance affecting the system is periodic, with a constant time period.

System Lifting

In order to design a repetitive controller, the periodic error throughout the trials is stored in the memory block, and used to calculate the input of the system for the following trial. This can be accomplished by transforming the linear time-variant state space model to a linear trial-invariant state space, by lifting. *By performing the lifting on a stable system, the resulting lifted system is also stable* [Houtzager, 2011]. The lifting is done for the period p corresponding to the period of the repetitive error. The period, p, also determines the size of the stacking vectors, depicted in Figure 13.2.

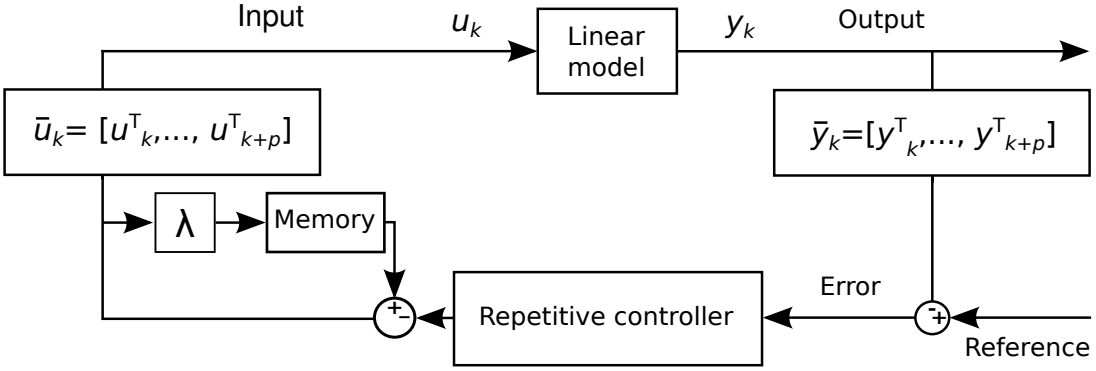

Figure 13.2: Control scheme for the repetitive control, with the stacking vectors for the output y_k, described as $\bar{y}_k$ and of the input u_k as $\bar{u}_k$. λ is the forgetting factor of the repetitive control scheme.

The different stacking vectors are described following, starting with the output stacked vector as:

$$\bar{y}_k = \begin{bmatrix} y_k^T & y_{k+1}^T & \cdots & y_{k+p-1}^T \end{bmatrix}^T$$

Consequently the input stacked vector is:

$$\bar{u}_k = \begin{bmatrix} u_k^T & u_{k+1}^T & \cdots & u_{k+p-1}^T \end{bmatrix}^T$$

and the disturbance stacked vector, which is inflicted by the disturbances of the wind, elaborated on Page 95, is:

$$\bar{d}_k = \begin{bmatrix} d_k^T & d_{k+1}^T & \cdots & d_{k+p-1}^T \end{bmatrix}^T$$

Consequently the stacked vectors for the next trial are noted by $\bar{y}_{k+p}$, $\bar{u}_{k+p}$, $\bar{d}_{k+p}$ respectively. These values are stacked throughout the trial, and used in the further calculations only when the trial length p is reached. The resulting stacked vectors are the base of the system lifting and are explained following.

The lifted state space, noted $\bar{S}$, contains the system matrices, lifted for one period p as following:

$$\bar{S}\begin{cases} x_{k+p} & = \Phi x_k + \Gamma_\mathrm{s}\bar{u}_k + \Gamma_\mathrm{d}\bar{d}_k \\ \bar{y}_k & = Hx_k + \mathcal{J}_\mathrm{s}\bar{u}_k + \mathcal{J}_\mathrm{d}\bar{d}_k \end{cases} \tag{13.2}$$

Where the state transition matrix is composed of the stable closed loop system state matrix $\tilde{A}$

$$\Phi = \tilde{A}^p$$

The following are the extended controllability matrices, composed of the stable closed loop state matrix $\tilde{A}$, the stable closed loop input matrix $\tilde{B}$ and the stable closed loop output matrix $\tilde{C}$:

$$\Gamma_\mathrm{s} = \begin{bmatrix} \tilde{A}^{p-1}\tilde{B} & \dots & \tilde{A}^k\tilde{B} & \tilde{B} \end{bmatrix}$$
$$\Gamma_\mathrm{d} = \begin{bmatrix} \tilde{A}^{p-1}\tilde{B}_\mathrm{d} & \dots & \tilde{A}^k\tilde{B}_\mathrm{d} & \tilde{B}_\mathrm{d} \end{bmatrix}$$
$$H = \begin{bmatrix} \tilde{C} \\ \tilde{C}\tilde{A} \\ \vdots \\ \tilde{C}\tilde{A}^{p-1} \end{bmatrix}$$

While the impulse matrices are:

$$\mathcal{J}_\mathrm{s} = \begin{bmatrix} 0 & 0 & \cdots & 0 \\ \tilde{C}\tilde{B} & 0 & \cdots & \vdots \\ \vdots & \ddots & \ddots & 0 \\ \tilde{C}\tilde{A}^{p-2}\tilde{B} & \tilde{C}\tilde{A}^{p-3}\tilde{B} & \cdots & 0 \end{bmatrix} \qquad \mathcal{J}_\mathrm{d} = \begin{bmatrix} 0 & 0 & \cdots & 0 \\ \tilde{C}\tilde{B}_\mathrm{d} & 0 & \cdots & \vdots \\ \vdots & \ddots & \ddots & 0 \\ \tilde{C}\tilde{A}^{p-2}\tilde{B}_\mathrm{d} & \tilde{C}\tilde{A}^{p-3}\tilde{B}_\mathrm{d} & \cdots & 0 \end{bmatrix}$$

Error Augmentation in the State Space Model

The error for the period p, is then augmented in the lifted state space $\bar{S}$, by augmenting the state space with the state corresponding to the error for the trial period. The error is described as the difference between the stacked output vector, $\bar{y}_k$, and the reference vector, $\bar{r}_k$:

$$\bar{e} = \bar{r}_k - \bar{y}_k = \bar{r}_k - Hx_k + \mathcal{J}_\mathrm{s}\bar{u}_k + \mathcal{J}_\mathrm{d}\bar{d}_k$$

Note that the reference is trial invariant, thus the system is aware of the error throughout the trials, and allows the design of a repetitive controller, capable of tracking the error from one trial to the next. The difference between two trials is denoted by Δ, thus in case of the input Δu, and in case of the states Δx are:

$$\Delta\bar{u}_k = \bar{u}_k - \bar{u}_{k-p}$$
$$\Delta x_k = x_k - x_{k-p}$$

The notation x_k refers to the value of the states at sample time k, corresponding to the initial states of the current trial, while the notation x_{k-p} refers to the values of the states at sample time $k-p$, or the initial

states of the previous trial. Thus, the states of the system are not stacked throughout the period p.

According to the statement from [Hätönen et al., 2008], *the disturbance has to be periodic with a period of p*, consequently the change from one period to another is zero. Thus in the following equations the disturbance term is not considered.

$$\Delta \bar{d}_k = \bar{d}_k - \bar{d}_{k-p} = 0$$

Note that in the first period, the repetitive control is not active, as it needs to stack the information, to be able to correct the error. Consequently the error is initialised as zero, and changes through the trials.

The tracking error is given as:

$$\bar{e}_k = \bar{e}_{k-p} - H\Delta x_k - \mathcal{J}_s \Delta \bar{u}_k \tag{13.3}$$

The differences in the initial conditions of $\bar{S}$, are found by applying the Δ operator, which lead to

$$\Delta x_{k+p} = \Phi \Delta x_k + \Gamma_s \Delta \bar{u}_k \tag{13.4}$$

By augmenting the error in the state space, the new state $\xi_k = \begin{bmatrix} \Delta x_k \\ \bar{e}_k \end{bmatrix}$ is obtained. Using Equation 13.3 and 13.4 the system $\bar{S}^{\mathrm{RC}}$ is designed for the repetitive control purposes as following:

$$\bar{S}^{\mathrm{RC}} \begin{cases} \xi_{k+p} & = \bar{\Phi}\xi_k + \bar{\Gamma}_s \Delta \bar{u}_k \\ \bar{e}_k & = \bar{H}\xi_k + \bar{\mathcal{J}}_s \Delta \bar{u}_k \end{cases} \tag{13.5}$$

Where:

$$\begin{aligned} \xi_k &= \begin{bmatrix} \Delta x_k \\ \bar{e}_k \end{bmatrix} \quad \bar{\Phi} = \begin{bmatrix} \Phi & 0 \\ -H & \lambda I \end{bmatrix} \\ \bar{\Gamma}_s &= \begin{bmatrix} \Gamma_s \\ -\mathcal{J}_s \end{bmatrix} \quad \bar{H} = \begin{bmatrix} -H & \lambda I \end{bmatrix} \\ \bar{\mathcal{J}}_s &= -\mathcal{J}_s \end{aligned}$$

Note that λ is the forgetting rate, which ensures that the system is stable even though the error has been augmented to the lifted state space. Moreover, the forgetting rate is a tuning parameter.

Repetitive Control Law

Based on the state space system for which the repetitive control is designed, different control approaches can be used for minimising the error. However, LQR is considered optimal, for its ability to control MIMO systems, as in the case when lifting the system. This is due to the fact that LQR works both for SISO and MIMO system, thus the general repetitive control designed can cover both systems. The LQR approach is used in the initial setup, by assuming that the system is not stochastic, and all the states are measured. However, in the case in which the system is corrupted by noise, or not all the states are measurable, a Kalman filter can be used for noise filtering and state estimation.

LQR Approach

The LQR approach is made with respect to [Stefani et al., 2002, p.676]. The main problem, regarding the LQR problem, is to solve the quadratic cost function, J, by finding the control signal, $\Delta\bar{u}$, that minimises:

$$J = \lim_{p\to\infty} \sum_{k=0}^{p-1} \left(\xi_k^T Q \xi_k + \Delta\bar{u}_k^T R \Delta\bar{u}_k\right) \tag{13.6}$$

where $Q \in \mathbb{R}^{n\times n}$ and $R \in \mathbb{R}^{l\times l}$ are the symmetric quadratic weighting matrices, where n is the dimension of ξ and l is the dimension of $\Delta\bar{u}$.
The controller, for the system noted in Equation 13.5, can be defined as:

$$\Delta\bar{u}_k = -K_{\text{LIFT}} \cdot \xi_k$$

Resulting in:

$$\begin{aligned}\xi_{k+p} &= \bar{\Phi}\xi_k - \bar{\Gamma}_\text{s}(K_{\text{LIFT}} \cdot \xi_k) + \bar{\Gamma}_\text{d}\Delta\bar{d}_k \\ \xi_{k+p} &= (\bar{\Phi} - K_{\text{LIFT}}\bar{\Gamma}_\text{s})\xi_k + \bar{\Gamma}_\text{d}\Delta\bar{d}_k\end{aligned}$$

Where:

$$K_{\text{LIFT}} = [R + \bar{\Gamma}_\text{s}^T \mathcal{Z} \bar{\Gamma}_\text{s}]^{-1} \bar{\Gamma}_\text{s}^T S \bar{\Phi}$$

This results in the final controller:

$$\bar{S}^{\text{LQR}} \begin{cases} \bar{\xi}_{k+p} & = (\bar{\Phi} - K_{\text{LIFT}}\bar{\Gamma}_\text{s})\xi_k + \bar{\Gamma}_\text{d}\Delta\bar{d}_k \\ \Delta\bar{u}_k & = -K_{\text{LIFT}}\bar{\xi}_k \end{cases} \tag{13.7}$$

In order to persuade the reader, that the repetitive control scheme is able to minimise a repetitive error, and drive the output signal of the system to the reference value without any steady state error, as time goes to infinity, a repetitive control scheme is implemented on the linearised pitch system, derived in Section 5.3 on page 39. This system is of a lower order than the wind turbine, thus the dynamics are more straight forward.

In the following section, a basic overview of the model is given, followed by its state space. The steps for designing the repetitive control, presented in Section 13.2 on page 92, are followed in order to determine the final performances. The results of using a repetitive controller are depicted throughout different plots. Finally, the results are summed for a conclusion, with respect to the final performances of the control scheme.

13.3 Repetitive Control Implementation on the Pitch Actuator System

The continuous time pitch system, modelled in Section 5.3 on page 39, is expressed in Equation 13.8, as a general equation for the i^{th} pitch system.

$$\dot{\theta}_{\text{p}i}(t) = \frac{1}{\tau_\theta}(\theta_{\text{p,ref}}(t) - \theta_{\text{p}i,\text{ref}}(t)) + d_{\text{p}i}(t) \qquad [^\circ/s] \quad (13.8)$$

Following the equation is written as a continuous time state space in Equation 13.9. Note that it is the individual pitch system which is considered, thus the state space consists of three states, corresponding to each blade.

$$\begin{bmatrix} \dot{\theta}_{\text{p1}}(t) \\ \dot{\theta}_{\text{p2}}(t) \\ \dot{\theta}_{\text{p3}}(t) \end{bmatrix} = \begin{bmatrix} -\frac{1}{\tau_\theta} & 0 & 0 \\ 0 & -\frac{1}{\tau_\theta} & 0 \\ 0 & 0 & -\frac{1}{\tau_\theta} \end{bmatrix} \begin{bmatrix} \theta_{\text{p1}}(t) \\ \theta_{\text{p2}}(t) \\ \theta_{\text{p3}}(t) \end{bmatrix} + \begin{bmatrix} \frac{1}{\tau_\theta} & 0 & 0 \\ 0 & \frac{1}{\tau_\theta} & 0 \\ 0 & 0 & \frac{1}{\tau_\theta} \end{bmatrix} \begin{bmatrix} \theta_{\text{p1,ref}}(t) \\ \theta_{\text{p2,ref}}(t) \\ \theta_{\text{p3,ref}}(t) \end{bmatrix} + \begin{bmatrix} d_{p1}(t) \\ d_{p2}(t) \\ d_{p3}(t) \end{bmatrix} \qquad [^\circ/s] \quad (13.9)$$

In order to force the system to act in a periodic manner, a periodic sine wave disturbance, $d_{\text{p}i}(t)$, is introduced to each of the pitch systems, presented in Figure 13.4(a). The sine waves are shifted with a period of $\frac{2\pi}{3}$, starting from the pitch system for blade 2.

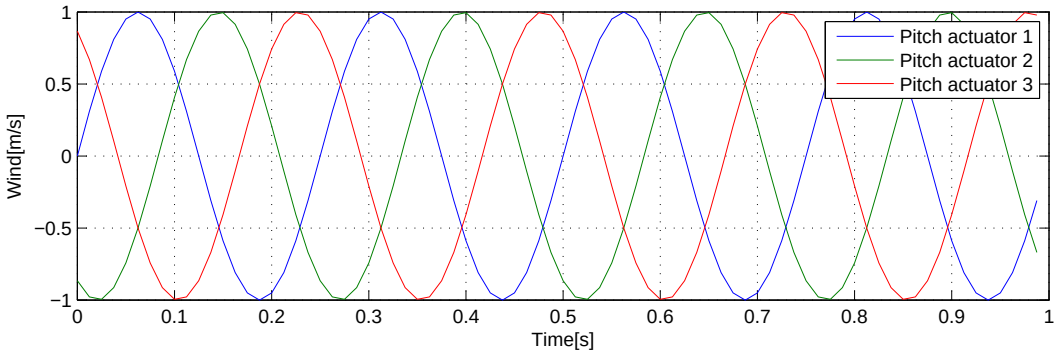

Figure 13.3: Disturbance d_{p} affecting the pitch systems.

Using the designed repetitive control algorithm, presented in Section 13.2 on page 92, the repetitive control design for the pitch system is derived as follows. The pitch system is a closed loop stable linear first order system, thus, there is no need of designing a stabilising controller for the state space. The state space discretisation is performed using Zero-Order Hold. Next the system is lifted, then augmented with the error, and finally a LQR design is used to minimise the repetitive deviation from the reference, caused by the disturbance. The control signal from the repetitive controller, displayed in Figure 13.4(a) and 13.4(b), is noted increasing, until a certain limit required in order to minimise the error. This increase is due to the learning capabilities of the controller.

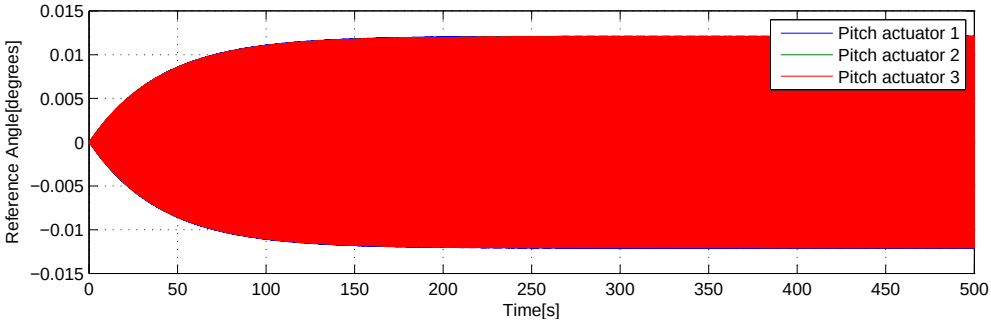

(a) Pitch reference of the linearised pitch actuator model.

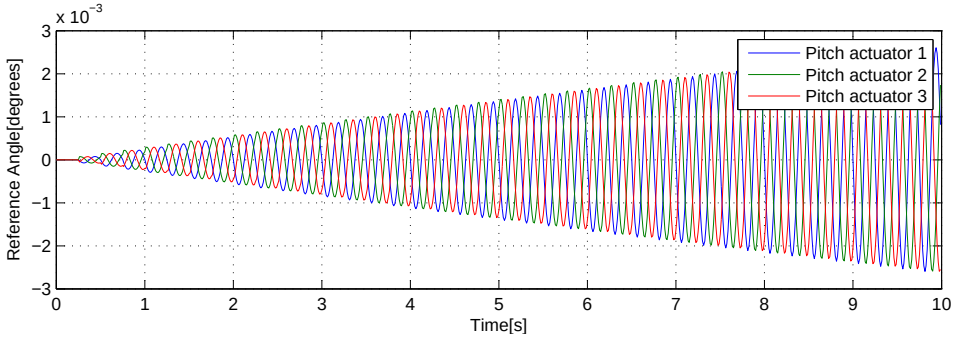

(b) Pitch reference of the linearised pitch actuator model, from time 0 to 10 s.

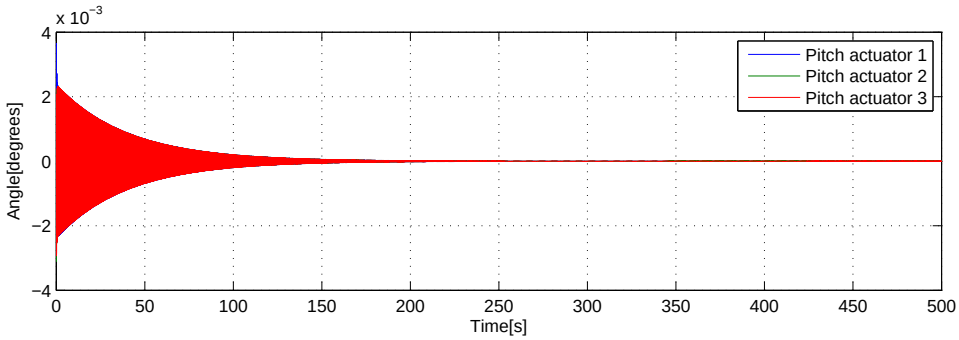

(c) Pitch angle of the linearised pitch actuator model.

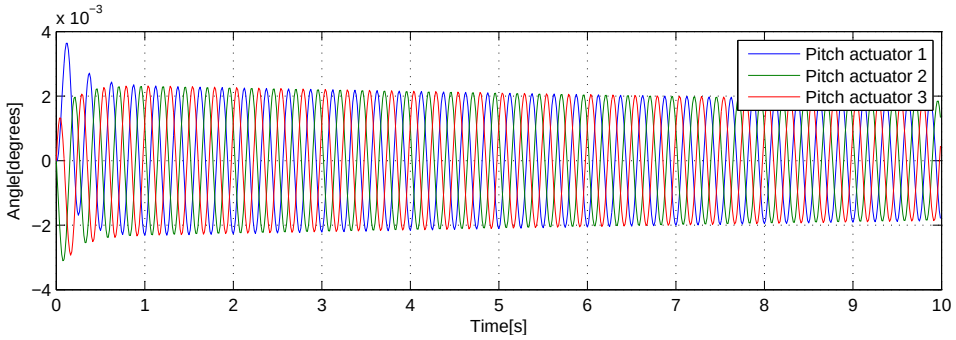

(d) Pitch angle of the linearised pitch actuator model, from time 0 to 10 s.

Figure 13.4: Control signals for the linear pitch system.

It is observed that the output of the system, presented in Figure 13.4(c) and 13.4(d), converges to zero as time goes to infinity, despite the presence of the repetitive disturbance noted in Figure 13.4(a), which

is affecting the pitch actuators. Note that because the reference is considered to be zero, the error is the output of the system. The requirements of the repetitive controller are fulfilled, and the implementation was successful. As an overview on the performance of the controllers, Figure 13.4 presents the asymptotic convergence of the error to zero as time goes to infinity.

The repetitive control algorithm has been presented together with an example in order to motivate the reader of this approach, for further implementation on the wind turbine. In the following section, the implementation of the repetitive control, on the developed wind turbine model in Chapter 6 on page 43, is elaborated thoroughly.

13.4 Repetitive Control Implementation on Wind Turbine System

This section elaborates on the implementation of the repetitive control scheme on the linear wind turbine model, derived in Chapter 6 on page 43 (the plant model). In order to design a repetitive controller for the system, the repetitive algorithm presented in Section 13.2 on page 92 is used. According to the algorithm, the system has to be closed loop stable. Thus, the augmentation of the linear control model with the two PI controllers, derived in Chapter 11 on page 73, is performed as the first step. This is followed by lifting the linear time variant system, in order to obtain a time-invariant system for the corresponding repeating period of the disturbance, also known as the trial-to-trial system. The error throughout the period is then augmented in the system, for satisfying the internal model principle, elaborated in Appendix G on page 173. These steps result in an increase in system dimensions, thus system reduction is performed. It is noted, that all the states of the designed system are observable and controllable. In the final step, a controller is used to minimise the overall error of the system throughout the chosen period. The determined control gain, is used in the simulations to determine the optimal inputs for the system. A series of test are performed with the designed controller implemented on the linear plant model, in order to evaluate its global performance. It is noted that the control model is used for designing the repetitive controller. The section concludes on the repetitive control implementation and its performances.

Introduction

During one rotor revolution, the turbine encounters wind phenomena like wind shear, tower shadow and wake, which are further elaborated in Chapter 1.4 on page 9. These phenomena, are repeating to a certain extend, at every revolution, thus resulting in the repetitive behavior of the wind disturbance. It is possible to minimise these periodic disturbances and even eliminate them, by means of the repetitive control scheme, as noted in the case of the pitch system in Section 13.3 on page 97. The impact of the repetitive wind disturbance on the wind turbine for a given period, p, is depicted in Figure 13.5(b), as the steady state behaviour of the blade tilt-wise displacement. Note that the controller designed in Chapter 11, is used to stabilise the blade displacement noted in Figures 13.5.

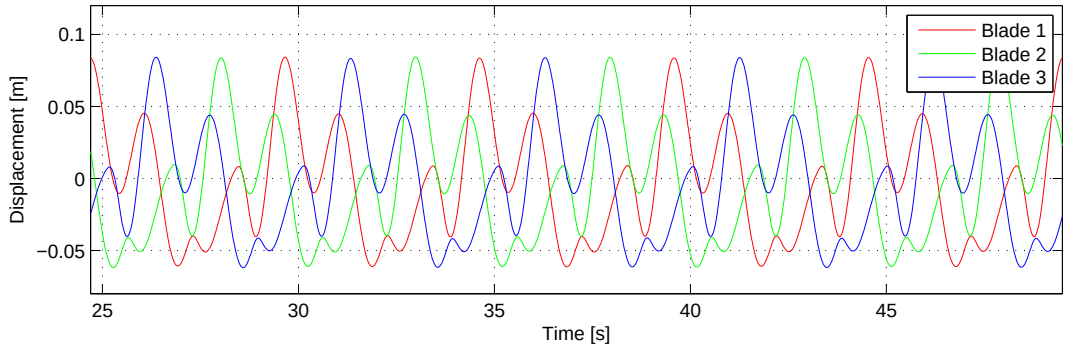

(a) Repetitive behavior of the displacement of the blades.

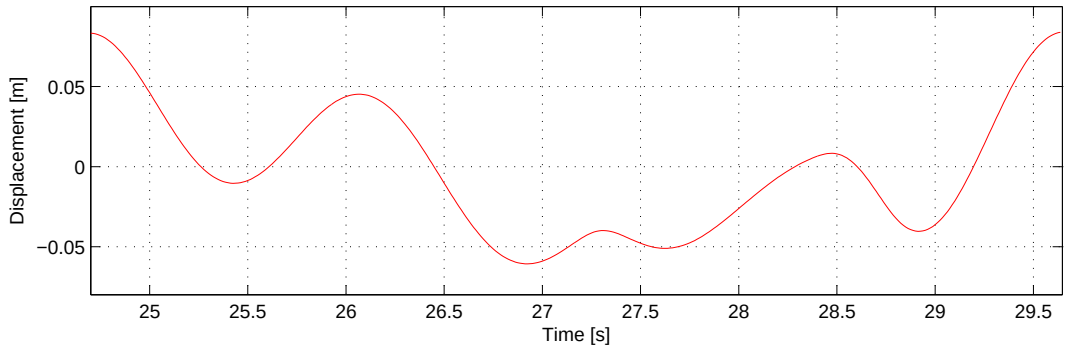

(b) Displacement of the first blade for a period p.

Figure 13.5: Repetitive behavior of the displacement of the blades in case of the linear plant model.

As noted in Figure 13.5 a repetitive behavior is present, thus the foundation for designing a repetitive control on the wind turbine is present, leading to augmenting the state space with the PI controllers.

Augmenting the State Space with PI Controllers

The PI controllers derived in Chapter 11 on page 73, are augmented in the linear control model. This is performed in order to obtain a stable closed loop system with respect to the desired reference points, when lifting the control model, thus the first requirement of the repetitive control design is fulfilled. In order to clarify the overall implementation strategy, it is noted that the repetitive controller is used to compensate and correct the control signal generated by the collective pitch controller implemented in Chapter 11 on page 73. It ensures that the system is stable, and that the required reference tracking is achieved. Namely keeping the output power at 5 MW and the angular velocity of the generator at 122.9 rad/s.

The linear discrete time control model, derived in Chapter 6 on page 43, S is described following:

$$S \begin{cases} x_{k+1} & = Ax_k + Bu_k + B_\mathrm{d} d_k \\ y_k & = Cx_k + Du_k \end{cases} \tag{13.10}$$

where

x_k is the state vector
u_k is the input vector
d_k is the disturbance vector
y_k is the output vector
A_k is the state matrix
B_k is the input matrix
B_d is the disturbance matrix
C_k is the output matrix
D_k is the feed forward matrix
k is the time step

The sampling time of the discretized control model is set to 0.0125 s according to the nonlinear NREL Fast 5 MW wind turbine model. In the initial implementation and tests, the sensor noise, according to Table D.3 on page 166, is used, though when implemented on the NREL 5 MW wind turbine, noise is neglected. In the case of the repetitive control scheme the plant input u_k, contains the individual pitch demands. Furthermore, the output y_k is set as the bending moments of the blades, individually. The wind affecting the blades is the disturbance, denoted by d_k (with respect to the azimuth angle of each individual blades). These are noted as following:

$$
\begin{aligned}
u_k &= [\theta_{\mathrm{p1}_k}\ \theta_{\mathrm{p2}_k}\ \theta_{\mathrm{p3}_k}]^T \\
y_k &= [x_{\mathrm{b1}_k}\ x_{\mathrm{b2}_k}\ x_{\mathrm{b3}_k}]^T \\
d_k &= [v_{1_k}\ v_{2_k}\ v_{3_k}]^T
\end{aligned}
$$

In order to design a repetitive controller, the state space described in Equation 13.10, is augmented with two new states corresponding to the integral effects of the two PI controllers. Consequently, in the following equations, $\boldsymbol{w}$, is the new state corresponding to the integral effect from the PI controller designed for keeping the output power constant, while $\boldsymbol{c}$, is the integral effect for the controller stabilising the angular velocity of the generator by means of collective pitch. The stable closed loop state space $\tilde{S}$ is presented following.

$$
\tilde{S}\begin{cases}
\begin{bmatrix} x_{k+1} \\ \boldsymbol{w}_{k+1} \\ \boldsymbol{c}_{k+1} \end{bmatrix} &= \tilde{A}\begin{bmatrix} x_k \\ \boldsymbol{w}_k \\ \boldsymbol{c}_k \end{bmatrix} + \tilde{B}u_k + \tilde{B}_\mathrm{d}d_k \\
y_k &= \tilde{C}\begin{bmatrix} x_k \\ \boldsymbol{w}_k \\ \boldsymbol{c}_k \end{bmatrix} \\
u_k &= -\tilde{K}\begin{bmatrix} x_k \\ \boldsymbol{w}_k \\ \boldsymbol{c}_k \end{bmatrix}
\end{cases}
\tag{13.11}
$$

Where:

$$\tilde{A} = \begin{bmatrix} A & 0 & 0 \\ C_4 & 0 & 0 \\ C_2 & 0 & 0 \end{bmatrix} \quad \tilde{B} = \begin{bmatrix} B \\ 0 \\ 0 \end{bmatrix} \quad \tilde{B}_{\mathrm{d}} = \begin{bmatrix} B_{\mathrm{d}} \\ 0 \\ 0 \end{bmatrix} \quad \tilde{C} = \begin{bmatrix} C & 0 & 0 \end{bmatrix} \tag{13.12}$$

$$\tilde{K} = \begin{bmatrix} 0 & 0 & 0 & K_{\mathrm{p},w} & 0_{1\mathrm{x}8} & K_{\mathrm{i},w} & 0 \\ 0 & K_{\mathrm{p},c} & 0 & 0 & 0_{1\mathrm{x}8} & 0 & K_{\mathrm{i},c} \\ 0 & K_{\mathrm{p},c} & 0 & 0 & 0_{1\mathrm{x}8} & 0 & K_{\mathrm{i},c} \\ 0 & K_{\mathrm{p},c} & 0 & 0 & 0_{1\mathrm{x}8} & 0 & K_{\mathrm{i},c} \end{bmatrix} \tag{13.13}$$

Note that C_2 and C_4, in Equation 13.12, are the corresponding rows from the output matrix C in Equation 13.10 on page 101. $K_{\mathrm{p},c}$ and $K_{\mathrm{i},c}$ are the feedback control gain, and the integral gain for the collective pitch angle. $K_{\mathrm{p},w}$ and $K_{\mathrm{i},w}$ are the control gain and integral gain for the torque of the generator.

The two PI controllers are augmented in the system, thus the following step is lifting the system which is elaborated in the following section.

Lifting the System

The augmentation of the state space has been performed, resulting in a stabilised closed loop state space system. In order to lift the state space system, the period of the trial, defined as $p \in \mathbb{N}^+$, needs to be determined. According to the repetitive control design, the period length has to be corresponding to the length of the repeating disturbance sequence. The following statements are given for the lifting of the system.

- The system is lifted for one full rotor revolution.
- The trial length p is calculated according to the angular velocity of the rotor (rated value 1.26 rad/s).
- The sampling time of the controller is $Ts_{contr} = 0.0125$ s.

The length of p is calculated as following:

1. Conversion from rad/s to rpm: $1.26 \cdot \frac{30}{\pi} \approx 12.1$ rpm
2. Time one rotor revolution takes: $60/12.1 \approx 4.96$ s
3. Size of $p = \frac{4.96}{0.0125} = 396$

In the case of the wind turbine, the wind disturbance has a repeating behaviour over each rotor revolution leading to the assumptions:

The wind disturbance affecting the system is periodic and constant, for a certain time period.

The angular velocity of the generator, is constant at all time.

The lifting is performed according *System Lifting* explained on Page 93.

Augmenting the System with the Periodic Error

The next step of the repetitive control design algorithm, is to include the error in the control model formulation. This is done by augmenting the state space with the states, corresponding to the error throughout the period. It is described as the difference of the stacked output vector, $\bar{y}_k$ which is composed of the individual blade moments $M_{\mathrm{b},i}$, and the desired reference throughout the trial $\bar{r}_k$. The reference is trial invariant, thus the value zero is considered sufficient for proper results. Consequently, the errors throughout the trials are the blade deviations, given by:

$$\bar{e} = \bar{r}_k - \bar{y}_k = \bar{r}_k - Hx_k + \mathcal{J}_\mathrm{s}\bar{u}_k + \mathcal{J}_\mathrm{d}\bar{d}_k$$

The difference between two trials according to Subsection 13.2 on page 95 is denoted by Δ, thus:

$$\Delta\bar{u}_k = \bar{u}_k - \bar{u}_{k-p}$$
$$\Delta x_k = x_k - x_{k-p}$$

Note that the states are not stacked throughout the trial period, resulting in the difference between the states from one trial to the next, is the difference between the initial conditions of the trials. Though in the case of the inputs, disturbance and outputs, the stacking is performed throughout the period. The wind disturbance is periodic, thus the difference between to periods is given as:

$$\Delta\bar{d}_k = \bar{d}_k - \bar{d}_{k-p} = 0$$

and the error is rewritten as:

$$\bar{e}_k = \bar{e}_{k-p} - H\Delta x_k - \mathcal{J}_\mathrm{s}\Delta\bar{u}_k \tag{13.14}$$

The difference in the initial conditions of the lifted system $\bar{S}$, is found by applying the Δ operator once again according to Equation 13.4 on page 95, thus

$$\Delta x_{k+p} = \Phi\Delta x_k + \Gamma_\mathrm{s}\Delta\bar{u}_k \tag{13.15}$$

By augmenting the determined error, $\bar{e}_k$ in Equation 13.14, into the lifted state space in Equation 13.2, defined with respect to the difference operator Δ in 13.15, the final form of the repetitive control is obtained, as described in Subsection 13.2 on page 95, $\xi_k = \begin{bmatrix}\Delta x_k \\ \bar{e}_k\end{bmatrix}$ being the new state of the system.

$$\bar{S}^{\mathrm{RC}} \begin{cases} \xi_{k+p} & = \bar{\Phi}\xi_k + \bar{\Gamma}_\mathrm{s}\Delta\bar{u}_k \\ \bar{e}_k & = \bar{H}\xi_k + \bar{\mathcal{J}}_\mathrm{s}\Delta\bar{u}_k \end{cases} \tag{13.16}$$

Where:

$$\bar{\Phi} = \begin{bmatrix}\Phi & 0 \\ -H & \lambda I\end{bmatrix} \quad \bar{\Gamma}_\mathrm{s} = \begin{bmatrix}\Gamma_\mathrm{s} \\ -\mathcal{J}_\mathrm{s}\end{bmatrix}$$
$$\bar{H} = \begin{bmatrix}-H & \lambda I\end{bmatrix} \quad \bar{\mathcal{J}}_\mathrm{s} = -\mathcal{J}_\mathrm{s}$$

Note that λ is the forgetting rate, used as tuning parameter in the implementation. It assures stability of the system, thus allows the implementation of an optimal controller on the designed repetitive control system. The design of the optimal controller is discussed following. However, as the order of the system is increased, due to the system lifting and the repetitive error augmentation, a state space reduction is performed in order to minimise it, and at the same time to eliminate the uncontrollable and unobservable states.

Reduction of the Lifted Model

The lifted model is desired to be minimised as much as possible, and still keep the dynamics of the complex model, by means of model reduction. Model reduction is further beneficial for ease of the computational load (the reduced model does also lead to reduced order for the control gain). One method is using the balanced truncation, which uses the Hankel Singular Value Decomposition. An advantage of using singular value decomposition is that the system stability is preserved. To find the Hankel singular values, the controllability and observability gramians of the lifted state space system, augmented with the periodic error, are determined. The implemented method is the balanced truncation based on the square root method. Though there are several square root methods, like the one proposed by [Mathworks, 2013] is used. This method is following described. It relies on finding the singular value decomposition for the controllability and observability matrices separately. The controllability and observability are found by the gramian method by the Lyapunov equation, noted following:

$$\bar{\Phi}\mathcal{P}\bar{\Phi}^T - \mathcal{P}\bar{\Phi}^T + \bar{\Gamma}\bar{\Gamma}^T = 0$$
$$\bar{\Phi}^T\mathcal{Q} + \mathcal{Q}\bar{\Phi} + \bar{H}^T\bar{H} = 0$$

where

- $\bar{\Phi}$ is the lifted augmented state matrix
- $\bar{\Gamma}$ is the lifted augmented input matrix
- $\bar{H}$ is the lifted output augmented matrix
- $\mathcal{P}$ is the controllability gramian
- $\mathcal{Q}$ is the observability gramian

The singular value decomposition is found by

$$\mathcal{P} = U_\mathcal{P}\Sigma_\mathcal{P}V_\mathcal{P}^T = \begin{bmatrix} U_{1\mathcal{P}} & U_{2\mathcal{P}} \end{bmatrix} \begin{bmatrix} \Sigma_{1\mathcal{P}} & 0 \\ 0 & \Sigma_{2\mathcal{P}} \end{bmatrix} \begin{bmatrix} V_{1\mathcal{P}}^T \\ V_{2\mathcal{P}}^T \end{bmatrix}$$
$$\mathcal{Q} = U_\mathcal{Q}\Sigma_\mathcal{Q}V_\mathcal{Q}^T = \begin{bmatrix} U_{1\mathcal{Q}} & U_{2\mathcal{Q}} \end{bmatrix} \begin{bmatrix} \Sigma_{1\mathcal{Q}} & 0 \\ 0 & \Sigma_{2\mathcal{Q}} \end{bmatrix} \begin{bmatrix} V_{1\mathcal{Q}}^T \\ V_{2\mathcal{Q}}^T \end{bmatrix}$$

Where index $_2$ denotes the undesired states of the system, that requires a more energy, than desired, to either observe or control.
The square root of the gramians are found by:

$$L_\mathcal{P} = U_\mathcal{P}\Sigma_\mathcal{P}^{-\frac{1}{2}} \tag{13.17}$$
$$L_\mathcal{Q} = U_\mathcal{Q}\Sigma_\mathcal{Q}^{-\frac{1}{2}} \tag{13.18}$$

Used for the singular value decomposition

$$L_\mathcal{Q}^T \cdot L_\mathcal{P} = U_{\mathcal{Q}\mathcal{P}}\Sigma_{\mathcal{Q}\mathcal{P}}V_{\mathcal{Q}\mathcal{P}} \tag{13.19}$$

which is noted with subscript $_{QP}$. The resulting left and right transformation matrices for the order reduction are:

$$T_\mathrm{l} = L_Q U_{QP} \Sigma_1 Q P^{-\frac{1}{2}}$$
$$T_\mathrm{r} = L_P V_{QP} \Sigma_{QP}^{-\frac{1}{2}}$$

Finally, the balanced truncation of the lifted and augmented state space matrices is performed according to:

$$\widehat{\Phi} = T_\mathrm{l} \Phi T_\mathrm{r}$$
$$\widehat{\Gamma} = T_\mathrm{l} \Gamma$$
$$\widehat{H} = H T_\mathrm{r}$$
$$\widehat{\mathcal{J}} = \mathcal{J}$$

In order to determine the most appropriate order for the model reduction by balanced truncation, several model orders are presented in Figure 13.6, with the dynamics of an arbitrary chosen input to output relation in Figure 13.7.

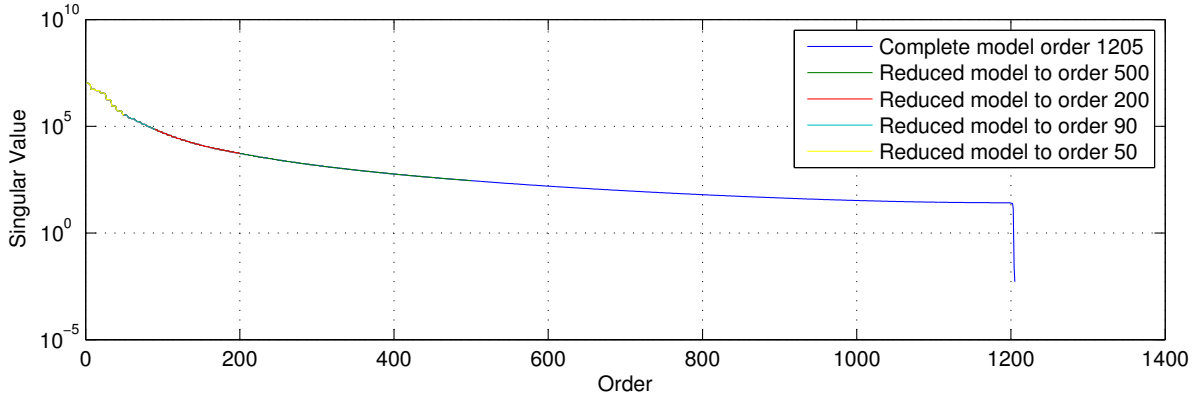

Figure 13.6: Hankel singular values of the lifted augmented system, reduced at different orders.

Figure 13.6 depicts the result of the balanced truncation model reduction technique. According to [Houtzager, 2011], the model order should be cut where a large gap in the Hankel singular values is noted. This is determined by considering the largest Hankel singular values, $\sum_{i=1}^{size(u\to y)} \sigma_\mathrm{i}$ of the relation between the input and output, $\underset{\|u\|\neq 0}{sup} \frac{\|y\|}{\|u\|}$. This approach guarantees the elimination of the uncontrollable and unobservable states of the system. Though to be sure that the dynamics are kept, a Bode diagram of the resulting model is considered.

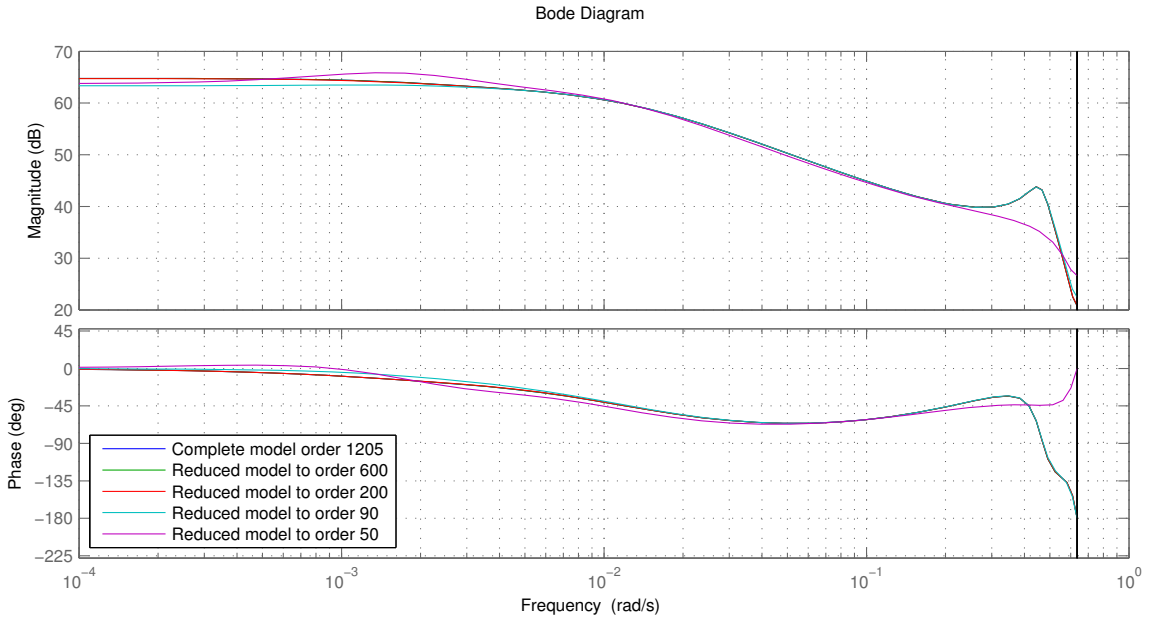

Figure 13.7: Bode diagram of the developed control model with respect to different order reductions.

The Bode diagram shows the results of model reduction for the repetitive control model presented on Page 104. Note that due to the size of the lifted system, 1205 inputs and outputs, the bode plot of an arbitrary input to an arbitrary output is presented in Figure 13.7. Though, several Bode diagrams have been examined, it is considered irrelevant to include them, due to the fact that they resemble the same differences due to model reduction as noted in Figure 13.7. To determine the order at which the lifted system can be reduced, a compromise is made between the size of the system, and its resemblance to the original full order model. Thus, the reduced model order is chosen as 90, noted by the cyan line, due to the resemblance of the original model as depicted in Figure 13.7. It is noted that for a model order lower than this, does not give good resemblence of the original. Consequently the chosen reduction order is considered optimal in the present case.

Optimal Control Design

The model reduction is complete, thus following, the implementation of an optimal controller is presented. The purpose of the controller is to minimise the error (deviation of the output of the linear plant model, from its reference point) and drive it to zero as time goes to infinity. When determining the appropriate controller, it is noted that the designed control model is of a high order MIMO system, thus only MIMO control structures are considered. As presented in the repetitive control design in Section 13.2 on page 92, the LQR controller leads to proper results, as proven through the implementation example of the pitch system in Section 13.3 on page 97. Consequently, an LQR design in combination with a Kalman filter is implemented as depicted in Figure 13.8. The Kalman filter, elaborated in Chapter 10 on page 67, is used for estimation of the unmeasured states, as these are needed in the repetitive control design.

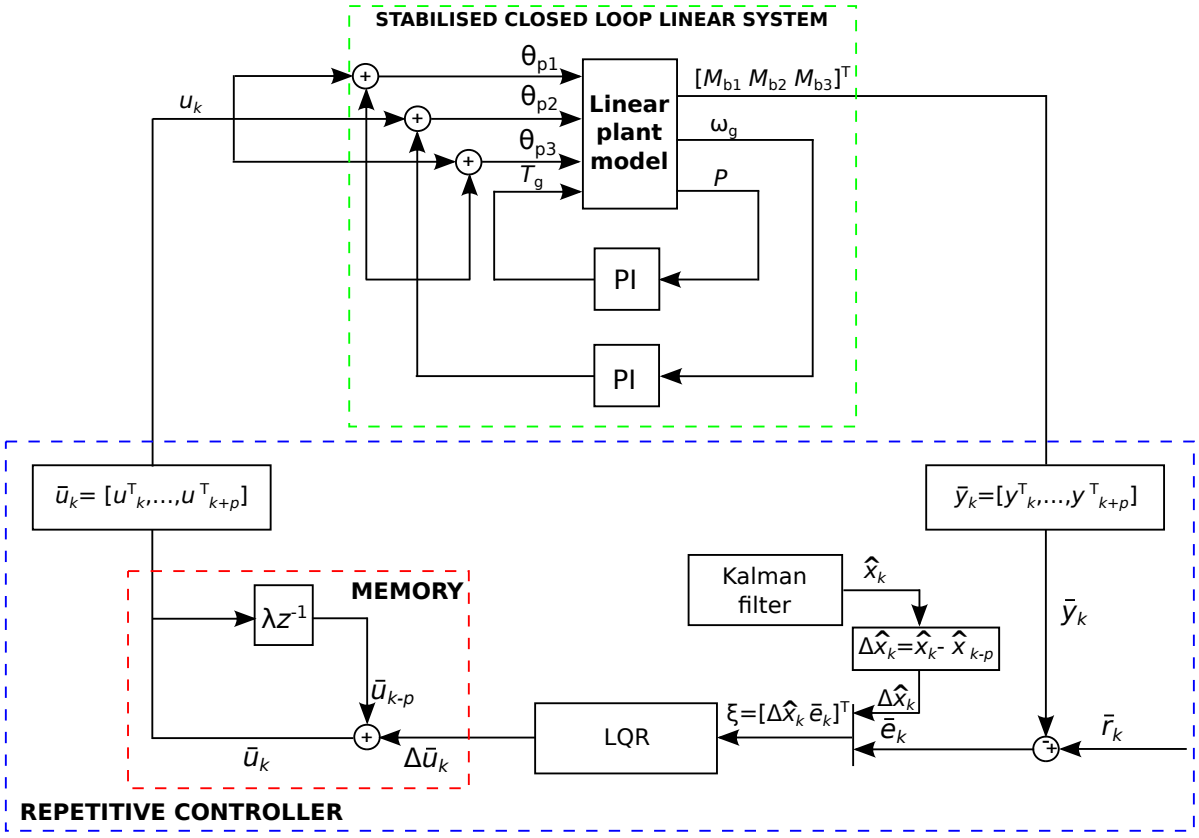

Figure 13.8: Lifted Repetitive control design scheme with LQR control and Kalman filter.

The LQR controller minimises the cost function:

$$J = \lim_{p\to\infty} \sum_{k=0}^{p-1} \left(\xi_k^T Q \xi_k + \Delta \bar{u}_k^T R \Delta \bar{u}_k \right) \tag{13.20}$$

In general the LQR controllers weighting matrices, Q and R are design with respect to Bryson's rule [Franklin et al., 2006, p.493]. This states that the weighting matrices have to be diagonal matrices with the elements determined according to:

$$Q = \frac{1}{max(\xi_j^2)} \tag{13.21}$$

$$R = \frac{1}{max(\Delta \bar{u}_l^2)} \tag{13.22}$$

Where $j \in \{1,2,...,s\}$ is the number of the corresponding state and s is the number of states in the system. $l \in \{1,2,...,o\}$ is the number of the input and o is the number of inputs of the system. Though Bryson's rule often gives good results, this approach cannot be used in the present case, due to the large size of inputs and outputs. Consequently, empirical tuning of the weighing matrices is performed, resulting the following values that are considered optimal for this design.

$$Q = I_{sxs} \cdot 10e-4$$
$$R = I_{oxo} \cdot 5e9$$

The control strategy used for control of the linear wind turbine model, developed in Chapter 6 on page 43, is elaborate, thus in the following part, the results of the simulation in `MATLAB` and `Simulink` environments are presented.

Controller Evaluation

In order to evaluate the performance of the repetitive controller, several tests are considered. The tests are run on the linear wind turbine plant model described in Chapter 6 on page 43. As the sensors for measuring the states are corrupted by noise, the Kalman state estimator is used throughout the simulations as presented in Chapter 10 on page 67. Throughout the tests the following are examined:

1. The repetitive controllers learning capabilities.
2. The repetitive controllers capabilities of minimising the loads on the structure and mechanism of the turbine.
3. The repetitive controllers robustness towards noise.

The first test is chosen in order to investigate the implemented memory and learning capability of the controller. This is carried out by running a simulation of the system, with the repetitive controller switched on and off several times. Note that as the repetitive controller is designed using the stabilised closed-loop system by the controllers presented in Chapter 11 on page 73, the resulting control signal is added to the collective pitch control signal. Consequently, when switching off the repetitive controller, the collective pitch controller solely generates the control signal. Figure 13.9(a) presents the control signal throughout the simulation. In the first period, the repetitive controller is switched on until 70 seconds, and switched off on the interval from 70 to 120 seconds. In the last part the repetitive controller it is switched on again, thus it needs to compensate for the error that the collective pitch controller did not minimised. This is noted as an overshoot in the system outputs in Figures 13.9 and 13.10. The improvement to the system dynamics, by using the designed repetitive controller scheme compared to the collective pitch controller, is visible throughout the figures. Furthermore, the repetitive controller is learning continuously and is aware of the systems error even when it is not controlling the system, thus as active, it can overcome it in a short period of time.

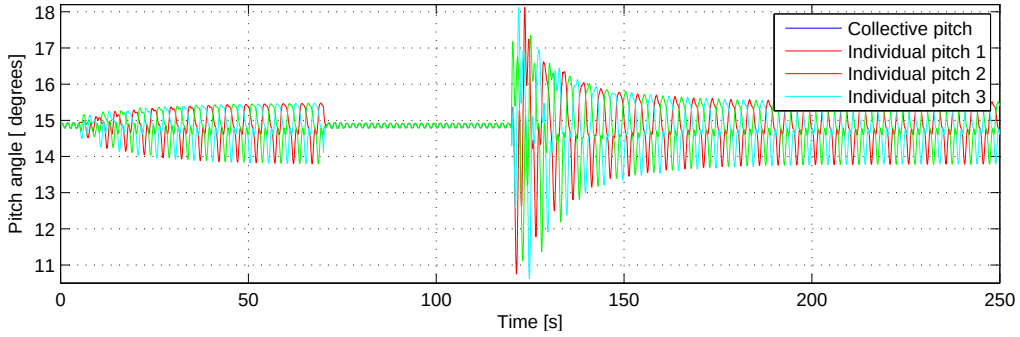

(a) Control input for the pitch actuators when running the memory test for the repetitive controller on the linear plant model.

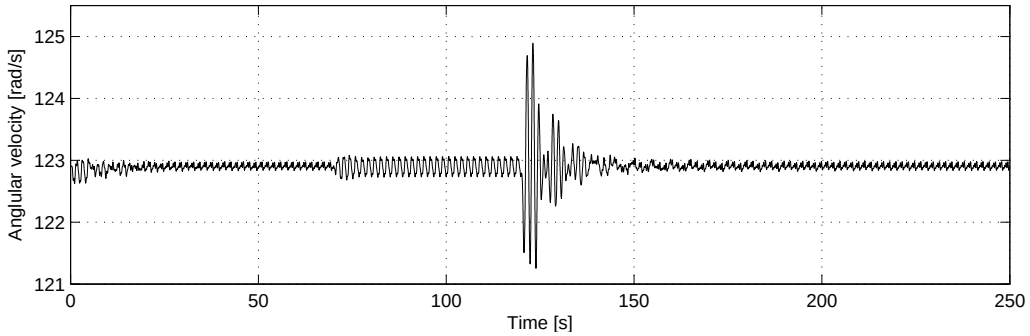

(b) Angular velocity of the generator output of the linearised model for verifying the memory of the repetitive controller.

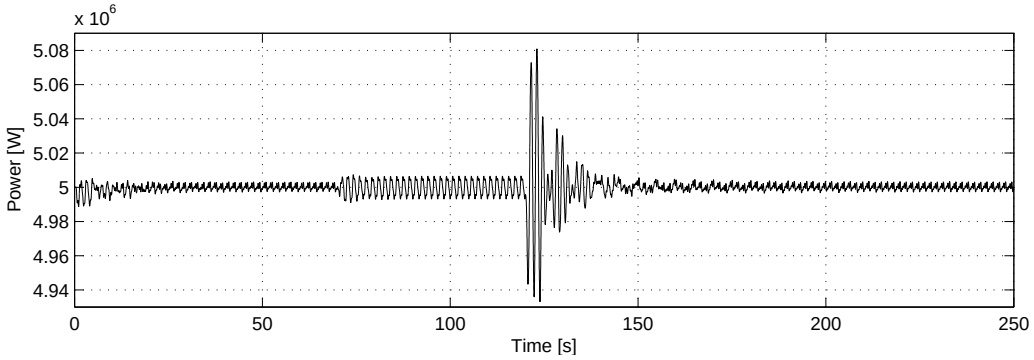

(c) Power output of the linearised model for verifying the memory of the repetitive controller.

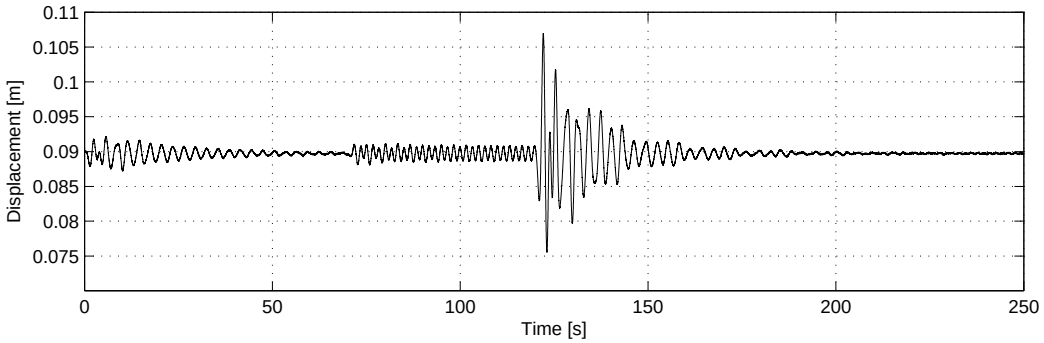

(d) Tower displacement output of the linearised model for verifying the memory of the repetitive controller.

Figure 13.9: Results for the repetitive controller implemented on the linear plant model.

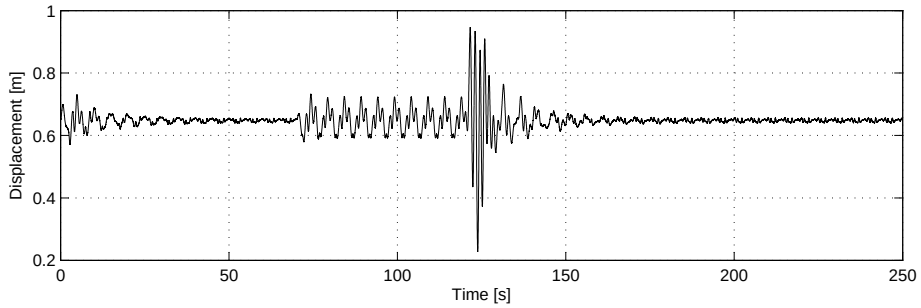

Figure 13.10: Blade 1 tilt-wise displacement of the linearised model for verifying the memory of the repetitive controller.

For the second test it is desired to investigate the implemented repetitive controller performances, with respect to the collective pitch controller designed in Chapter 11 on page 73. The wind model used in this test is composed of wind shear, tower shadow and wake, as presented in Chapter 3 on page 25. The result of the test should illustrate whether the repetitive controller is able to improve the overall system performances. The results are displayed for smaller time intervals, in order to visualise the differences. Figure 13.11(a) depicts the control input of the system. The repetitive controller generates individual pitch signals, with respect to the error stacked throughout the previous trial, while the collective pitch controller generates the same control signal for all the pitch actuators. In Figure 13.11(b) and 13.11(c), the angular velocity and power output are depicted. As noted, by using the repetitive controller scheme, the deviation from the reference point is minimised significantly.

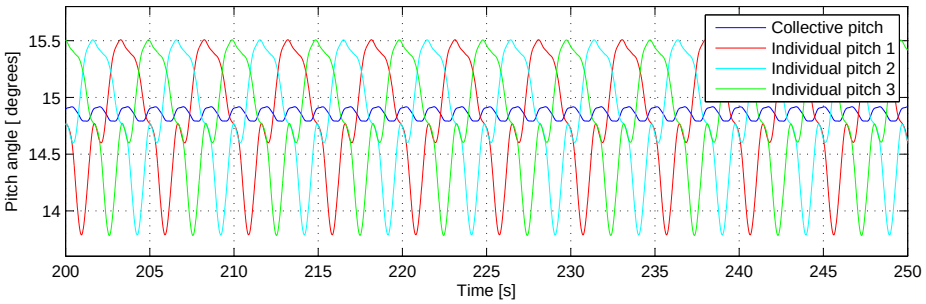

(a) Control input for the linear plant model, when comparing the repetitive controller with the collective pitch control.

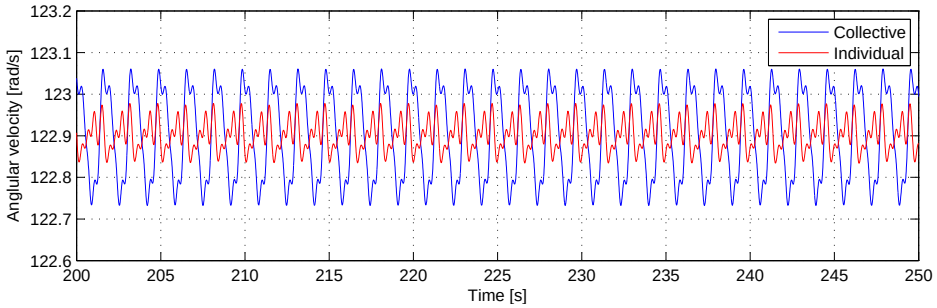

(b) Angular velocity of the generator for the repetitive controller compared with the collective pitch control, run on the linear plant model.

Figure 13.11: Results for the repetitive controller implemented on the linear plant model.

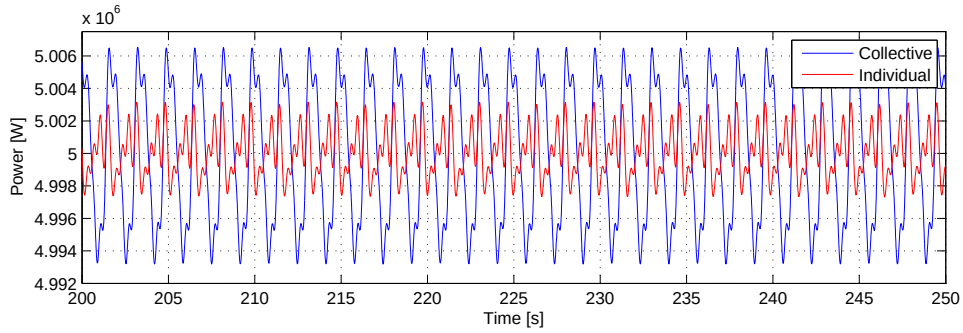

Figure 13.12: Power output of the linear plant model when comparing the repetitive controller with the collective pitch control.

In Figure 13.12(a), the variation in the tower displacement is noted to be minimised considerably by using the repetitive controller. The controller is designed to compensate for the blades bending moments, thus the main minimisation of the error is visible for the displacement of the blades, as depicted in Figure 13.12(b).

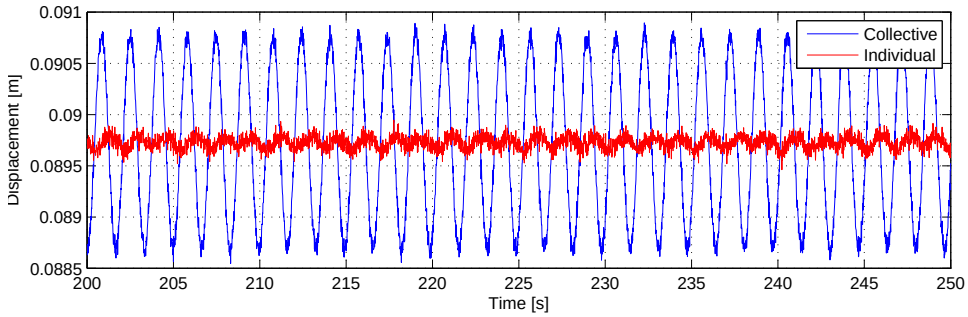

(a) Tower displacement of the linearised model when comparing the repetitive controller with the collective pitch control.

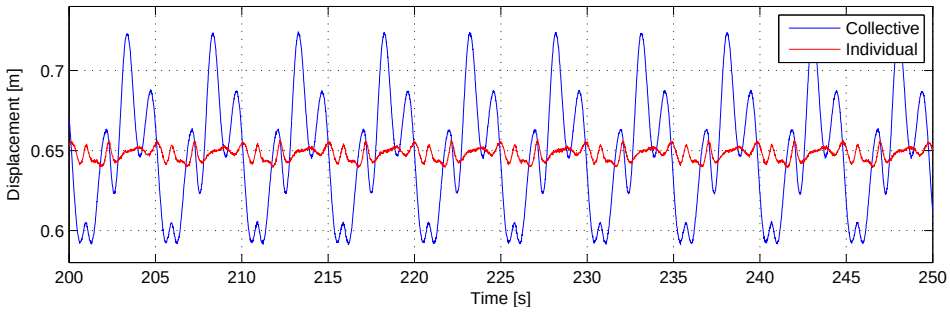

(b) Blade 1 tilt-wise displacement of the linearised model, when comparing the repetitive controller with the collective pitch control.

Figure 13.13: Results for the repetitive controller implemented on the linear plant model.

In the third test it is of interest to investigate whether the repetitive controller is able to provide proper results, if the disturbance affecting the system is corrupted by noise. Note that in the repetitive controller design, the robustness towards noise has not been considered. In order to verify this, the wind turbulence is added to the wind profile as noise source for the system. The results are compared once again to the collective pitch controller. As noted in Figure 13.13(a), the control signal for the individual pitch control,

is generated by the designed repetitive controller. By considering the outputs of the system, it is noted that the repetitive controller is not capable of minimising the error in the case of the parts of the wind turbine affected by the 3P loads, like the tower structure and mechanism of the turbine. Consequently the angular velocity of the generator, the mechanical power and the tower displacement are not affected by the repetitive controller as depicted in Figures 13.13(b), 13.13(c) and 13.14(a). The only minimised error is in the case of the blade displacement, affected by the 1P loads, as depicted in Figure 13.14(b).

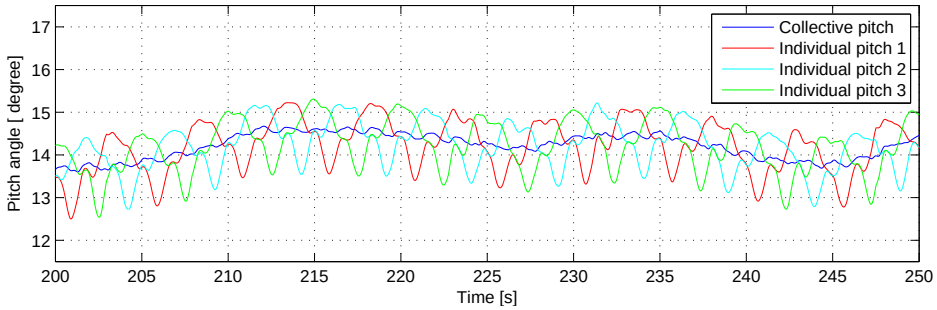

(a) Control input for the linear plant model when comparing the repetitive controller with the collective pitch control.

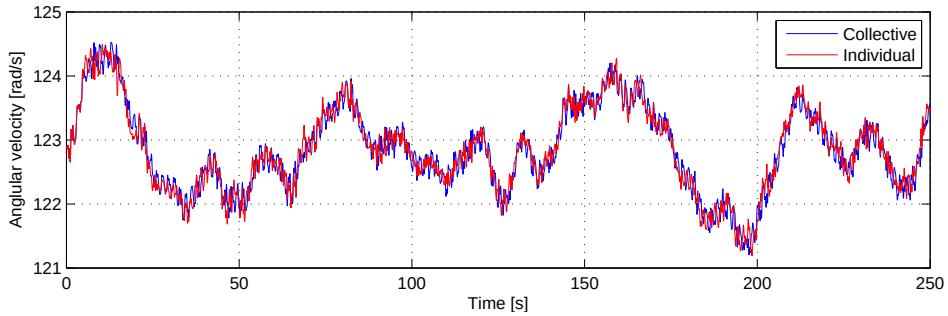

(b) Angular velocity of the generator output of the linear plant model, when comparing the repetitive controller with the collective pitch control.

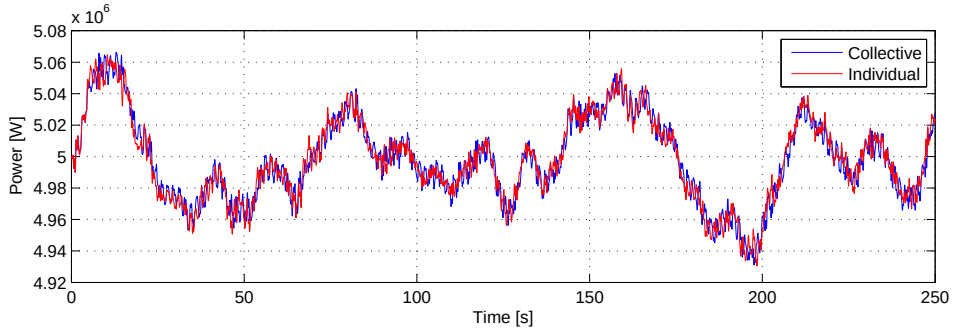

(c) Power output of the linear plant model, when comparing the repetitive controller with the collective pitch control.

Figure 13.14: Results of the comparison between the collective and individual controller, affected by a turbulent wind.

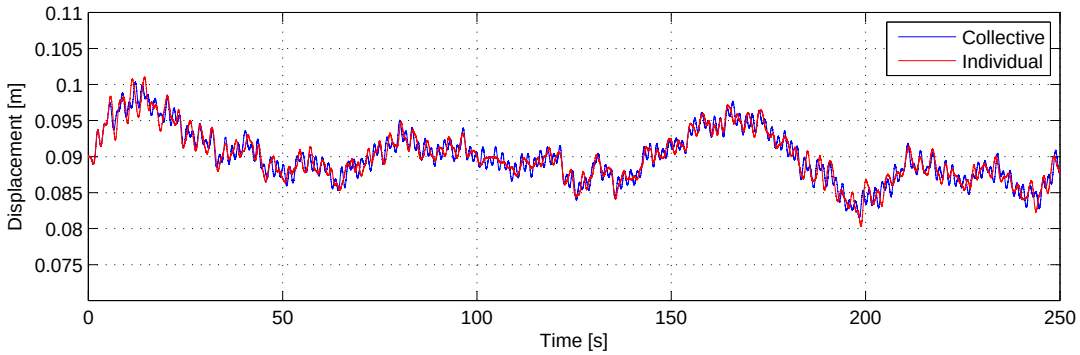

(a) Tower displacement output of the linear plant model when comparing the repetitive controller with the collective pitch control.

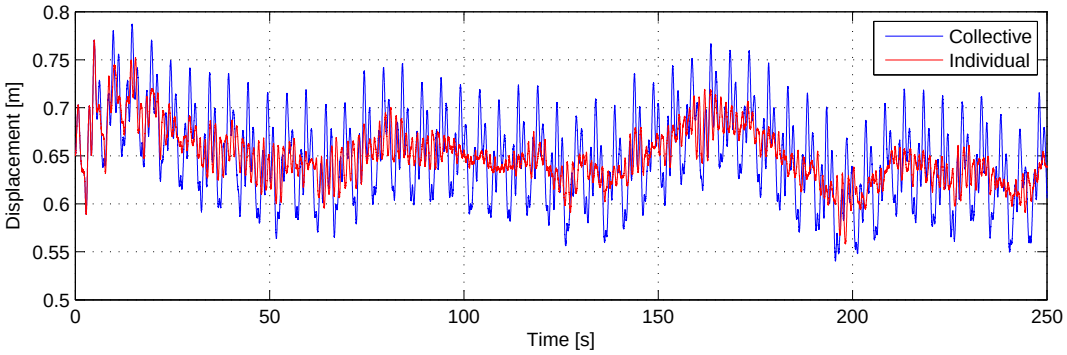

(b) Blade one tilt-wise displacement, when comparing the repetitive controller with the collective pitch control implemented on the linear plant model.

Figure 13.15: Results for the tower and blade displacements when comparing the collective and the repetitive controller on the linear plant model.

According to the tests, it is concluded that the repetitive controller outperforms the collective pitch controller, presented in Chapter 11 on page 73. Moreover, the learning capabilities of the controller are tested and proven working. The implementation is a success, thus the error is minimised accordingly. It is noted that the statement: *The error converges to zero as time goes to infinity*, is not fulfilled. From the control input it is noted that it stabilises after a certain time interval, thus providing the optimal signal for the pitch actuators. However, due to the limitation of the pitch actuators the repetitive controller is restricted, consequently the error cannot be entirely eliminated.

In the following a last test is performed. The purpose is to determine the efficiency of the designed repetitive controller scheme with respect to the multi-bladed coordinate transformation presented in Chapter 12 on page 79 method designed as well for Individual pitch purposes. The comparison includes the collective pitch controller for a final comparison of all the control strategies implemented throughout the project.

Due to the fact that both multi-bladed coordinate transformation and repetitive controller are individual pitch control methods, the control signal from the two strategies are presented in Figures 13.15(a) and 13.15(b), respectively. It is noted that the control signals have approximatively the same amplitude, thus the same pitch actuation is present, leading to the same degradation of the actuators. The only difference

lies in the fact that the control signal generated by the repetitive controller is shifted to the negative side as it learns the effect of the wind disturbance on the system.

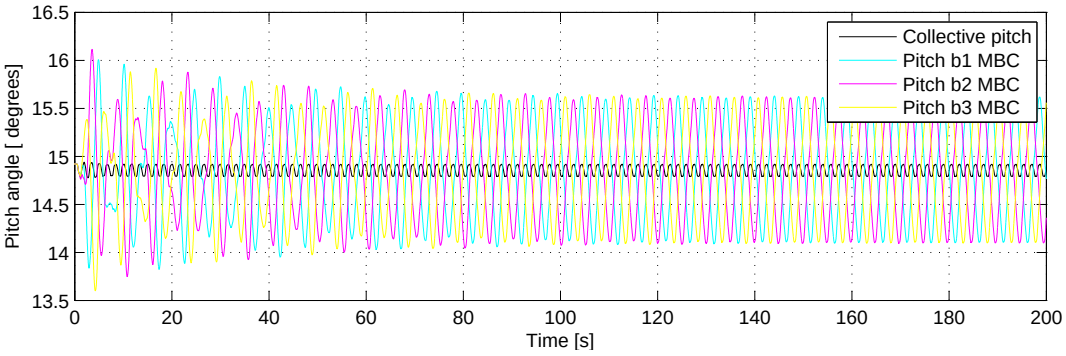

(a) Control signal generated by multi-bladed coordinate transformation.

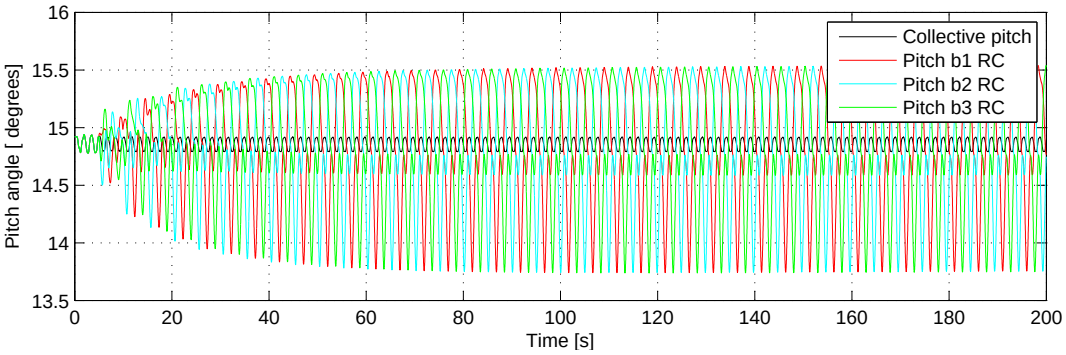

(b) Control signal generated by repetitive controller (RC).

Figure 13.16: Resemblance of the multi-bladed control signal and the repetitive control signal, compared to the collective pitch control.

The performance of the repetitive controller with respect to the multi-bladed coordinate transformation, in the case of the 3P loads, is noted in the following figures. The multi-bladed coordinate transformation improves the performance of the linear plant system, while it does not take the 3P loads into account. This is due to the fact that the multi-bladed coordinate transformation is designed and used to only minimise the 1P loads, corresponding to the loads on the blades, resulting in blade displacements. The repetitive controller is design to minimise all the harmonics of the disturbances iterated through the structure and mechanism of the turbine, as the 3P frequency and its higher order harmonics. Thus, the angular velocity of the generator, power output and tower displacement, are also minimised by the repetitive controller, as depicted in Figures 13.16(a) on the following page, 13.16(b) on the next page and 13.17(a) on page 119.

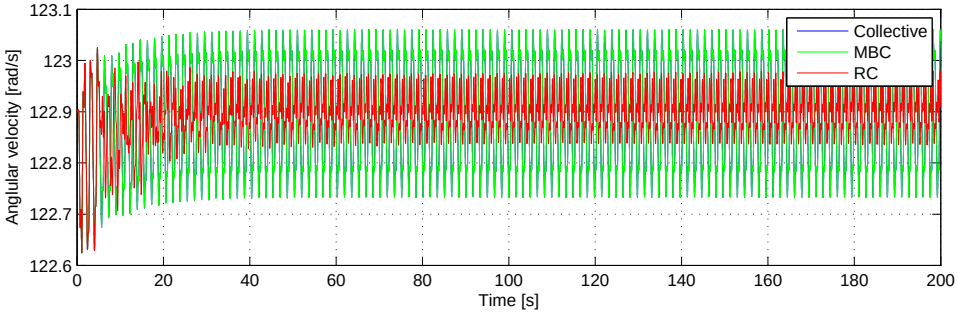

(a) Comparison of the three control strategies for the angular velocity of the generator output of the linear plant model.

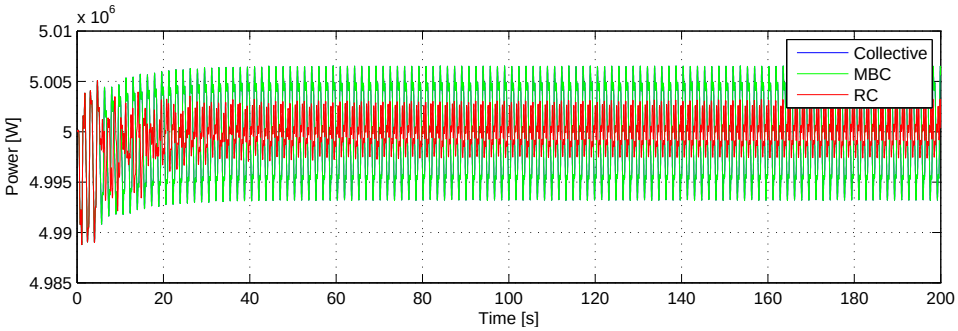

(b) Comparison of the three control strategies for the power output of the linear plant model.

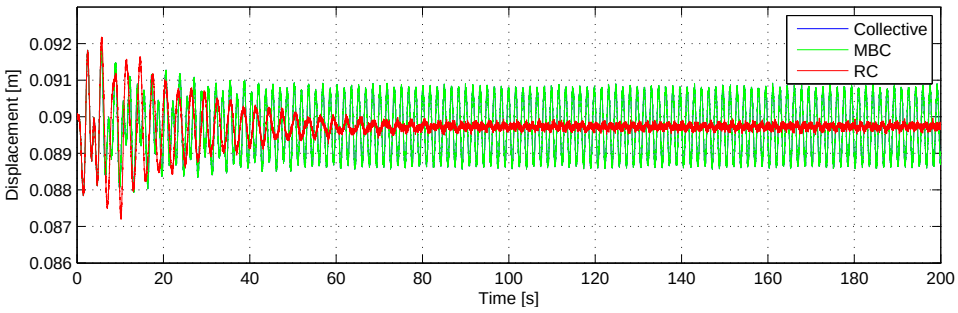

(c) Comparison of the three control strategies for the tower displacement output of the linear plant model.

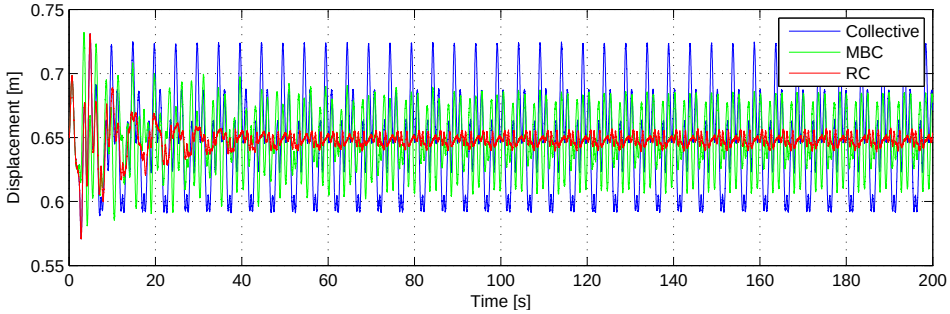

(d) Comparison of the three control strategies for the first blade tilt-wise displacement output of the linear plant model.

Figure 13.17: Results for angular velocity of the generator, power output, tower and blade displacement dynamics caused by the collective and individual controller implemented on the linear plant model.

In the case of the blade displacement, presented in Figure 13.17(b), the designed repetitive controller scheme, outperforms the multi-bladed coordinate transformation, and minimises the blade deflection.

In order to determine whether the repetitive controller is minimising all the harmonics of the error, the power spectral density of the first blades tilt-wise bending moment is illustrated in Figure 13.18. It is noted that the multi-bladed coordinate transformation minimises and eliminates the 1P frequency, according to its design purpose. Furthermore, the repetitive controller minimises the 1P frequency and all its harmonics as desired. As noted in the figure, the 1P frequency is not minimised as much as in the case of the multi-bladed controller, due to the system limitations.

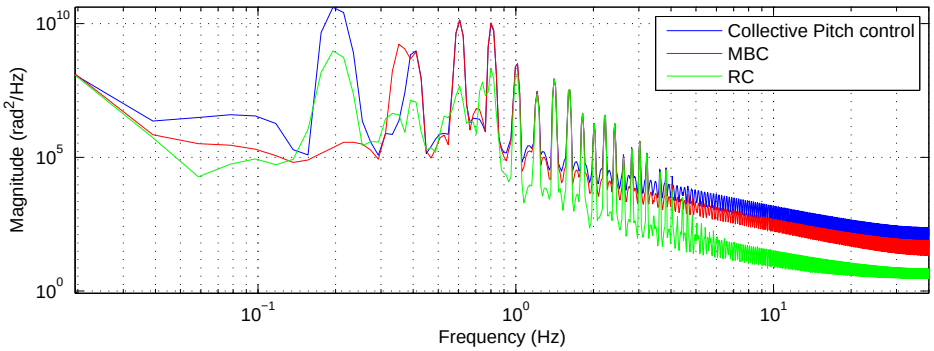

Figure 13.18: Power spectrum density of the blade bending moment for the collective pitch control, multi-bladed controller (MBC) and the repetitive controller (RC).

13.5 Conclusion

With respect to the results of the simulation noted in *Controller Evaluation* on Page 110, the designed repetitive controller is able to learn the error, caused by the repetitive disturbance that is affecting the system. It minimises the deflection of the blades, present as 1P load, for which it is designed. Further it minimises the effect of the wind disturbance iterated as the 3P loads throughout the tower and mechanism of the turbine. As noted, it outperforms both; the collective pitch controller, designed with the purpose of stabilising the power and angular velocity, while keeping them at their respective reference values, and the multi-bladed coordinate transformation, designed to minimise the blade deflection error caused by the 1P loads. Due to the system limitations, the repetitive controller does not drive the error to zero as time goes to infinity, though it does still improve the performance of the system. It is concluded that the implementation is a success.

Considering the assumptions on Page 103, it is concluded that the first assumption, regarding the disturbance, is satisfied, as the wind is periodic with period p. The second assumption is violated, as the angular velocity of the generator is not kept constant, it has small fluctuations from the desired reference value. Even in the presence of these oscillations, the stacking is not corrupted. The third assumption is satisfied, as the repetitive control algorithm is able to learn the error for an entire rotor revolution.

As the efficiency of the designed repetitive controller, with respect to the multi-bladed coordinate transformation is proven, the implementation of the multi-bladed coordinate transformation is neglected in the acceptance test.

Part IV

Epilogue

14 ACCEPTANCE TEST

14.1 Introduction

In order to run and validate the acceptance tests, the designed repetitive controller in Chapter 13 on page 91 for the developed linear states space system in Chapter 6 on page 43, evaluated in Subsection 13.4 on page 110, is following implemented on the nonlinear NREL FAST 5 MW wind turbine model, discretised by Zero-Order Hold. Note that for the tests, the sensor noise is not included. The corresponding `Simulink` implementation is depicted in Appendix H on page 175.

For the first test it is desired to investigate the performance of the controller in the neighborhood of the linearisation point, presented in Chapter 7 on page 47, namely at the wind velocity of 18 m/s. To perform this test, a wind profile is created using *TurbSim*, composed of a mean wind velocity of 18 m/s, wind shear and tower shadow, used to drive the system towards a repetitive behavior, upon which the performances of the developed repetitive controller in Chapter 13 on page 91 are tested. Because the FAST 5MW model only allows to extract the wind at hub height, the wind profile is not presented as it would be a straight line at 18 m/s. However the loads due to the wind shear and tower shadow can be seen in the tower and blade deflection of the wind turbine. The results of the implementation are presented in the following figures. Note that the investigated outputs are with respect to the project requirements, presented in Chapter 2 on page 15. It is further desired to investigate the stress on the tower tilt-wise displacement. Due to the fact that the collective pitch controller, designed by NREL, takes approximatively 100 seconds to stabilise at 18 m/s, all of the following tests results are considered from 100 seconds.

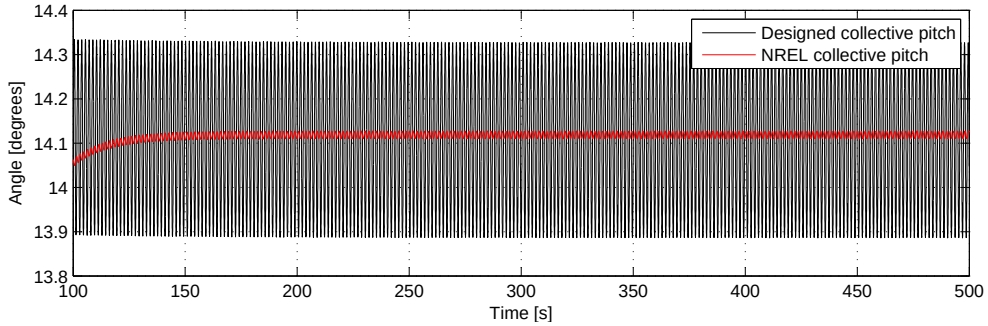

(a) Control signal for the collective pitch control.

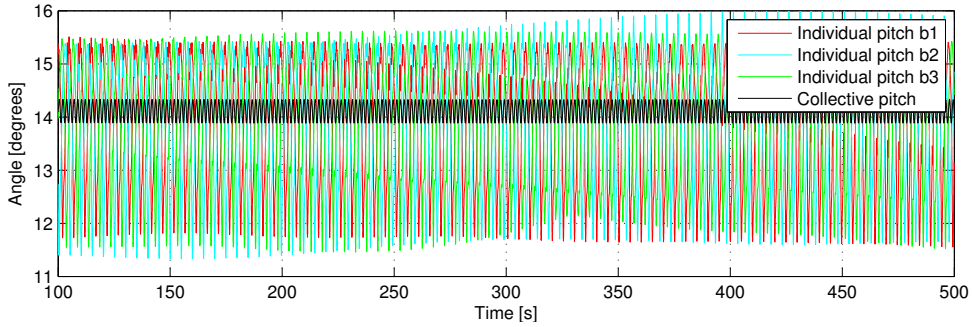

(b) Control signal for the collective and individual pitch control.

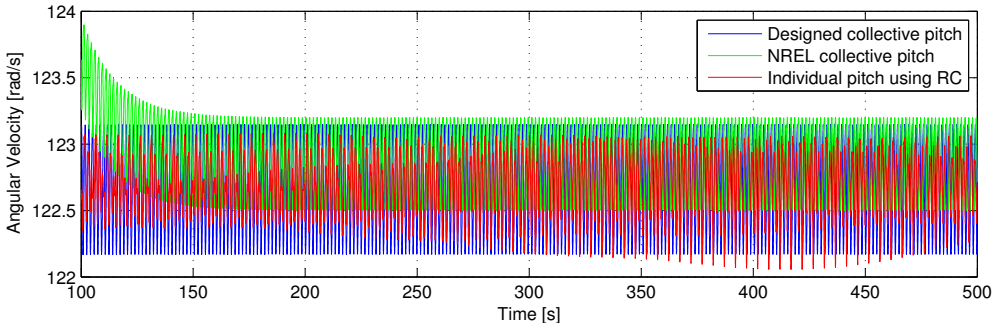

(c) Angular velocity of the generator.

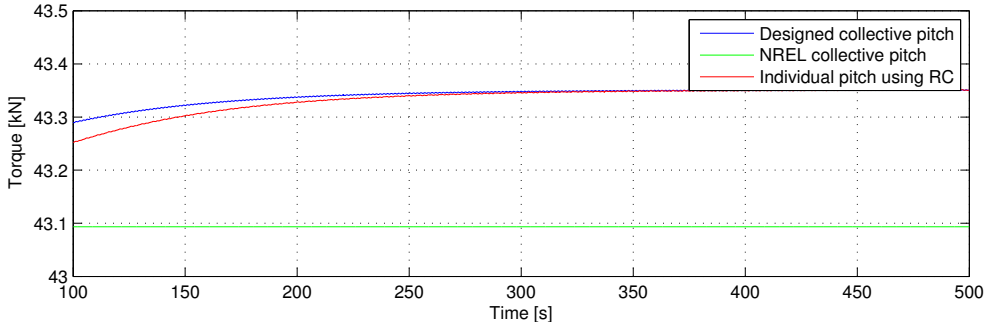

(d) Torque of the generator.

Figure 14.1: Results of the comparison of the designed collective pitch controller in Chapter 11 on page 73, and the NREL collective pitch controller, implemented on the nonlinear FAST 5 MW wind turbine model.

It is noted from the comparison between the collective pitch actuation using the developed collective pitch controller, and the NREL collective pitch controller in Figure 14.1(a), that the designed controller has a higher oscillation amplitude. Consequently, the actuation is more severe, which can be due to a mismatch between the pitch models or because the high integrative effect of the designed collective pitch controller. Furthermore, by comparing the collective pitch control, and the repetitive controller designed throughout the project and implemented on the FAST model, it is noted that the repetitive controller generates individual pitch signals, in order to encounter the deviation of the blades tilt-wise deflection.

By considering the outputs of the NREL 5 MW model, it is noted that by using the designed collective pitch controller and the repetitive controller scheme, the angular velocity of the generator stabilises at the same value, as in the case of the basic NREL collective pitch controller as displayed in Figure 14.2(a). By a closer inspection, it is noted that in fact, by using the designed repetitive controller, the error is slightly minimised, compared to the basic collective control, used by the FAST model. The generator torque, displayed in Figure 14.2(b), is not kept constant at the desired reference value of 43 kN. This is due to the fact that in the present project, the deviations in the output power are counteracted by the generator torque, resulting in a steady power output noted in Figure 14.3.

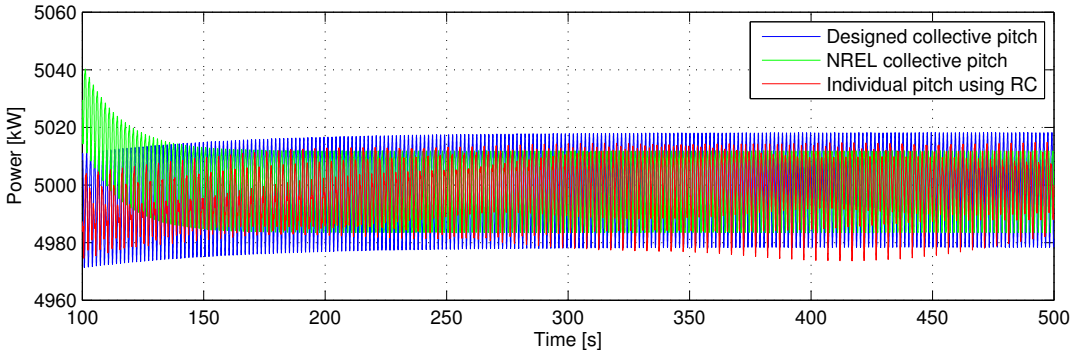

Figure 14.2: Power output for comparing the designed collective pitch controller from Chapter 11 on page 73, the NREL collective pitch controller, and the designed repetitive controller from Chapter 13 on page 91, implemented on the nonlinear FAST 5 MW wind turbine model.

In the case of the power output presented in Figure 14.3, the performance of the repetitive controller is similar to the performance of the NREL collective pitch controller, while the designed collective pitch controller tends to oscillate at a higher amplitude. This may be due to the strong integral effect of the PI controller, used to stabilise the power. Another reason could be model mismatches.

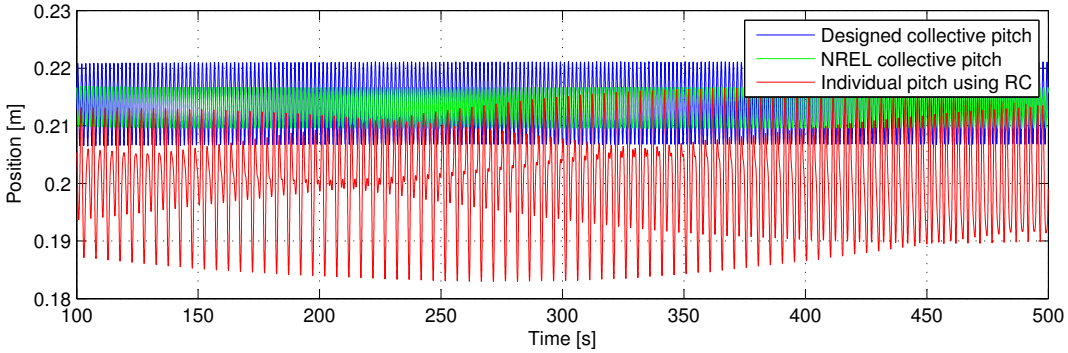

Figure 14.3: Tower tilt-wise displacement for comparing the designed collective pitch controller in Chapter 11 on page 73, the NREL collective pitch controller, and the designed repetitive controller in Chapter 13 on page 91, implemented on FAST 5 MW wind turbine model.

Regarding the tower deflection, presented in Figure 14.4, it is noted that in the case of the repetitive controller, it is more severe than in the case of the collective pitch controllers. The reason for this could be due to tower and blade modeling mismatches between the linearised and the nonlinear FAST model. When looking at the blade displacement depicted in Figure 14.5, it is noted that the performances of the designed collective pitch controller and the FAST collective pitch controller are similar, thus the same fatigue is present. In the case of the designed repetitive controller, this fatigue is minimised as expected.

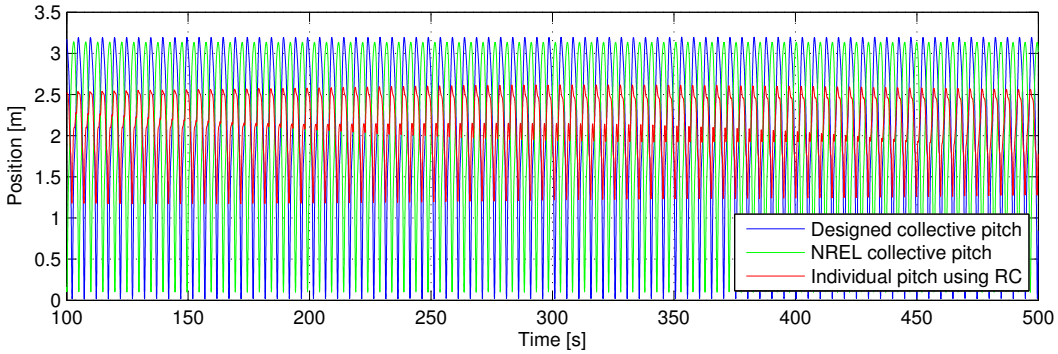

Figure 14.4: Blade one tilt-wise displacement for comparing the designed collective pitch controller in Chapter 11 on page 73, the NREL collective pitch controller, and the designed repetitive controller in Chapter 13 on page 91, implemented on FAST 5 MW wind turbine model.

As the project requirements, presented in Chapter 2 on page 15, are with respect to the above rated region of the wind turbine: from a wind velocity of 11.4 m/s to 25 m/s, a new set of tests is run with a wind profile, increasing from 12 m/s to 24 m/s by steps of 3 m/s. Moreover, the profile contains wind shear and tower shadow, and is presented in Figure 14.6. As it is only possible to extract the wind at hub height, from the nonlinear NREL 5 MW model, the wind profile depicted only contains the mean wind. The wind shear and tower shadow effects are visible in the tower and blades displacement. Due to the fact that when using the collective pitch controller designed by NREL it takes approximatively 70 seconds to startup, the wind turbine and reach the third region of operation, in all of the following tests, the results are considered form 70 seconds.

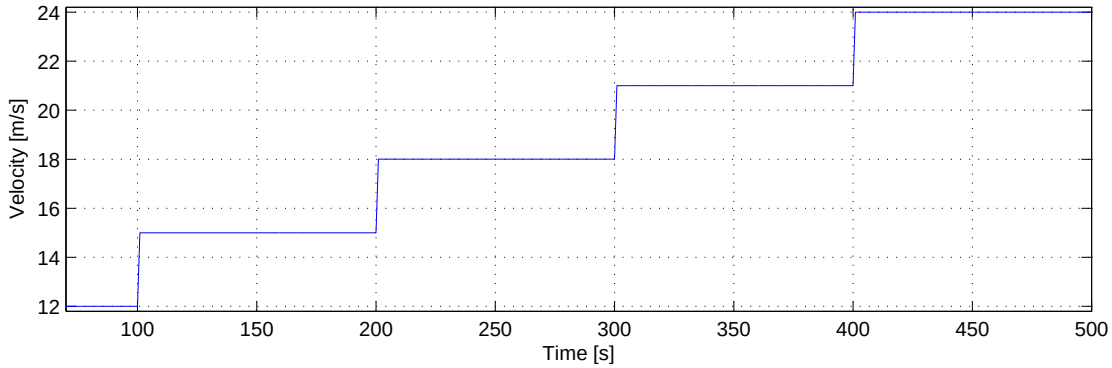

Figure 14.5: Wind profile used for comparing the designed collective pitch controller in Chapter 11 on page 73, the NREL collective pitch controller, and the designed repetitive controller in Chapter 13 on page 91, implemented on the nonlinear FAST 5 MW wind turbine model

Figures 14.7(a) and 14.7(b) present the evolution of the pitch signals with respect to the wind profile. By investigating Figure 14.7(a) it is noted that the most accurate match between the developed collective pitch controller for the model and the one designed by NREL, is at 14.94°, corresponding to the linearisation point of the model. As the wind velocity deviates from the linearisation point, 18 m/s, as much the deviation from the desired pitch angle increases. In the case of Figure 14.7(b) it is noted that the pitch angle, corresponding to the designed collective pitch controller and the designed individual pitch resulting, is individual by use of the developed repetitive controller scheme.

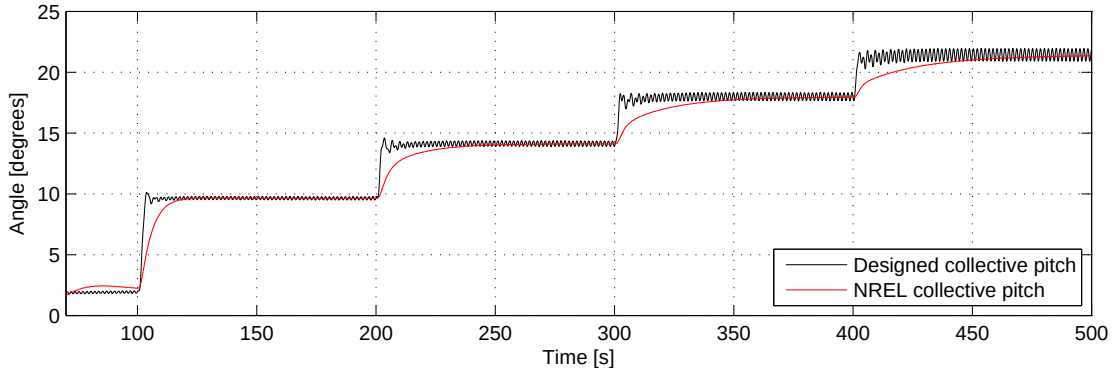

Figure 14.6: Control signal for comparing the designed collective pitch controller in Chapter 11 on page 73, and the NREL collective pitch controller, implemented on the nonlinear FAST 5 MW wind turbine model operating in above rated region (12 to 24 m/s).

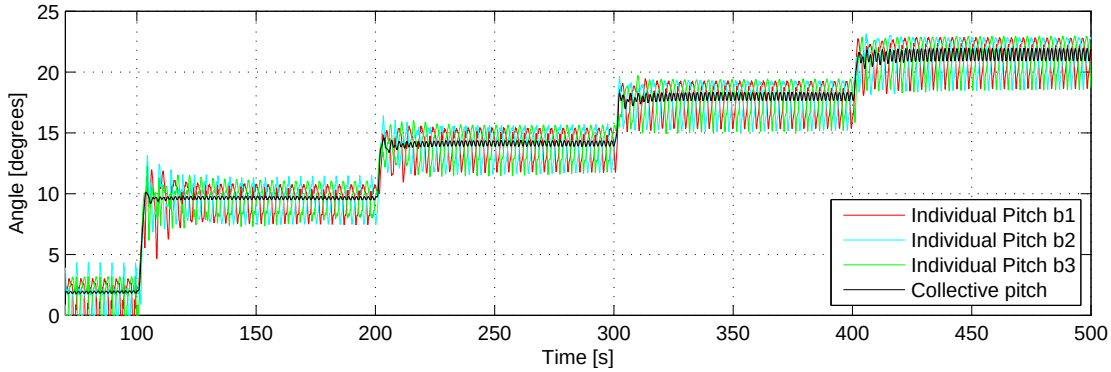

Figure 14.7: Control signal for comparing the designed collective pitch controller in Chapter 11 on page 73, and the designed repetitive controller in Chapter 13 on page 91, implemented on the nonlinear FAST 5 MW wind turbine model operating in above rated region (12 to 24 m/s).

The angular velocity of the generator, presented in Figure 14.8(a), does not have as high overshoot for the designed collective pitch controller and the designed repetitive controller, as for the collective pitch controller designed by NREL. This can be considered as an improvement, and may be a result of the more severe pitch actuation. In the case of the generator torque, displayed in Figure 14.8(b), a deviation from the desired constant generator torque is noted for the designed collective and the designed individual pitch controller. This is caused by the power control design, as a result of the severe deviation of the output power which is counteracted by the generator torque. Consequently at a high increase in the angular velocity of the generator, in order to keep the power constant, the generator torque has to be decreased and vice-versa.

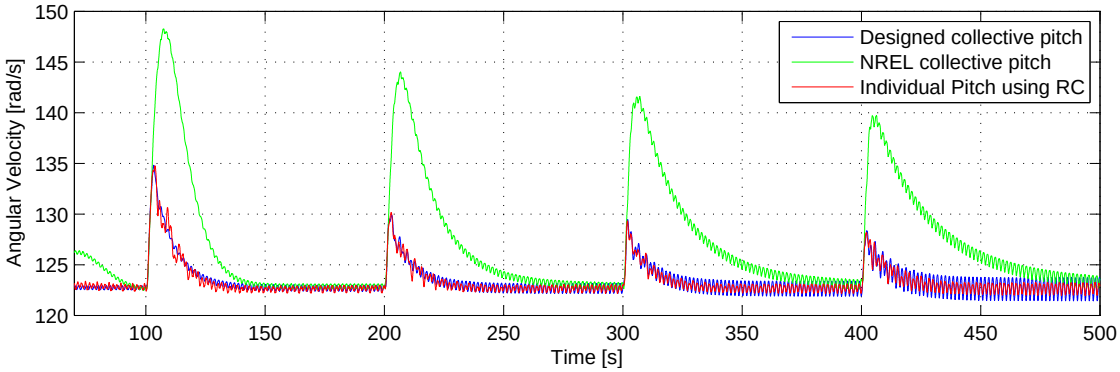

Figure 14.8: Angular velocity of the generator for comparing the designed collective pitch controller in Chapter 11 on page 73, the NREL collective pitch controller, and the designed repetitive controller in Chapter 13 on page 91, implemented on the nonlinear FAST 5 MW wind turbine model operating in above rated region (12 to 24 m/s).

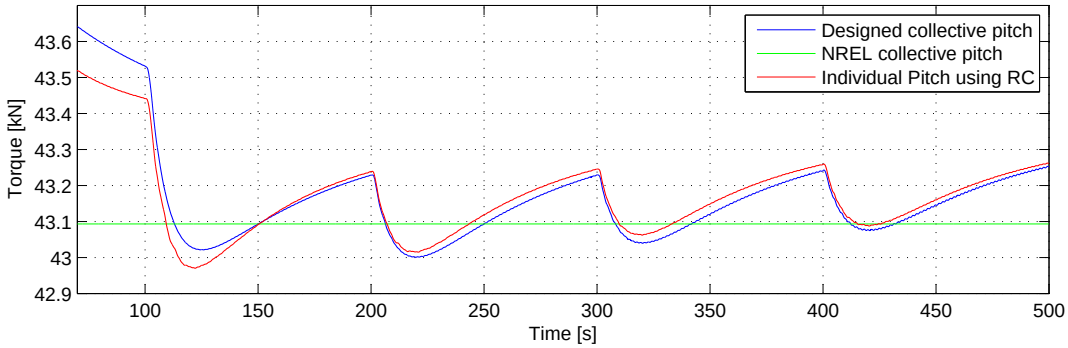

Figure 14.9: Torque of the generator for comparing the designed collective pitch controller in Chapter 11 on page 73, the NREL collective pitch controller, and the designed repetitive controller in Chapter 13 on page 91, implemented on the nonlinear FAST 5 MW wind turbine model operating in above rated region (12 to 24 m/s).

The output power, presented in Figure 14.9, presents high overshoots in the case of the NREL collective pitch controller, whereas the designed collective pitch controller and repetitive controller schemes, tend to diminish the overshoot. Moreover, by using the developed repetitive control scheme, the steady-state error is also minimised compared to the existing controller.

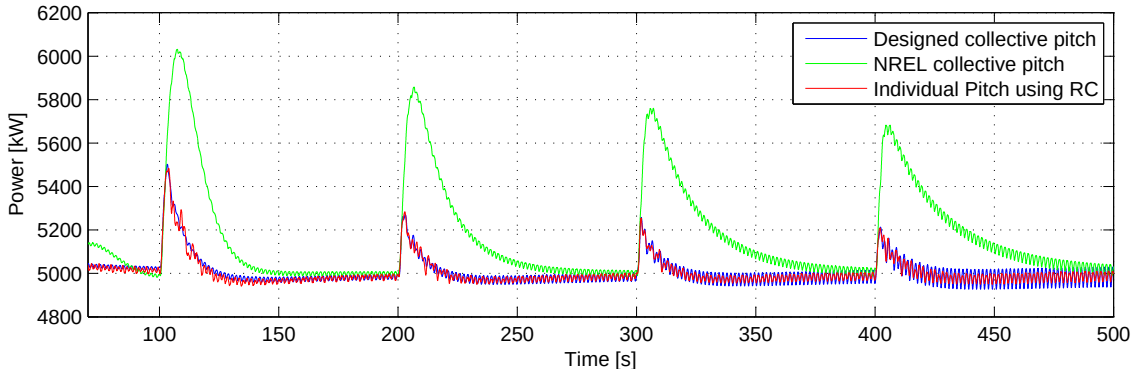

Figure 14.10: Power output for comparing the designed collective pitch controller in Chapter 11 on page 73, the NREL collective pitch controller, and the designed repetitive controller in Chapter 13 on page 91, implemented on the nonlinear FAST 5 MW wind turbine model operating in above rated region (12 to 24 m/s).

By using the collective pitch control and repetitive control schemes developed in this project, the tower tilt-wise displacement is increased, as mentioned in the previous set of tests, this may be due to the mismatches between the model of the turbines structure of the designed linearised state space model in Chapter 6 on page 43 and the NREL FAST 5 MWs structure model.

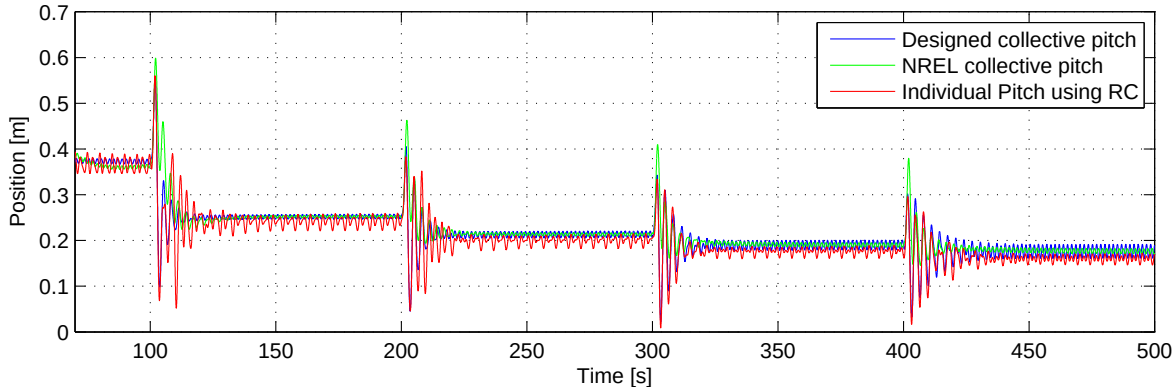

Figure 14.11: Tower tilt-wise displacement for comparing the designed collective pitch controller in Chapter 11 on page 73, the NREL collective pitch controller, and the designed repetitive controller in Chapter 13 on page 91, implemented on the nonlinear FAST 5 MW wind turbine model operating in above rated region (12 to 24 m/s).

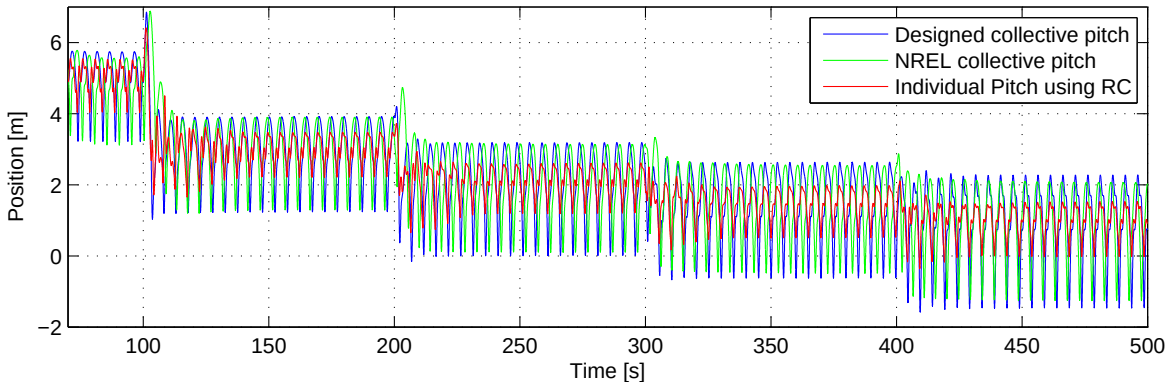

Figure 14.12: Blade 1 tilt-wise displacement for comparing the designed collective pitch controller in Chapter 11 on page 73, the NREL collective pitch controller, and the designed repetitive controller in Chapter 13 on page 91, implemented on the nonlinear FAST 5 MW wind turbine model operating in above rated region (12 to 24 m/s).

The blade tilt-wise displacement, displayed in Figure 14.11 is noted minimised by use of the developed repetitive control algorithm, in the above rated operating region of the wind turbine. This is expected as the repetitive controller is designed to minimise the 1P loads present on the blades. Furthermore, in the case of all the plots oscillations are noted. The reason is that the drivetrain damper has not been modeled.

By having studied the behavior of the system and by considering the requirements presented on Page 15, the first requirement is fulfilled, as the power is kept constant at 5 MW, with the error tolerance of $\pm 1\%$ in the above rated region. The second requirement, involving the angular velocity, is also fulfilled, as is it kept constant at all time at 122.9 rad/s, with an error tolerance of $\pm 1\%$ when operating in above rated region. The third requirement, and the most important requirement of the present project, to minimise the loads is fulfilled as well, as the blade displacement is minimised compared to the basic collective pitch control scheme used by the FAST model in above rated operating region.
As noted in the Figures 14.7(b) and 14.7(a) the pitch actuation of the designed repetitive controller, using individual pitch, and the designed collective pitch controller, compared to the NREL collective pitch

controller, is higher in both cases. Thus this could lead to a more rapid degradation of the pitch actuators then normal.

The fifth requirement, of keeping the generator torque constant at 43 kN when operating in the above region, is partially fulfilled as it is not constant at all time, deviations are present due to the collective pitch control implementation, noted in Figure 14.8(b). This however, is considered trivial as the project main scope was of minimising the loads on the turbine, which have been successfully accomplished.

As a conclusion of the acceptance test, the designed collective pitch controller, implemented on the nonlinear NREL FAST 5 MW turbine, performs similar to the already existing collective pitch controller. Consequently the designed repetitive controller scheme was tested, resulting in significant reduction of the 1P loads on the blades, and small reduction on the structure and mechanism of the turbine. It is thus concluded, that the implementation of the repetitive control strategy developed in the present project on the nonlinear NREL FAST 5 MW wind turbine, was successful. The performance of the implemented repetitive controller lives up to the expectation of the repetitive controller scheme.

15 CONCLUSION

The requirements of the project, presented in Chapter 2 on page 15, with the project scope, presented in Section 1.5 on page 12, are restated following.

Project scope

Is it possible to reduce the periodic loads on the components of a modern wind turbine operating in above-rated region, by means of individual pitch control?

Project Requirements

1. The power produced by the wind turbine should be kept constant at all time, at 5 MW with an error tolerance of $\pm 1\%$, for wind velocities from 12 to 24 m/s.
2. The angular velocity of the generator should be kept constant at all time at 122.9 rad/s, with an error tolerance of $\pm 1\%$, for wind velocities from 12 to 24 m/s.
3. The displacement of the tower and blades of the wind turbine should be diminished compared to the already exiting control of the FAST 5 MW turbine.
4. The pitch action should be minimised compared to the existing pitch control of the NREL FAST 5 MW wind turbine.
5. The generator torque should be kept constant at the reference value of 43050 Nm, with an error tolerance of $\pm 1\%$, for wind velocities from 12 to 24 m/s.

To be able to satisfy the requirements, and give an answer to the project scope, modelling of the wind turbine was required. The model has been designed based on the nonlinear NREL FAST 5MW wind turbine model. Consequently several models were developed to compose the final linear wind turbine model, designed and implemented. The final wind turbine model being composed of:

1. A nonlinear aerodynamic model, linearised for later control implementation and testing purposes.
2. Models for the mechanisms of the turbine: drivetrain, generator and pitch system.
3. Models for the structure of the turbine: tower and blades.

The designed models have been combined in a continuous-time linear state space model, further used as the model for tests and also for the controller implementation. A parameter estimation has been performed in order to find the optimal parameters, with respect to the NREL 5 MW wind turbine model. A comparison has been presented with the appertaining conclusion, that the model is sufficient for the goal

of the project. Furthermore, the model used to test the controllers, is a continuous-time model, but the measurements are obtained according to a sampling time of $T_s = 0.0125$, corresponding to the sampling time of the FAST model. The measurements are considered with noise, thus a Kalman filter and state estimator is designed. For the control implementation, the model is discretised using Zero-Order Hold. All the implemented controllers are in discrete-time.

To be able to run the simulation, a wind profile has been developed. The wind profile is composed of shear, tower shadow, wake and a turbulence model, in order to be as accurate to the real life environment as possible.

Three controllers have been designed to accomplish the requirements of the project. A collective pitch controller, composed of two discrete-time PI controllers has been developed to drive the output power, and angular velocity of the generator to their respective reference values. This controller is further used as a basis for the individual pitch controllers, that were developed.

To overcome the repetitiveness of the wind disturbances affecting the turbine, two approaches were proposed and implemented: multi-bladed coordinate transformation and repetitive control. With respect to the obtained results, the first approach has minimised the blades tilt-wise bending, caused by the 1P loads. It did not affect the other components of the turbine, as the purpose of this approach was to minimise the 1P loads, and generate individual pitch signals. Consequently this approach is considered passed when implemented on the developed linearised model. For the second approach, an algorithm has been developed, which can be used on any system encountering periodic behaviour. Before implementing it on the developed model, it has been tested on a simpler model, namely the pitch model used by the wind turbine. The results of the implementation are as expected, thus by using the developed repetitive control algorithm, the repetitive error converges to zero as time goes to infinity. In the case of the wind turbine model, the implementation was also done according to the designed algorithm. The first step was to stabilise the closed-loop system, which was accomplished by using the designed collective pitch controller. Following the system has been lifted corresponding to the period of the disturbance affecting the system. The errors augmentation in the lifted state space was performed. Due to the fact that the obtained system was of a large size, model reduction has been performed using the balanced truncation method. An LQR controller has been designed for the obtained states space together with a Kalman filter used to estimate the unmeasured states.

With respect to the results obtained when implementing the repetitive control algorithm on the developed linear model of the wind turbine, it minimises the deviations form the reference values, for all the components of the turbine. The control signal is an individual pitch control, as desired. When comparing it to the performance of the collective pitch control and the multi-bladed coordinate transformation, it is noted that it outperforms both implementations. Moreover, the repetitive controller minimises not only the 1P loads present on the blades of the turbine, but also the other harmonics of this frequency. Thus the repetitive control implementation has been considered a success.

In order to perform the acceptance tests, the designed controllers except the multi-bladed coordinate transformation, were implemented on the nonlinear NREL FAST 5 MW wind turbine, considered the real plant and according to which the model was developed. Corresponding to the results of the acceptance tests, it is concluded that the project scope has been accomplished. Consequently the answer to the

project scope is positive, as it is possible to minimise the loads present on a wind turbine by means of individual pitching.

16 FUTURE WORK

The development of the control strategies presented throughout the project is not ending here. Improvements can be conducted on the modelling, control and implementation as well. Remarks on the improvements and further work that can be carried out, are presented in sections corresponding to modelling, control and implementation.

Modelling

For the present project, a wind model containing wind shear, tower shadow, wake and turbulence has been implemented. However, regarding the wake, it has not been considered as having a meandering effect, thus this should be modelled as well, in order to have an even more realistic wake model. The wind field is perpendicular on the area swept by the rotor. Furthermore, the wind model was not validated.

Due to the limitations of the developed kinematic model, the aerodynamic model does not affect other tower or blades displacements than the ones in the direction of the x-axis.
For the wind turbine model used throughout the project, a mass-spring-damper system is considered as the blades model. For a more accurate model of the blades dynamics hinged blade approach could be developed. This would result in more realistic behaviour of the developed model.

The generator model should include the necessary converters in order to make the transition from mechanical power to electrical power more realistic.

The model for the yaw was also neglected, and considered that the turbine is always in upwind position. This however is not realistic, consequently a further yaw model is required for more true results and interpretations.

The developed linear model presented only a good match, according the nonlinear NREL FAST 5MW wind turbine model, in the neighbourhood of the operating points chosen in the linearisation. To be able to obtain a better estimate to the nonlinear model, gain scheduling or feedback linearisation could be implemented.

The considered pitch model is a simple first order electric pitch system. For proper results and implementation on a real turbine, the pitch system needs to be re-modelled accordingly.

Control

The start-up and shut-down of the wind turbine were not considered, as the main goal of the project was to develop a controller for the third region of operation. Furthermore, to cover the whole range of wind

velocities, gain scheduling or bumpless transfer can be used for the linear controllers.

The Kalman estimator can be improved by performing further tuning of the state covariance matrix. As the wind velocities had been estimated, a second approach of repetitive control could be considered, involving constraints to the current LQR controller by using Model Predictive Control.

As the iterative learning control design, is similar to the one of the repetitive controller implemented in the present project, a further research could be of determining weather the iterative learning strategy can provide better results.

For the multi-bladed coordinate transformation to minimise the following P loads, present in the system, further transformations can be performed with respect to the P loads, that are desired to be minimised. This will lead to considerable results, worth of comparing it to the performance of the repetitive controller implemented in this project.

A new approach for improving the performance of the system by using repetitive controller, could be its implementation as a part of the multi-bladed coordinate transformation. By doing so, the system would learn to minimise the tilt-wise and yaw-wise moments, and possibly result in a better performance than both the individual pitch control strategies presented throughout the project.

The performance of the designed repetitive controller could be improved by adding more memory loops. By doing so, period mismatches may be encountered. Also by including a noise model in the control design, the controllers robustness towards noise may be assured.

Another improvement to repetitive controller is to consider the period length of one third of the revolution. This is possible due to the fact that all three blades gather information, thus by concatenating the information for one-third of a revolution, a whole revolution is obtained. To accomplish it, either the information of the disturbance throughout the period has to be shifted from one blade to the other, or the control signal used in the following period, has to be shifted to the corresponding blades. This could lead to better results and faster convergence of the error. Moreover, the number of state will be decreased thus the computational time with it.

Implementation

As no sensor noise has been considered in the case of the control strategies implemented on the nonlinear NREL FAST 5 MW wind turbine, it would be of interest to determine the performances of the developed controller under these circumstances.

BIBLIOGRAPHY

3Tier. *Global Mean Wind Speed at 80m*. 2008.

Karl Johan Aastrom. *Control System Design*. 2002.

alternativeenergysource.org. *Renewable Energy*. 2011. URL http://www.alternativeenergysource.org/pros_cons.html.

Wind Atlas Analysis and Application Program. Turbulence modelling, 2009. URL http://130.226.56.171/products/WAT/wathelp/WATmodelling.htm.

Athanasios Constantinos Antoulas. *Approximation of Large-scale Dynamical Systems*. 2005.

Mines ParisTech / Armines. *Yearly Mean of Daily Irradiation in UV in the World*. 2008. URL http://www.soda-is.com/eng/map/maps_for_free.html.

Walter Benenson, John W. Harris, Horst Stocker, and Holger Lutz. *Handbook of Physics*. 2002.

Fernando D. Bianchi, Hernán De Battista, and Ricardo J. Mantz. *Wind Turbine Control Systems*. 2007.

Yuval Bistritz. *Reflections on Schur-Cohn Matrices and Jury-Marden Tables and classification of related unit-circle zero location criteria*. 1996.

Anders Bech Borchersen. *FAST Installing*. 2012. URL http://kom.aau.dk/~anb/fast/fastinstall.html.

E. A. Bossanyi. *Individual Blade Pitch Control for Load Reduction*. 2002.

E. A. Bossanyi, Garrad Hassan, and Partners Ltd. *Further load reductions with individual pitch control*. 2005.

Tony Burton, David Sharpe, Nick Jenkins, and Ervin Bossanyi. *Wind Energy Handbook*. 2001.

Robert P. Coleman and Arnold M. Feingold. *Theory of self-excited mechanical oscillations of helicopter rotors with hinged blades*. 1957.

Dale S. L. Dolan and Peter W. Lehn. *Simulation Model of Wind Turbine 3p Torque Oscillations due to Wind Shear and Tower Shadow*. 2006.

Energy Research Centre of the Netherlands. *Aerodynamics of turbine wakes*. 2009.

Renewable energy UK. *Betz Limit*. 2012. URL http://www.reuk.co.uk/Betz-Limit.htm.

EWEA. *Wind in power*. 2012.

B.A. Francis and W.M. Wonham. *The Internal Model Principle for Linear Multivariable Regulators*. 1975.

Steen T. Frandsen. *Turbulence and Turbulence Generated Structural Loading in Wind Turbine Clusters*. 2007.

Gene F. Franklin, J. David Powell, and Abbas Emami-Naeini. *Feedback Control of Dynamic Systems*. 2006.

Martin O. L. Hansen. *Aerodynamics of Wind Turbines*. 2009.

Shinji Hara, Yutaka Yamamoto, Tohru Omata, and Michio Nakano. *Repetitive Control System: A New Type Servo System for Periodic Exogenous Signals*. 1988.

J. Hätönen, D. H. Owens, and R. Ylinen. *A New Optimality Based Repetitive Control Algorithm for Discrete-Time Systems*. 2008.

Simon Haykin. *Kalman Filtering and Neural Networks*. 2001.

Ivo Houtzager. *Towards Data-Driven Control for Modern Wind Turbines*. 2011.

Florin Iov, Anca Daniela Hansen, Poupl Sørensen, and Frede Blaabjerg. *Wind Turbine Blockset in Matlab/Simulink*. 2004.

Mate Jelavic, Vlaho Petrovic, and Nedjeljko Peric. *Estimation based Individual Pitch Control of Wind Turbine*. 2010.

N. O. Jensen. *A Note on Wind Generator Interaction*. 1983.

J. Jonkman, S. Butterfield, W. Musial, and G. Scott. *Definition of a 5-MW Reference Wind Turbine for Offshore System Development*. 2009.

Jason M. Jonkman and Marshall L. Buhl Jr. *FAST User's Guide*. 2005.

Morten Knudsen. *Experimental modelling of dunamic systems*. 2004.

NREL Laboratories. *Computer-Aided Engineering Tools*. 2013. URL `https://wind.nrel.gov/designcodes/simulators/`.

Matthew A. Lackner and Gijs van Kuik. *A Comparison of Smart Rotor Control Approaches using Trailing Edge Flaps and Individual Pitch Control*. 2009.

Jay H. Lee, Seshatre Natarajan, and Kwand S. Lee. *A model-based predictive control approach to repetitive control of continuous processes with periodic operations*. 2001.

Jay H. Lee Manish Gupta. *Period-robust repetitive model predictive control*. 2005.

J. F. Manwell, J. G. McGowan, and A. L. Rogers. *Wind Energy Explained*. 2009.

Mathworks. *Balanced model truncation via square root method*. 2013. URL `http://www.mathworks.se/help/robust/ref/balancmr.html`.

Caroline Mawer. *Vertical Axis Windmill in Nishtafun*. June 2012. URL http://architectureforguerillas.blogspot.dk/.

NREL. *Power Technologies Energy Data Book*. 2013. URL http://www.nrel.gov/analysis/power_databook/calc_wind.php.

Peter F. Odgaard and Kathryn E. Johnson. *Wind turbine fault detection and fault tolerant control - a second challange*. 2012.

Katsuhiko Ogata. *Discrete-Time Control Systems*. 1987.

R. H. Park. *Two-Reaction Theory of Synchronous Machines; Generalized Methods of Analysis - Part 1*. 1929.

R. C. P. Prinsen. *Investigation into reduction of the Cost-Of-Energy of the Upwind 5.0 MW Wind Turbine using Higher-Harmonic Individual Pitch Control*. 2011.

Tohru Omata Shinji Hara, Yutaka Yamamoto and Michio Nakano. *Repetitive Control System: A New Type Servo System for Periodic Exogenous Signals*. 1988.

Raymond T. Stefani, Bahram Shahian, Clement J. Savant, and Gene H. Hostetter. *Design of Feedback Control Systems*. 2002.

Rochester Solar Technologies. *About turbines*. 2012. URL http://www.solarrochester.com/Wind%20Turbine%20information.asp.

L. J. Vermeer, J. N. Sørensen, and A. Crespo. *Wind Turbine Wake Aerodynamics*. 2003.

Youqing Wang, Furong Gao, and Francis J Doyle III. *Survey on iterative learning control, repetitive control, and run-to-run control*. 2008.

Jinghau Zhong. *PID Controller Tuning: A Short Tutorial*. 2006.

LIST OF FIGURES

LIST OF TABLES

Appendix

A NREL FAST 5 MW WIND TURBINE

This chapter shortly elaborates on the open source NREL FAST 5 MW wind turbine software. The FAST version used is *v7.01.00a-bjj*. The 5 MW wind turbine is version *v1.05.00*. AeroDyn, used for generating the wind profile, is version *v13.00.01a-bjj*. NWTC, the subroutine library, is version *v1.05.00*.

A.1 FAST Setup

The FAST model can be downloaded from [Laboratories, 2013]. For UNIX operating systems, a special compiling has to be run, for the FAST to work. This can e.g. be done by using the compiling algorithm developed by [Borchersen, 2012]. Though for Windows operating system, it runs out of the box. FAST can either be run from a terminal, or from `Simulink`. By using `Simulink`, FAST is run by using the following commands in the *Command Window* of `MATLAB`:

1. Run `Simsetup.m`
2. A line appears where the behaviour file `.fst`, is entered.
3. The model, `.mdl`, which include the FAST model is opened, and run.

All the mentioned files should be in the same folder, together with the rest of the FAST model dynamic files. When the model is run ones, it is a good idea to close the model, before running a new test, starting from the first number in the above enumerations.

The main file for determining the behaviour of the FAST model is the `.fst` file. It is e.g. possible to choose from where the FAST model should be controlled (`Simulink`, baseline (`DISCON.f90`) or none at all). Further it is also possible to determine which outputs are wanted. The `.fst` file uses the `.ipt` to determine tower shadow, shape of the blade, wind profile among others.

The reader is encouraged to read [Jonkman and Jr., 2005] for further installation and operating instructions.

A.2 Baseline Controller

This section elaborates on the controllers used for the nonlinear baseline NREL 5 MW wind turbine. The region of which these controllers are elaborated in, are for wind velocities from 11.4 m/s to 25 m/s. The control is, from NREL, made in FORTRAN code, and is found in the file `DISCON.f90`.

The torque controller is split up in five regions, as noted in Figure A.1.

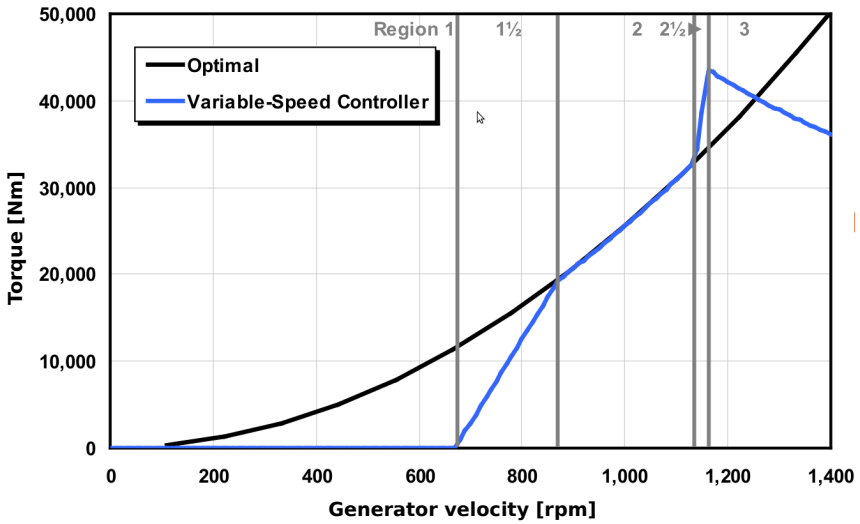

Figure A.1: Gain scheduling regions for the torque controller, [Jonkman et al., 2009, p.20].

The region of interest is just at the beginning of region 3. Though it is hard to note in Figure A.1, that the torque is kept constant, at 43050 Nm, for a constant angular velocity of the generator, at 1173 rpm. This is done by pitching the blades according to the angular velocity of the rotor, where the gain scheduled PI controller is composed of a P = 0.0188 and a I = 0.0080. A reference table for the wind to pitch is noted in Table D.2 on page 163.

B IDEAL ROTOR MODEL

This chapter is written with respect to [Manwell et al., 2009, p.92-96]. For this chapter only, the wind velocities are noted different than the rest of the report. V_1 and V_4 are the wind velocities at different distances with respect to rotor of the wind turbine.

In order to find the maximum energy extraction efficiency of a wind turbine, a model with infinite number of thin blades is considered, upon which a constant wind stream is blowing. As the turbine extracts kinetic energy from the wind, the velocity of the wind upstream is greater than downstream, due to the velocity induced onto the rotor. This is noted in Figure B.1 by the blue line, $V_1 > V_4$. The wind velocity effect on the turbine results in a thrust force which at the rotor is the mass flow rate times the difference between the wind velocity from the inlet of the tube to its outlet. These changes are depicted in Figure B.1. The mass flow rate through the tube, enclosing the rotor, is the same for the whole tube, thus the following equation is given:

$$\rho A_1 V_1 = \rho A_\mathrm{r} V_\mathrm{r} = \rho A_4 V_4 \qquad [\cdot] \quad \text{(B.1)}$$

Because of the decrease in wind velocity over the rotor, the following equation is given:

$$F_\mathrm{T}(t) = (V_1(t) - V_4(t))\,\rho A_\mathrm{r} V_\mathrm{r}(t) \qquad [\mathrm{N}] \quad \text{(B.2)}$$

Where:

ρ	is the density of the air	[kg/m^3]
A_i	is the cross sectional area for the given position; *1, r, 4*	[m^2]
$V_1(t)$	is the wind velocity at the inlet of the tube	[m/s]
$V_4(t)$	is the wind velocity at the outlet of the tube	[m/s]
$V_\mathrm{r}(t)$	is the wind velocity at rotor	[m/s]
$F_\mathrm{T}(t)$	is the force of thrust	[N]

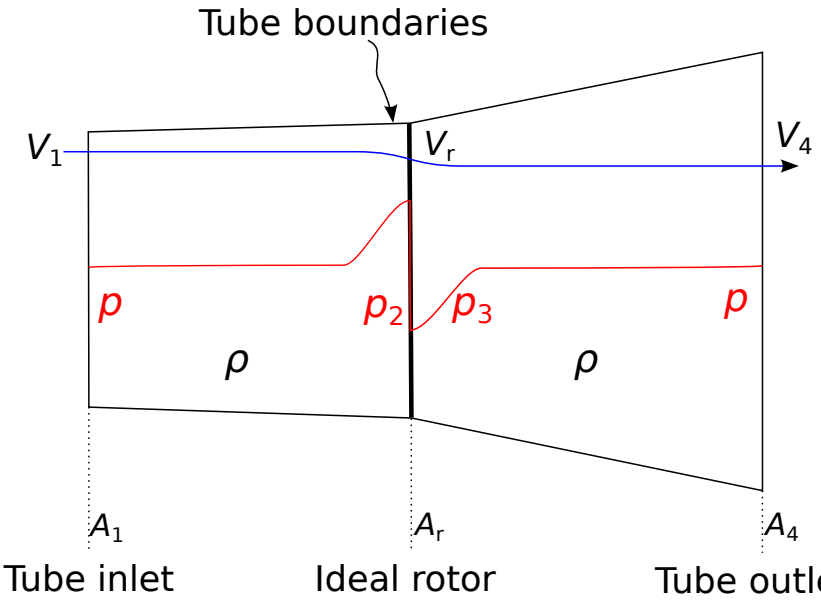

Figure B.1: The tube principle, based on momentum theory, with an ideal rotor. Blue line depicts pressure drop, red line depicts the pressure and the vertical black line in the middle, depicts the rotor.

A part of the wind energy is absorbed by the turbine, thus the wind velocity across the rotor is reduced by: $V_1 - V_4$, and a pressure drop from one side of the rotor to the other, occurs. At the beginning and end of the tube, the two pressure points are equal. The pressure drop is depicted by the red line, and the drop in wind velocity is depicted by the blue line in Figure B.1. These changes affects the turbine by inducing a thrust force F_T, given by Equation B.3.

$$F_T(t) = (p_2(t) - p_3(t))A_r \quad [\text{N}] \quad \text{(B.3)}$$

The pressure drop across the rotor is expressed by using the Bernoulli equation, [Manwell et al., 2009]. It takes both upstream and downstream pressure of the turbine into consideration:

$$p(t) + \frac{1}{2}\rho V_1^2(t) = p_2(t) + \frac{1}{2}\rho V_r^2(t) \quad [\text{Pa}] \quad \text{(B.4)}$$

$$p_3(t) + \frac{1}{2}\rho V_r^2(t) = p(t) + \frac{1}{2}\rho V_4^2(t) \quad [\text{Pa}] \quad \text{(B.5)}$$

By substituding Equation B.4 in Equation B.5, Equation B.6 is given.

$$(p_2(t) - p_3(t)) = \frac{1}{2}\rho(V_1^2(t) - V_4^2(t)) \quad [\text{Pa}] \quad \text{(B.6)}$$

It is known that the force of thrust, F_T Equation B.3, can be defined using the axial induction factor, a, to

$$F_T = (V_1 - V_4)\rho A_r V_1(1-a) \quad [\text{N}] \quad \text{(B.7)}$$

By inserting Equation B.6 into B.3 which is equal to Equation B.7, Equation B.8 is given:

$$V_4(t) = V_1(t) \cdot (1-2a) \quad [\text{m/s}] \quad \text{(B.8)}$$

It is known that the wind velocity at the rotor, Equation B.2, also can be rewritten using a:

$$V_r(t) = V_1(t) \cdot (1-a) \quad [\text{m/s}] \quad \text{(B.9)}$$

By inserting Equation B.8 into Equation B.2, and replacing V_r by Equation B.9, the total power extracted from the wind by the rotor, is obtained as the force of thrust acting on the rotor times the wind velocity at the rotor.

$$P(t) = F_\mathrm{T}(t)V_\mathrm{r}(t) = 2\rho A V_\mathrm{r}^3(t)a(1-a)^2 \quad [\mathrm{W}] \quad \text{(B.10)}$$

The subscript, r, for V_r is neglected unless other wind velocities are present. The power coefficient describes how well the performance of the wind turbine is. It is defined as the power dissipated to drive the rotor divided by the wind power.

$$C_\mathrm{p}(t) = \frac{P(t)}{\frac{1}{2}\rho V^3(t)A} \quad [\cdot] \quad \text{(B.11)}$$

$$\Downarrow$$

$$C_\mathrm{p}(t) = 4a(1-a)^2 \quad [\cdot] \quad \text{(B.12)}$$

In order to determine the maximum power coefficient, called the Betz limit, the first order derivative of the power coefficient is equaled to zero. Thus, for operating at maximum power production the power coefficient for $a = \frac{1}{3}$ is:

$$C_{\mathrm{p,\,max}} = 0.5926 \quad [\cdot] \quad \text{(B.13)}$$

The coefficient of thrust is obtained as the thrust force divided by the dynamic force acting on the rotor [Manwell et al., 2009]:

$$C_\mathrm{t}(t) = \frac{P(t)}{\frac{1}{2}\rho V^2(t)A} \quad [\cdot] \quad \text{(B.14)}$$

The evolution of the power and thrust coefficients are presented in Figure B.2. The maximum limit for C_t is one and the maximum value for C_p is 0.59, meaning 59 % of the wind can be transformed into rotational energy by the turbine. The maximum limit for an operating wind turbine is usually between 0.35-0.45 [energy UK, 2012]. As noted in Figure B.3, for the FAST model, the maximum C_p value is 0.485.

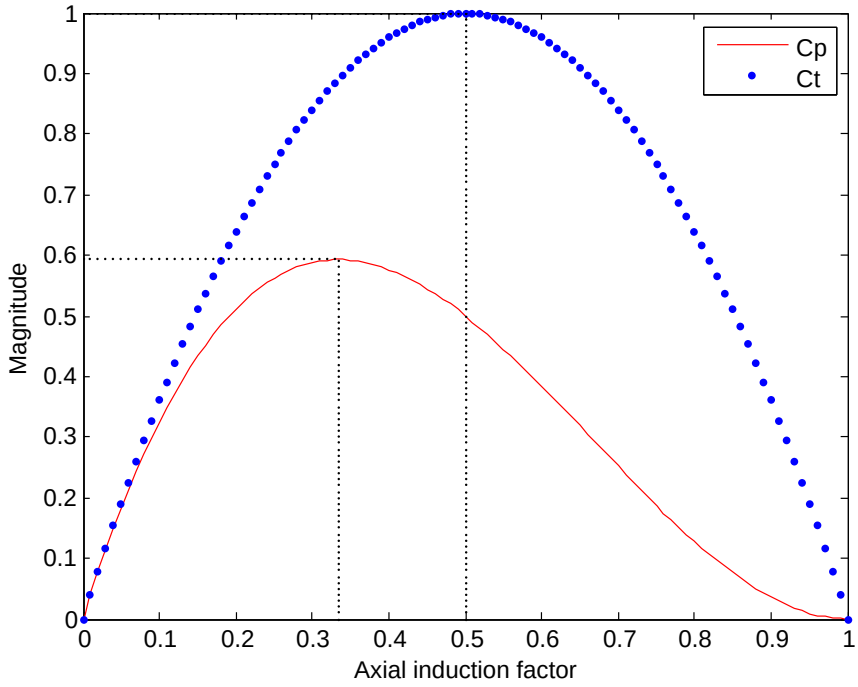

Figure B.2: Performance coefficients for an ideal wind turbine.

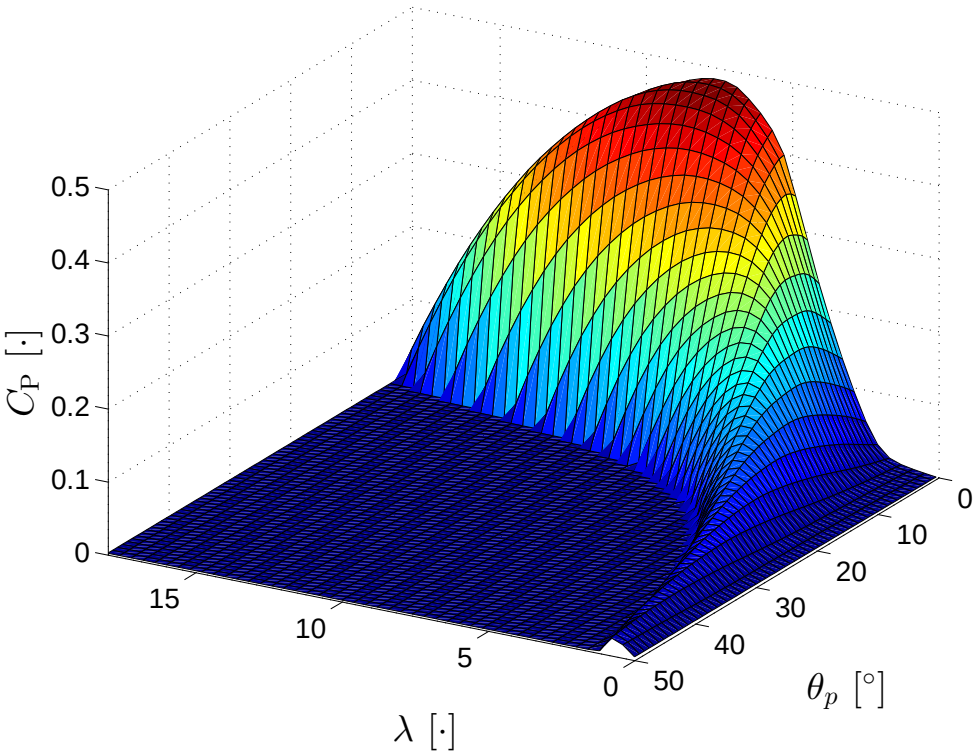

Figure B.3: C_p curve for the NREL 5 MW wind turbine.

The maximum value is relative high, when comparing to a real wind turbine. This high value is reached because it is a model, and not a real wind turbine. It is further noticed that the pitch angle does not cover the whole pitch region from 0 to 90 degrees. This is not necessary when looking at Table D.1 on page 162, where the maximum pitch angle, at wind velocity of 25 m/s, is 23.47°. At wind velocities

above 25 m/s the turbine shuts down, thus pitch angles above are not considered.

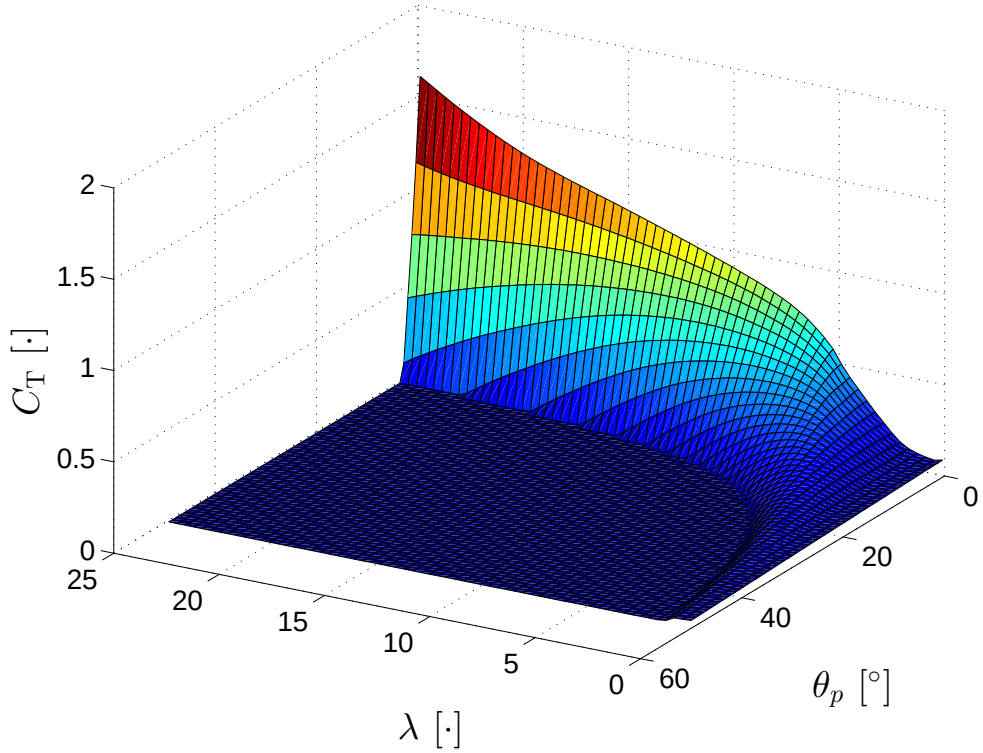

Figure B.4: C_t surface for the NREL 5 MW wind turbine.

The maximum value for the C_t surface is 1.6207, which is noted in Figure B.4. The reason that the value is higher than what is noted in Figure B.2 on page 154 is because of the axial induction factor, a, which is higher than 1/3, given by isolating a in:

$$C_p = 4a(1-a)^2 \qquad [\cdot] \quad \text{(B.15)}$$

This leads to $a = 0.51$, with a maximum C_p of 0.485. With a above 1/3, according to [Hansen, 2009], simple momentum theory does not hold. Thus the Glauert Correction and the Prandtl's tip loss factor is used. This is shortly explained:

- Prandtl's tip loss factor takes the fact that a turbine does not really have an infinite number of blades, into account. Having a turbine with an finite number of blades has a different vortex system than that of an infinite.
- Glauert correction takes the different empirical relations between a and the thrust coefficient into consideration.

Thus the calculations for the C_t-curve is made by

$$C_t(t) = \frac{F_T}{\frac{1}{2}\rho V^2 A} \qquad [\cdot] \quad \text{(B.16)}$$

where:

F_T	is the force of thrust	[N]
ρ	is the air density	[kg/m^3]
V	is the wind velocity	[m/s]
A	is the area of the rotor	[m^2]

For further explanation on this subject, the reader is encouraged to read [Hansen, 2009].

C LINEARISATION OF NONLINEARITIES

When working with a state space (see Section 6 on page 43 for elaboration upon state space), it is desired to have only linear terms, to investigate the behavior of the system near the equilibrium point. A simple solution to this problem is by linearising with respect to an operating point. Though this results in the fact that the system is most likely only to show good results within a short neighborhood region of its linearisation point. To overcome this problem, several models with different working points can be derived, also called gain scheduling, for the linear model. When looking at the derived models, it is clear that the aerodynamic model has some nonlinearities. These are noted and linearised in the following sections.

C.1 Linearisation of the Torque

The aerodynamic model contains nonlinear terms caused by the wind velocity. These are the angular velocity of the rotor, the wind affecting the system and the pitch angle. The goal of the following part is to linearise the equations at the predefined operating points V_0, $\omega_{r,0}$ and $\theta_{p,0}$, which are for the wind, angular velocity of the generator and the pitch angle respectively. Moreover, the operating point for the torque, from Equation 4.12 on page 35, is given as:

$$F_{Q,0} = \frac{P_0}{\omega_{r,0}} = \frac{1}{2\omega_{r,0}} \rho \pi R^2 V_0^3 C_p(\lambda_0, \theta_{p,0}) \tag{C.1}$$

where the tip-speed-ratio is given by:

$$\lambda_0 = \frac{\omega_{r,0} R}{V_0} \tag{C.2}$$

The first order Taylor expansion of the torque acting on the rotor is given by:

$$F_Q(t) = F_{Q,0} + \left.\frac{\partial F_Q}{\partial \omega_r}\right|_{\omega_{r,0}} \Delta\omega_r(t) + \left.\frac{\partial F_Q}{\partial \theta_p}\right|_{\theta_{p,0}} \Delta\theta_p(t) + \left.\frac{\partial F_Q}{\partial V}\right|_{V_0} \Delta V(t) \tag{C.3}$$

where

$$\left.\frac{\partial F_Q(t)}{\partial \omega_r}\right|_{\omega_{r,0}} = \frac{1}{2}\rho\pi R^2 \Delta V_0^3 \left(-\frac{1}{\omega_r^2} C_p(\lambda_0, \theta_{p,0}) + \frac{1}{\omega_{r,0}} \left.\frac{\partial C_p(\lambda(t), \theta_p(t))}{\partial \lambda}\right|_{\lambda_0} \left.\frac{\partial \lambda}{\partial \omega_r}\right|_{\omega_{r,0}} \right) \tag{C.4}$$

$$\left.\frac{\partial F_Q(t)}{\partial \theta_p}\right|_{\theta_{p,0}} = \frac{1}{2\omega_{r,0}} \rho\pi R^2 V_0^3 \left(\left.\frac{\partial C_p(\lambda(t), \theta_p(t))}{\partial \theta_p}\right|_{\theta_{p,0}} \right) \tag{C.5}$$

$$\left.\frac{\partial F_Q(t)}{\partial V_p}\right|_{V_{p,0}} = \frac{1}{2\omega_{r,0}} \rho\pi R^2 \left(3V_0^2 C_p(\lambda_0, \theta_{p,0}) + V_0^3 \left.\frac{\partial C_p(\lambda(t), \theta_p(t))}{\partial \lambda}\right|_{\lambda_0} \left.\frac{\partial \lambda}{\partial V}\right|_{V_0} \right) \tag{C.6}$$

By substituting the above computed partial derivatives into the Taylor expansion of the torque, the following expression for the torque is given:

$$\begin{aligned} F_{\mathrm{Q}}(t) = F_{\mathrm{Q},0} &+ \frac{1}{2}\rho\pi R^2 \Delta V_0^3 \left(-\frac{1}{\omega_{\mathrm{r}}^2} C_{\mathrm{p}}(\lambda_0, \theta_{\mathrm{p},0}) + \frac{1}{\omega_{\mathrm{r},0}} \left.\frac{\partial C_{\mathrm{p}}(\lambda(t), \theta_p(t))}{\partial \lambda}\right|_{\lambda_0} \left.\frac{\partial \lambda}{\partial \omega_{\mathrm{r}}}\right|_{\omega_{\mathrm{r},0}} \right) \Delta\omega_{\mathrm{r}}(t) \\ &+ \frac{1}{2\omega_{\mathrm{r},0}} \rho\pi R^2 V_0^3 \left(\left.\frac{\partial C_{\mathrm{p}}(\lambda(t), \theta_{\mathrm{p}}(t))}{\partial \theta_{\mathrm{p}}}\right|_{\theta_{\mathrm{p},0}} \right) \Delta\theta_{\mathrm{p}}(t) \\ &+ \frac{1}{2\omega_{\mathrm{r},0}} \rho\pi R^2 \left(3V_0^2 C_{\mathrm{p}}(\lambda_0, \theta_{\mathrm{p}0}) + V_0^3 \left.\frac{\partial C_{\mathrm{p}}(\lambda(t), \theta_{\mathrm{p}}(t))}{\partial \lambda}\right|_{\lambda_0} \left.\frac{\partial \lambda}{\partial V}\right|_{V_0} \right) \Delta V(t) \end{aligned} \tag{C.7}$$

where

$$\left.\frac{\partial \lambda}{\partial \omega_{\mathrm{r}}}\right|_{\omega_{\mathrm{r},0}} = \frac{R}{V_0} \tag{C.8}$$

$$\left.\frac{\partial \lambda}{\partial V}\right|_{V_0} = \frac{-\omega_{\mathrm{r},0} \cdot R}{V_0^2} \tag{C.9}$$

where $\frac{\partial C_{\mathrm{p}}}{\partial \lambda}$ and $\frac{\partial C_{\mathrm{p}}}{\partial \theta_{\mathrm{p}}}$ usually are given by a C_{p} look-up table or curve, specific for each individual type of wind turbine. By subtracting the operating point of the torque, $F_{\mathrm{Q},0}$ expressed by Equation C.1 on page 157, on both sides of the equality sign, the linear torque force is obtained.

C.2 Linearisation of the Thrust Force

The linearisation of the thrust force is done in the same manner as the linearisation of the torque, having the force of thrust $F_{\mathrm{T}}(t)$ as:

$$F_{\mathrm{T}}(t) = \frac{1}{2}\rho\pi R^2 V^2(t) C_{\mathrm{t}}(\lambda(t), \theta_{\mathrm{p}}(t)) \tag{C.10}$$

and the operating point of the thrust force:

$$F_{\mathrm{T},0} = \frac{1}{2}\rho\pi R^2 V_0^2 C_{\mathrm{t}}(\lambda_0, \theta_{\mathrm{p},0}) \tag{C.11}$$

with

$$\lambda_0 = \frac{\omega_{\mathrm{r},0} R}{V_0} \tag{C.12}$$

The first order Taylor expansion of the thrust acting on the rotor of the turbine is given by:

$$F_{\mathrm{T}}(t) = F_{T,0} + \left.\frac{\partial F_{\mathrm{T}}}{\partial \omega_{\mathrm{r}}}\right|_{\omega_{\mathrm{r}0}} \Delta\omega_{\mathrm{r}}(t) + \left.\frac{\partial F_{\mathrm{T}}}{\partial \theta_{\mathrm{p}}}\right|_{\theta_{\mathrm{p},0}} \Delta\theta_{\mathrm{p}}(t) + \left.\frac{\partial F_{\mathrm{T}}}{\partial V}\right|_{V_0} \Delta V(t) \tag{C.13}$$

where

$$\left.\frac{\partial F_{\mathrm{T}}(t)}{\partial \omega_{\mathrm{r}}}\right|_{\omega_{\mathrm{r},0}} = \frac{1}{2}\rho\pi R^2 V_0^2 \left(\left.\frac{\partial C_{\mathrm{t}}(\lambda(t), \theta_p(t))}{\partial \lambda}\right|_{\lambda_0} \left.\frac{\partial \lambda}{\partial \omega_{\mathrm{r}}}\right|_{\omega_{\mathrm{r},0}} \right) \tag{C.14}$$

$$\left.\frac{\partial F_{\mathrm{T}}(t)}{\partial \theta_{\mathrm{p}}}\right|_{\theta_{\mathrm{p},0}} = \frac{1}{2}\rho\pi R^2 V_0^2 \left(\left.\frac{\partial C_{\mathrm{t}}(\lambda(t), \theta_{\mathrm{p}}(t))}{\partial \theta_{\mathrm{p}}}\right|_{\theta_{\mathrm{p},0}} \right) \tag{C.15}$$

$$\left.\frac{\partial F_{\mathrm{T}}(t)}{\partial V}\right|_{V_0} = \frac{1}{2}\rho\pi R^2 \left(2V_0 C_{\mathrm{t}}(\lambda_0, \theta_{\mathrm{p},0}) + V_0^2 \left.\frac{\partial C_{\mathrm{t}}(\lambda(t), \theta_{\mathrm{p}}(t))}{\partial \lambda}\right|_{\lambda_0} \left.\frac{\partial \lambda}{\partial V}\right|_{V_0} \right) \tag{C.16}$$

By substituting the above computed partial derivatives into the Taylor expansion of the thrust force, the expression of the thrust is:

$$\begin{aligned} F_{\mathrm{T}}(t) = F_{\mathrm{T},0} &+ \frac{1}{2}\rho\pi R^2 V_0^2 \left.\frac{\partial C_{\mathrm{t}}(\lambda(t),\theta_p(t))}{\partial\lambda}\right|_{\lambda_0} \left.\frac{\partial\lambda}{\partial\omega_{\mathrm{r}}}\right|_{\omega_{\mathrm{r},0}} \Delta\omega_{\mathrm{r}}(t) \\ &+ \frac{1}{2}\rho\pi R^2 V_0^2 \left.\frac{\partial C_{\mathrm{t}}(\lambda(t),\theta_{\mathrm{p}}(t))}{\partial\theta_{\mathrm{p}}}\right|_{\theta_{\mathrm{p},0}} \Delta\theta_{\mathrm{p}}(t) \\ &+ \frac{1}{2}\rho\pi R^2 \left(2V_0 C_{\mathrm{t}}(\lambda_0,\theta_{\mathrm{p},0}) + V_0^2 \left.\frac{\partial C_{\mathrm{t}}(\lambda,\theta_{\mathrm{p}})}{\partial\lambda}\right|_{\lambda_0} \left.\frac{\partial\lambda}{\partial V}\right|_{V_0}\right) \Delta V(t) \end{aligned} \tag{C.17}$$

Where

$$\left.\frac{\partial\lambda}{\partial\omega_{\mathrm{r}}}\right|_{\omega_{\mathrm{r},0}} = \frac{R}{V_0} \tag{C.18}$$

$$\left.\frac{\partial\lambda}{\partial V}\right|_{V_0} = \frac{-\omega_{\mathrm{r}0}\cdot R}{V_0^2} \tag{C.19}$$

Where $\frac{\partial C_{\mathrm{t}}}{\partial\lambda}$ and $\frac{\partial C_{\mathrm{t}}}{\partial\theta_{\mathrm{p}}}$ usually are given by a C_{t} look-up table or curve, specific for each individual type of wind turbine. By subtracting the operating point of the thrust force, $F_{\mathrm{T},0}$ which is given by Equation C.11 on page 158, on both sides of the equality sign, the linear thrust force is obtained.

C.3 Linearisation of the Power

The linearisation of the power is done by looking at the small perturbation around the operating point of the torque $T_{\mathrm{g},0}(t)$, angular velocity $\omega_{\mathrm{g},0}(t)$ and the output power $P_0(t)$, by using Taylor approximation of the nonlinear part. For ease of understanding, Equation 5.20 on page 41 for the power is repeated:

$$P(t) = \eta_{\mathrm{g}}\omega_{\mathrm{g}}(t)T_{\mathrm{g}}(t) \tag{C.20}$$

The small perturbations for the nonlinearities are noted

$$P(t) = P_0 + P_\Delta(t) \tag{C.21}$$

Thus by inserting the perturbations into Equation C.20, the following equation is given:

$$\underbrace{\eta_{\mathrm{g}}\omega_{\mathrm{g}}(t)T_{\mathrm{g}}(t)}_{P(t)} \approx \underbrace{\eta_{\mathrm{g}}\omega_{\mathrm{g},0}T_{\mathrm{g},0}}_{P_0} + \underbrace{\eta_{\mathrm{g}}\omega_{\mathrm{g},0}T_{\mathrm{g}\Delta}(t) + \eta_{\mathrm{g}}\omega_{\mathrm{g}\Delta}(t)T_{\mathrm{g},0}}_{P_\Delta(t)} \tag{C.22}$$

By substituting $P(t)$, by Equation C.21

$$P_0 + P_\Delta(t) = \eta_{\mathrm{g}}\omega_{\mathrm{g}0}T_{\mathrm{g}0} + \eta_{\mathrm{g}}\omega_{\mathrm{g}0}T_{\mathrm{g}\Delta}(t) + \eta_{\mathrm{g}}\omega_{\mathrm{g}\Delta}(t)T_{\mathrm{g}0} \tag{C.23}$$

and by isolating $P_\Delta(t)$, the linearised first order differential power equation is found:

$$P_\Delta(t) = \eta_{\mathrm{g}}\omega_{\mathrm{g}0}T_{\mathrm{g}\Delta}(t) + \eta_{\mathrm{g}}\omega_{\mathrm{g}\Delta}(t)T_{\mathrm{g}0} \tag{C.24}$$

D PARAMETERS

The parameters used for the linearised control model, derived in Chapter II on page 21, and various parameters through out the report, are denoted in this chapter. The parameters are set with respect to the NREL FAST 5 MW wind turbine model, [Jonkman et al., 2009]. If a subscript is followed by an i, the parameter has an influence on more than one subject. This could e.g. be the mass of the blades, which are noted by M_{bi}, where i specifies blade 1 to 3.
First the optimal pitch angles for the NREL 5 MW turbine is noted. Then the dynamics NREL 5 MW FAST parameters, going to parameter estimation and ends with parameters for the sensor noise.

D.1 Pitch Table - Above Rated

For a wind velocities over 11.4 m/s, the angular velocity of the rotor is kept constant, by blade pitching with respect to a given wind velocity. Table D.1 contains the pitch angles with respect to the wind velocities. The table is from [Jonkman et al., 2009, p.23]. It is used for control purpose in `Simulink`.

Wind speed [m/s]	**Rotor speed** [rpm]	**Pitch angle** [°]
11.4	12.1	0.00
12.0	12.1	3.83
13.0	12.1	6.60
14.0	12.1	8.70
15.0	12.1	10.45
16.0	12.1	12.06
17.0	12.1	13.54
18.0	12.1	14.92
19.0	12.1	16.23
20.0	12.1	17.47
21.0	12.1	18.70
22.0	12.1	19.94
23.0	12.1	21.18
24.0	12.1	22.35
25.0	12.1	23.47

Table D.1: Pitch angle with respect to angular velocity of the rotor and the wind velocity, [Jonkman et al., 2009, p.23].

D.2 Dynamic parameters

Gross properties			
Notation	**Part**	**Value**	**Unit**
P	Rated power output	5	[MW]
$[\cdot]$	Number of blades	3	$[\cdot]$
R	Rotor diameter	126	[m]
$[2 \cdot r_0]$	Hub diameter	3	[m]
H	Hub height	90	[m]
$[\cdot]$	Cut-in, rated, cut-out	3, 11.4, 25	[m/s]
$[\cdot]$	Rated tip speed	80	[m/s]
M_r	Rotor mass	110,000	[kg]
M_n	Nacelle mass	240,000	[kg]
M_t	Tower mass	347,460	[kg]
Blade structural properties			
L_b	Blade length	61.5	[m]
M_bi	Blade mass	17,740	[kg]
$[\cdot]$	Center of mass location w.r.t. root	20.475	[m]
Drive train properties			
ω_r	Rated rotor speed	1.267	[rad/s]
ω_g	Rated generator speed	122.9	[rad/s]
N_g	Gearbox ratio	97:1	$[\cdot]$
J_r	Rotor inertia about low-speed shaft	35444067	[kg·m^2]
J_g	Generator inertia about high-speed shaft	534.116	[kg·m^2]
Baseline control system properties			
T_g	Rated generator torque	43,093.55	[Nm]
$T_{\mathrm{g,\,max}}$	Maximum generator torque	47,402.91	[Nm]
$\tau_{T_{\mathrm{g,max}}}$	Maximum generator torque rate	15,000	[Nm/s]
τ_T	Generator torque time constant rate	0.1	[s]
$\theta_{\mathrm{pi,\,min}}$	Minimum blade-pitch setting	0	[°]
$\theta_{\mathrm{pi,\,max}}$	Maximum blade-pitch setting	90	[°]
τ_θ	Maximum absolute blade-pitch rate	8	[°/s]

Table D.2: Parameters from the nonlinear FAST 5 MW turbine, [Jonkman et al., 2009].

D.3 Parameter estimation

For calculating the stiffness of the tower and the blades, the following equation is used:

$$\omega^2 = \frac{K_\mathrm{x}}{M_\mathrm{x}} \quad [\mathrm{Hz}] \quad \text{(D.1)}$$

$$K_\mathrm{x} = M_\mathrm{x} \cdot (2\pi f_\mathrm{t})^2 \quad [\mathrm{N/m}] \quad \text{(D.2)}$$

where:

K_x	is the stiffness of x	[N/m]
M_x	is the mass of x	[kg]
x	is t for tower and bi for blade $i = 1,\ 2,\ 3$	$[\cdot]$
f_t	is the resonance frequency ($\omega = 2\pi f_\mathrm{t}$)	[Hz]

According to [Jonkman et al., 2009], the resonance frequency of the tower fore-aft is 0.324 Hz, and for the blade flap-wise is 0.6993 Hz. This gives the following values for the stiffness of the blade and tower:

$$K_\mathrm{t} = 347460 \cdot (2\pi \cdot 0.324)^2 = 1.4400e6 \quad [\mathrm{N/m}] \quad \text{(D.3)}$$

$$K_\mathrm{b} = 17740 \cdot (2\pi \cdot 0.6993)^2 = 3.4248e5 \quad [\mathrm{N/m}] \quad \text{(D.4)}$$

The damping constant B_x is calculated by rearranging:

$$\zeta_x = \frac{B_\mathrm{x}}{2\sqrt{M_\mathrm{x} K_\mathrm{x}}} \quad [\cdot] \quad \text{(D.5)}$$

Where the damping ratio ζ according to [Jonkman et al., 2009], usually is between 0.6 and 0.7 for the blade. Therefore 0.65 is chosen. The tower fore-aft damping ratio is found to be 0.01. The damping for the two structures are found to be:

$$B_\mathrm{x} = \zeta_\mathrm{x} 2\sqrt{M_\mathrm{x} K_\mathrm{x}} \quad [\mathrm{N(s/m)}] \quad \text{(D.6)}$$

$$B_\mathrm{t} = 0.01 \cdot 2\sqrt{347460 \cdot 1.44e6} = 1.4147e4 \quad [\mathrm{N(s/m)}] \quad \text{(D.7)}$$

$$B_\mathrm{b} = 0.65 \cdot 2\sqrt{17740 \cdot 3.4248e5} = 1.0133e5 \quad [\mathrm{N(s/m))}] \quad \text{(D.8)}$$

Parameter Estimation using *SENSTOOLS*

`SENSTOOLS` is a toolbox for `MATLAB` developed at AAU. It is added to the `MATLAB` toolbox library, for it to be used in `MATLAB`. `SENSTOOLS` is included on the attached dvd on the inside of the last page of the report, found in the folder `matlab/Sens.tar`. As the keen reader may have noted, the toolbox is a UNIX based software (*.tar*), and is only tested in this environment. It has several other usages than parameter estimation, though these are not elaborated.
`SENSTOOLS` is used to estimate, M_t, K_t, B_t, M_bi, K_bi, B_bi, to get better dynamics of the blades and the tower. `SENSTOOLS` needs certain inputs for it to estimate these parameters. These are included in the files `simKEEP.m` and `progprogKEEP.m`, in folder `matlab/parameter_estimation/sens`. These files contains the following information:

1. A control model.

2. Data, from the states which the control model is wanted to be matched to.

3. Start estimates, set as `par0`.

4. Initial value for the control model states.

5. Driving input for the model.

and further elaborated:

1)
The linear control model is described in Chapter II on page 21, and is not further elaborated here.

2)
The data from the states, which the linear control model is wanted to resemble, are:

Angular velocity of the rotor	ω_r
Tower displacement	x_t
Tower acceleration	$\dot{x}_t$
Blade displacement	x_{bi}
Blade acceleration	$\dot{x}_{bi}$

These are made by running the FAST model, under certain circumstances. The file (`.fst`) concerning the setup for the FAST model is found on the cd in directory
`matlab/parameter_estimation/lin_at_18ms_pitch_14_92/FAST/`.

3)
The start guess for the parameters, `par0`, are chosen to be those given in Table D.2, and those calculated from Equation D.3 to D.8. The parameters which are estimated are renamed by e.g. `par(1) = Mt` for estimating the mass of the tower. Though the parameter should then be commented in the initialisation of the parameters of the model.

4)
The model is linearised, thus the initial values for the states are zeros for all.

5)
The model is excited by the wind profile, noted in Figure 7.1(a). By using `MATLAB`'s `lsim` (linear simulation), the simulation is run for the length of the data file from FAST. The input and state files need to be of the same length.
For further information for the toolbox `SENSTOOLS` the reader is referred to the Paper by [Knudsen, 2004].

D.4 Sensor Noise

Table D.3 presents the noise level for the available sensors on the turbine.

Sensor type	Symbol	Unit	Noise power
Anemometer (wind velocity at hub height)	$V_{\mathrm{H,n}}$	0.0071	[m/s]
Rotor velocity	$\omega_{\mathrm{r,n}}$	10^{-4}	[rad/s]
Generator velocity	$\omega_{\mathrm{g,n}}$	$2{\cdot}10^{-4}$	[rad/s]
Generator torque	$T_{\mathrm{g,n}}$	0.9	[Nm]
Generated power	P_{n}	10	[W]
Pitch angle of the i^{th} blade	$\theta_{\mathrm{p}i,\mathrm{n}}$	$1.5 \cdot 10^{-3}$	[°]
Azimuth angle on the low speed side	ϕ_{n}	10^{-3}	[rad]
Blade root moment of the ith blade	$M_{\mathrm{B}i\mathrm{n}}$	10^{3}	[Nm]
Tower top acceleration fore-aft ($x_{\mathrm{t,n}}$) measurement	$\ddot{x}_{\mathrm{t,n}}$	$5 \cdot 10^{-4}$	$\left[\mathrm{m/s^2}\right]$

Table D.3: Noise level for different sensors on the 5MW NREL wind turbine, [Odgaard and Johnson, 2012]

Note that in the present project, the tower and blades position is considered as being measured, thus the same noise power is considered as in the case of the tower top acceleration, of $5 \cdot 10^{-4}$ m/s^2.

E EIGENVALUES OF THE CONTROL MODEL

Following the eigenvalues are noted for investigating the open loop stability:

Value
-0.2493
-0.6701 +13.5728i
-0.6701 -13.5728i
-0.0462 + 2.0764i
-0.0462 - 2.0764i
-0.4029 + 4.3229i
-0.4029 - 4.3229i
-0.4085 + 4.2701i
-0.4085 - 4.2701i
-0.4085 + 4.2701i
-0.4085 - 4.2701i
-10.0000
-5.0000
-5.0000
-5.0000

They are calculated by `MATLAB eig` function.

F TUNING THE PI CONTROLLERS

The tuning method used for the two PI controllers, elaborated in Chapter 11 on page 73, is based on the Ziegler-Nichols frequency response method, also known as oscillation method, [Franklin et al., 2006, p.199]. The method is based on the intersection, where the Nyquist curve on the Nyquist plot of the system crosses the negative real axis. This intersection is found by tuning two parameters, namely the frequency ω_c (ultimate period), and the gain at that frequency K_c (ultimate gain), which typically is given as:

- The *ultimate gain*, $K_u = \frac{1}{K_c}$.
- The *ultimate period*, $T_u = \frac{2\pi}{\omega_c}$.

The approach to parametrise these values as following: a controller consisting only of a proportional controller with a small gain, is applied to the system. This gain is increased until the system becomes marginally stable. The corresponding gain is called the ultimate gain and the period of this oscillation is the ultimate period. By knowing K_u and T_u, the optimal controller gains are chosen according to the following table:

Controller	K	T_i	T_d
P	$\frac{K_u}{2}$		
PI	$\frac{K_u}{2.2}$	$\frac{T_u}{1.2}$	
PID	$\frac{K_u}{1.7}$	$\frac{T_u}{2}$	$\frac{T_u}{8}$

Table F.1: Controller parameters for Ziegler-Nichols method, [Aastrom, 2002].

This approach is used to design the optimal PI controllers for the power control and the pitch control, which are investigated following.

Tuning the PI Controllers for Power Output Stabilising

When tuning the PI controller for the power output, a Nyquist plot of the input output relation of the generator torque reference, and power, is used. It is depicted in Figure F.1.

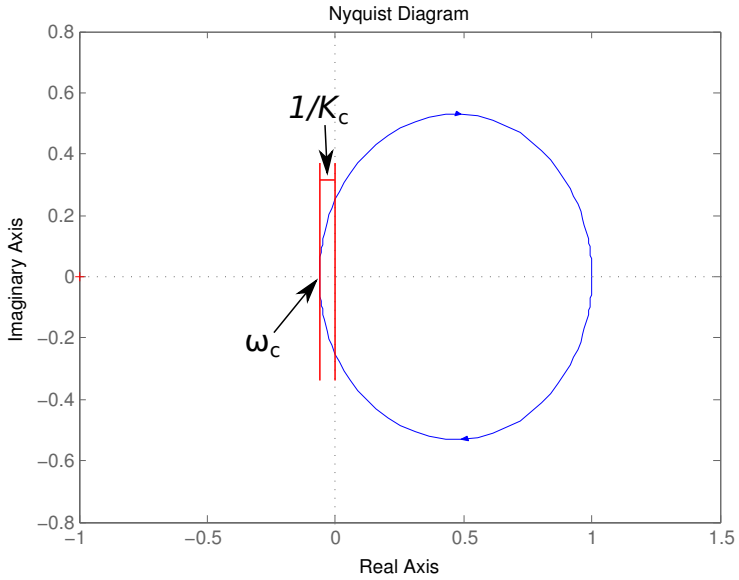

Figure F.1: Nyquist plot of the discretized system for controlling the power output.

Where the ultimate gain $K_u = 16.02$ and the ultimate period is $T_u = 0.025$. By using Table F.1 on page 169, the values for the PI controller are given as follows: K_p=7.28 and $K_i = 0.02$, which results in the following step response of the discretized system.

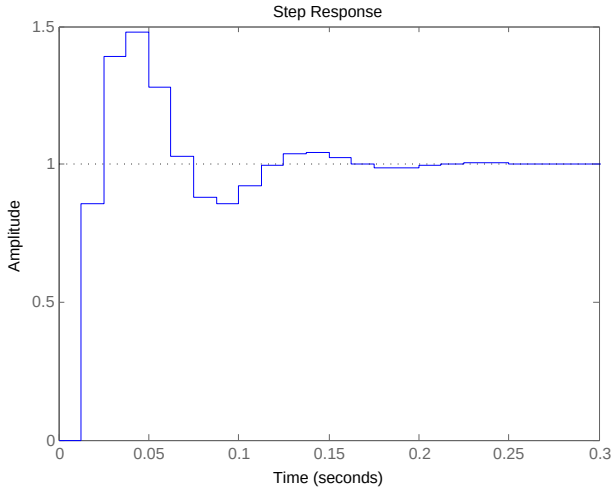

Figure F.2: Step response of the system with tuned value for the PI controller.

As noted in Figure F.1 the system is discretized. The sample time used is set with respect to NREL 5 MW FAST wind turbine at 0.0125.

Tuning the PI controllers for collective pitch

The same procedure is used for tuning the PI controller used for the collective pitch of the wind turbine. The input-output relation is given as the pitch angle to the generator speed. Thus the following step response is given.

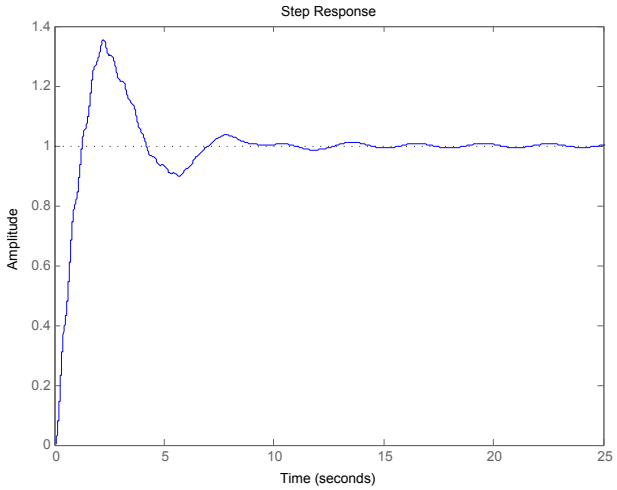

Figure F.3: Step response of the discretized system with the PI controller.

The values for the PI controller are calculated to be $K_\mathrm{p} = 0.59564$ and $K\mathrm{i} = 1.1974$.
The Ziegler-Nichols tuning method is a straight forward method for tuning PID controllers, where by tuning the proportional gain, a PID controller can be derived. Another advantage is the understanding of the behaviour of the system because it gives, including the overall dynamics of the system, with respect to specified input/output.
Applying Ziegler-Nichols tuning method does not always result in optimal controller values.

Further Tuning

As the two PI controllers do not give a satisfactory response, a further tunning of the parameters is performed with respect to Table F.2.

Response	Rise time	Overshoot	Settling time	S-S error
K_p	Decrease	Increase	Small change	Decrease
K_i	Decrease	Increase	Increase	Eliminate
K_d	Minor change	Decrease	Decrease	No effect in theory

Table F.2: The affect the PID parameters has on a system, [Zhong, 2006].

The new gains for the power controller is given as $K_\mathrm{p} = -0.013$ and $K_\mathrm{i} = -0.13$. The gains for the angular velocity controller is derived to be $K_\mathrm{p} = 0.01$ and $K_\mathrm{i} = 1.15e-3$

G INTERNAL MODEL PRINCIPLE

The following description of the Internal Model Principle (IMP), is made with respect to [Hara et al., 1988]. It states that the output of the controller is able to track a periodic error, for a fixed period p, without any steady state error, for the stable closed loop system, if the disturbance is known in advance. For repetitive disturbances in time domain, this can e.g. be done by implementing a memory block, as noted in Figure G.1(b), which is affect by the periodic signal depicted in Figure G.1(a). The memory block stores the control signal of the last period, and uses the information for the given period. From the system, which is wanted controlled, the controller behaves like a non-causal controller.

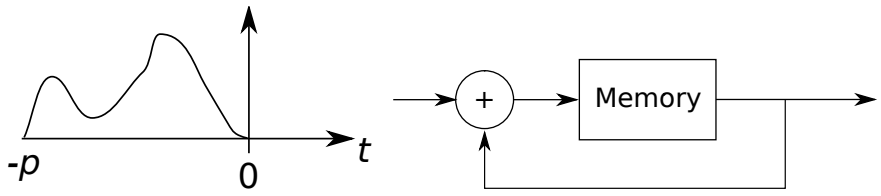

(a) Repetitive signal. (b) Periodic and initial signal.

Figure G.1: Periodic signal block, [Hara et al., 1988]

Though by using this scheme, the disturbance is first know after the first period, thus the control of the system is first initiated after 1 p.

When examining the frequency domain, this scheme has infinitely many poles on the imaginary axis, $jk\omega_p$, $k = 0, \pm 1, \pm 2, \ldots$, and $\omega_p = \frac{2\pi}{p}$, according to [Hara et al., 1988]. Because of that, the internal model principle the tracking of the periodic disturbance should converge asymptotically. Thus can be used by implementing

$$\frac{e^{-p \cdot s}}{1 - e^{(p \cdot s)}}$$

as a controller, in the closed loop for tracking the disturbance, then the scheme is often noted as a repetitive controller as noted in Figure G.2.

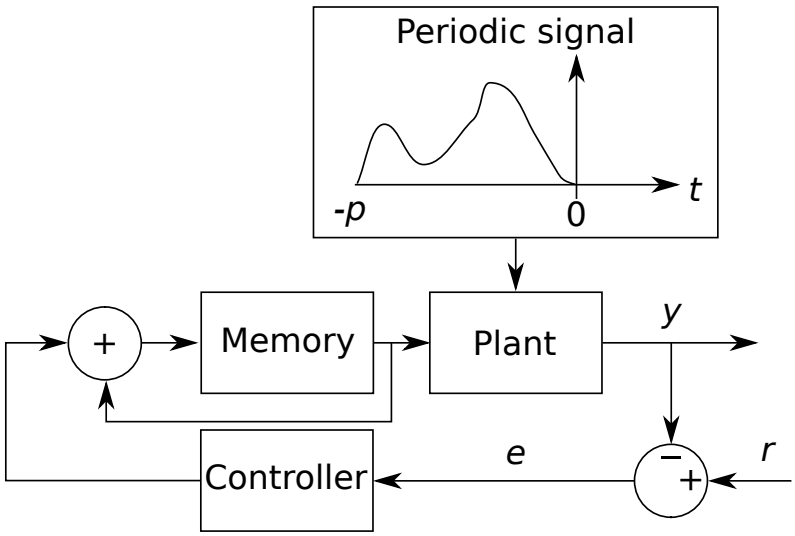

Figure G.2: Repetitive control scheme.

H Repetitive Controller Implemented in Simulink

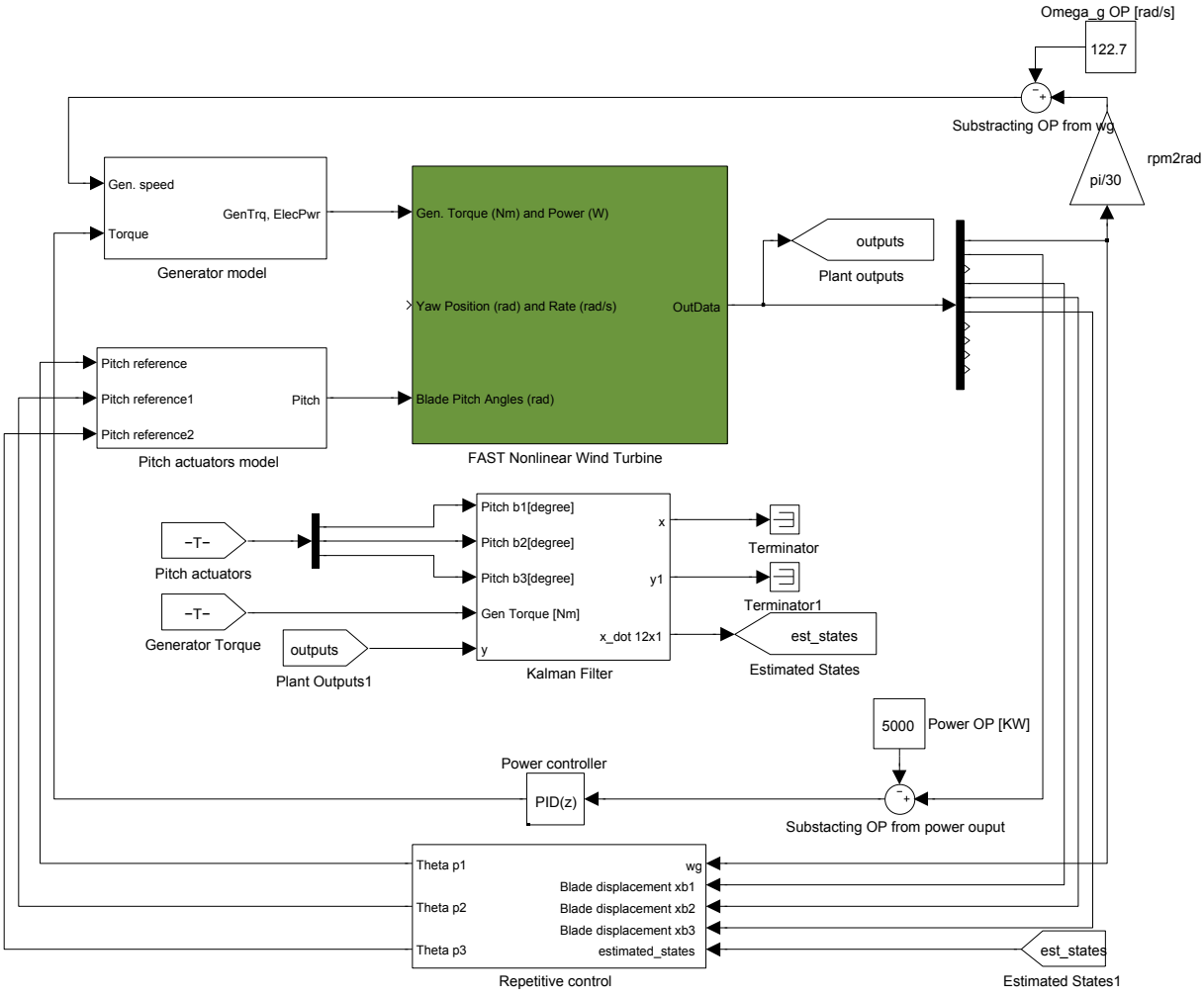

Figure H.1: Repetitive controller implemented on the nonlinear FAST 5 MW model in Simulink.

For the implementation of the developed repetitive control scheme, the models of the generator and pitch actuators are implemented for the NREL FAST 5MW nonlinear wind turbine model as presented in Chapter 5 on page 37. As the nonlinear model is working with large signals, it is desired to substract the operating point corresponding to the linearisation point of the designed model in Chapter 6 on page 43 at the output and add them in the input. Consequently the designed repetitive controller for the linearised plant model can be used on the nonlinear plant. The Kalman filter is present in order to estimate the unmeasured states required by the repetitive control algorithm.

I CONTENT OF THE CD

The included CD has the following content:

- Literature from bibliography

  `literature/`

- Digital copy of the report

  `report.pdf`

- `MATLAB` and `Simulink` files

  `matlab/`

  Linear turbine model

  Model validation

  Implemented controllers

  Acceptance test

  Parameter estimation